A SPATIO-TEMPORAL ANALYSIS OF NEAR-SURFACE AIR TEMPERATURE WITHIN THE WEST CASTLE WATERSHED, ALBERTA

KYLE J. BEXTE
Bachelor of Science, **University of Lethbridge, 2017**

A thesis submitted
in partial fulfilment of the requirements for the degree of

MASTER OF SCIENCE

in

GEOGRAPHY

Department of Geography
University of Lethbridge
LETHBRIDGE, ALBERTA, CANADA

A SPATIO-TEMPORAL ANALYSIS OF NEAR-SURFACE AIR TEMPERATURE WITHIN THE WEST CASTLE WATERSHED, ALBERTA

KYLE BEXTE

Date of Defence: June 13th, 2019

Dr. P. Bonnaventure	Assistant Professor	Ph.D.
Dr. M. G. Letts	Professor	Ph.D.
Thesis Co-Supervisors		
Dr. S. Kienzle	Professor	Ph.D.
Thesis Examination Committee Member		
Dr. C. Hopkinson	Professor	Ph.D.
Thesis Examination Committee Member		
Dr. C. Coburn	Professor	Ph.D.
Chair, Thesis Examination Committee		

Abstract

Modelling surface air temperature across regions of relatively complex terrain has historically presented a challenging task. Using topographically derived variables in association with land cover, monthly linear regression models were derived for mapping surface air temperature across the West Castle Watershed, Alberta. Hourly, daily, and monthly surface lapse rates were determined for the study period (July 1st, 2017 – June 30th, 2018). The monthly surface lapse rates observed varied between -8.0 ˚C km^{-1} in October and -2.2 ˚C km^{-1} in February. The role of frequent chinook events was observed in tche distinct surface lapse rate in January compared against the previous and following months; January had a surface lapse rate of -5.8 ˚C km^{-1} compared to December and February of -2.3 ˚C km^{-1} and -2.2 ˚C km^{-1} respectively. Inverted surface lapse rates were found to exhibit a seasonal pattern in occurrence and were present for 18.5 % of the study period.

Acknowledgements

The completion of this thesis would not be possible without the support provided by so many people. First and foremost a sincere thank you to my supervisor, Dr. Philip Bonnaventure, for the invaluable guidance and assistance throughout this process which without, I undoubtedly would have had a much more difficult experience. Thank you for teaching me that research involves both hard work and dedication but requires laughter, comradery, and a drink around a campfire with friends. I would also like to thank the members of my committee for their helpful insight and guidance; Dr. Letts for providing monetary support in association with his valuable insight, Dr. Hopkinson who shared data relevant to this projects, and Dr. Kienzle who inspired me to pursue my passion for mapping and geography.

I would be remiss not to thank explicitly my lab mates, Rory, Madeleine, Seamus, Oliver and Trevor. The hours of both casual conversation and laughter provided to me a sense of belonging and comfort through the process of this research. Also, without whom, field work and logistics of this research would have been nigh on impossible.

To all my friends, the Core Five, Da By's, and others too many to mention, who kept me sane through this process, reminding me to stay humble, I cannot thank you enough. I honestly cannot fathom having made it through this process without their constant reassurances and untimely distractions. And finally, a special thanks to my family, who provided me with endless love, support, affirmations, and a warm hearth to which I could always escape to when I needed moments of clarity and respite.

Contents

i. List of figures

ii. List of tables

iii. List of Equations

iv. List of Abbreviations

AMAT	Annual Mean Air Temperature
ANUSPLIN	Australia National University Spline
ASL	Above sea level
DEM	Digital Elevation Model
DJF	December, January, February – winter
GIS	Geographic Information System
JJA	June, July, August – summer
IPCC	International Panel on Climate Change
MAM	March, April, May – spring
MAT	Monthly Average Temperature
MAAT	Mean Annual Air Temperature
PAR	Photosynthetically Active Radiation
PISR	Potential Incoming Solar Radiation
PRISM	Parameter Regression on Independent Slopes Model
RPC	Representative Concentration Pathway
SON	September, October, November – fall
TPI	Topographic Position Index
WCW	West Castle Watershed

1.0 Introduction

Inherently, some of the most challenging terrain to collect data and model climate is located in the mountains. Mountainous terrain generally lack climatic infrastructure and are often logistically difficult to access and sample (Li & Heap, 2014). Commonly, climate stations in mountains are clustered near roads and easily accessed sites are concentrated around locations of particular relevance to human populations (Stahl et al., 2006). As such, examining climatic trends within complex topography presents a substantial challenge, compared to adjacent lowlands and valleys. Mountain climates represent complex systems with complex interactions between topography, solar irradiation, snow cover, and vegetation (Fridley, 2009). Thus, these environments represent terrain where we have a limited understanding of existing feedbacks or how they will respond to climate change (Pepin et al., 2015).

The need for high-resolution climate models covering areas with topographically variable terrain has become particularly important to accurately assess potential climate change while capturing heterogeneity in localized phenomena (Pepin et al., 2015). These include the microclimatological effects of vegetation, snow cover and the impact of inversions in surface lapse rate (SLR), with the latter being particularly poorly understood (Lewkowicz & Bonnaventure, 2011). Many existing climate models over mountainous regions infer fixed SLR over different seasons and landforms (Minder et al., 2010). Much of this stems from observations of adiabatic lapse rates in the lower free atmosphere, as well as from research in highly-studied mountains such as the European Alps where

inversions show a limited impact on the local climatology and mountains are distinct from other ranges (Kirchner et al., 2013).

It has been demonstrated that inversions in SLR, which occur mostly in winter in northern locales, can play an essential role in the spatial distribution of temperature across North American mid- and high-latitude topography, with the relationship between temperature and elevation often being seasonally or even annually reversed (Lewkowicz & Bonnaventure, 2011). This relationship results from cold stable air masses which pool at low elevations (Clements et al., 2003; Minder et al., 2010; Lewkowicz & Bonnaventure, 2011). The full impact of this effect is, however, often not incorporated into climate models that extend into mountain areas (Hijmans et al., 2005). This can result in significant errors modelling temperature in mountainous regions due to the presence of inversions (Way & Bonnaventure, 2015). Thus, the nature and effect of inversions, as well as contributing factors, are essential to the understanding of the spatial variability of air and ground temperatures, as well as the presence and distribution of cryospheric components (e.g. permafrost, glaciers, seasonal snowpack) (Taylor et al., 1998; Pigeon & Jiskoot, 2008). Understanding these concepts can thus improve models in complex terrain subsequently refining the evolution of temperature fields in the past, present and into the future. As much of the observed and predicted change in climate is seasonally and spatially asymmetric, with greater warming intensity expected in winter, at higher latitudes, and within mountainous regions (Pepin & Lundquist, 2008; Serreze & Barry, 2011; Cohen et al., 2012; IPCC, 2014; Pepin et al., 2015; Kienzle, 2017) refining the understanding of heterogeneous topography, inversions, and surface air temperature in the mountains is critical to many aspects of environmental modelling.

2.0 Objectives

2.1 Primary Research Objective

The primary objective of this research is the collection of surface air temperature data for the purpose of modelling a topographically derived surface of monthly and annual surface air temperature for further insight into the spatial and temporal patterns within West Castle Watershed, Alberta.

2.2 Secondary Research Objectives

1) Develop a distributed network of monitoring stations that capture the heterogeneity of air temperature within mountainous regions with respect to elevation, land cover, and other topographically derived variables.
2) Compare the modelled temperatures derived for this research with established coarse-resolution models that are spatially coincident with the study area.
3) Perturb modelled surface air temperature to predict potential future climates in association with climate change using Representative Concentration Pathways (RCP) set out by the International Panel on Climate Change (IPCC).
4) Examine the spatiotemporal patterns of surface lapse rates, inversions, and chinooks within the complex topography.

3.0 Background

3.1 Introduction

Weather and climate are essential controls to daily life; they influence how we dress, what we eat, and are tied to many of the economic, social, and behavioural patterns seen in society (Ross, 2017). Although these terms are related, their differences are vast, and it is essential to understand the relationship we have with each of them. The day-to-day nature of weather can complicate life, from delaying travel to cancelling outdoor activities altogether. Forecasting weather has become essential to modern day life. So much so, that inaccurate forecasting can have negative economic and societal repercussions. In connection with the uncertainty of weather forecasts, many question the ability to look into the future and understand how climate shifts with any degree of certainty. Although at their core these two phenomena are related though they are governed under very different systems (Chaotic v. Deterministic) (Ruddiman, 2001).

Climate exhibits deterministic behaviour in comparison to the chaotic nature of weather (Palmer, 2000). The chaotic nature of weather systems means that any uncertainty in understanding the initial state or interactions between elements within the system will result in the compounding of errors in prediction of that system's future state and it is this that makes weather forecasting such a challenge (Lorenc, 1986). The deterministic characteristic of climate is fundamentally different from that of a chaotic system, where understanding the current state of the system allows accurate prediction of past or future system conditions. It is with the predictable nature of climate that the

distribution of plants and animals, influences on the presence of cryospheric elements, and soil formation can be understood throughout history and into the future (Jenny, 1994; Hock, 2003; Gottfried et al., 2012).

Of the seven elements of climate (Ross, 2017), temperature is perhaps the most evident to the average person. Average near-surface air temperature plays a crucial role in the distribution of elements present within all the earth's spheres. Although the nature of this element is well known, both modelling and observation have shown that current temperature distribution patterns and behaviour have begun to change (IPCC, 2014; SWIPA, 2017). Understanding these changes and their effect onto both weather and climate is a significant focus for humanity today. The Meteorological Service of Canada began observing weather in 1871, which has since become incorporated into Environment Canada and has been providing progressively accurate short-term weather predictions as well as climate records and interpolations. Although this record and history of observation represent an impressive accomplishment, an essential aspect of any monitoring program is the distribution of monitoring sites (Way & Bonnaventure, 2015). Even today, climate stations show location bias, being concentrated in regions of economic importance and transportation hubs which are easily accessed and in proximity to human population centres (Stahl et al., 2006) which generally occur in locations of lower elevation (**Figure 1**). Because of this bias, our fundamental understanding of the geographical and seasonal variability of weather and climate in northern and mountain environments is relatively poor in comparison to lowland and urban locations (Stahl et al., 2006). Some of this has been addressed with the use of satellite-derived data, especially in

uniform polar areas (Cowtan & Way, 2014) as well as through statistically downscaled data derived from global circulation models (Wood et al., 2019), but these methods are arguably less effective in modelling fine-resolution air temperature in areas of complex topography (Prömmel et al., 2010) and still require validation. Not only are these locations predicted to respond sensitively to change and may potentially change in an asymmetric manner, they are also vastly under-represented in sampling (Stahl et al., 2006; Pepin et al., 2015) (**Figure 1**). Because of the systematic under-sampling of the total elevation range present within these regions, models tend to break down regarding prediction accuracy (Bradley et al., 2004; Stahl et al., 2006). Due to the lack of knowledge regarding climate within mountainous regions, there is a resulting lack of understanding of how these systems will change in response to climate change (Bradley et al., 2004). Most networks of climate stations directly avoid high-elevation locations and other hard to access sites (Pepin et al., 2015). As a result, it is imperative to establish a baseline of the climates in these complex and heterogeneous environments.

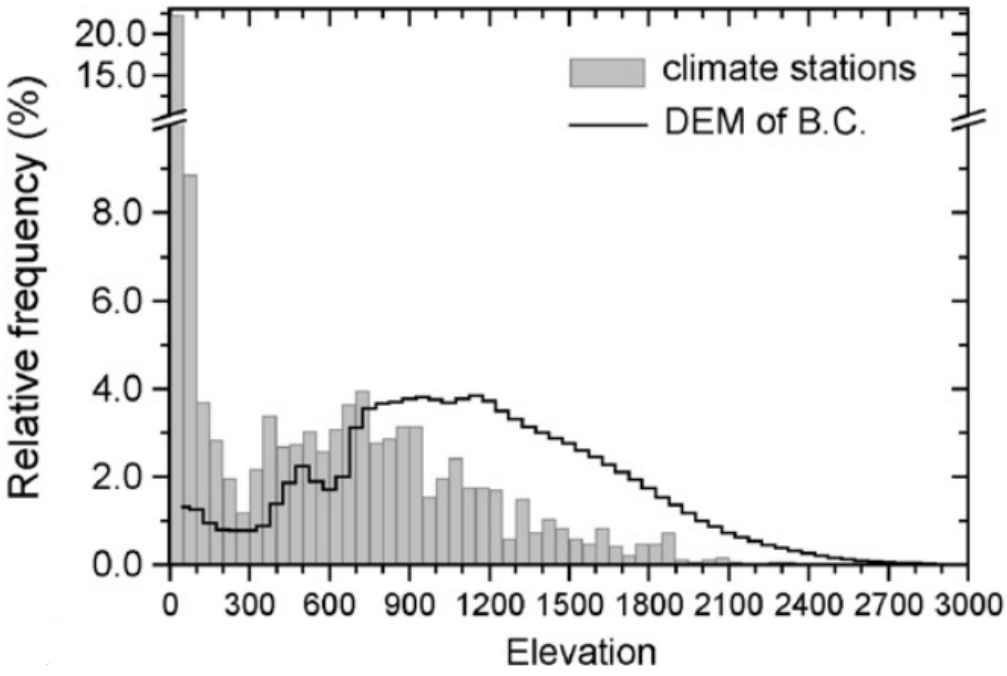

Figure 1: The distribution of climate stations within the province of British Columbia compared with the hypsometry of the province (Stahl et al., 2006).

3.2 Climate Change

3.2.1 Global Overview

Since Arrhenius (1896) determined that an increase in CO_2 concentration within our atmosphere would consequently increase temperature, the body of knowledge of the changing climate has grown (IPCC, 2014). Climate change can be understood as the shifting of states of the climate system which is usually observed through the change in the means and trends over multiple decades or longer (IPCC, 2014). The climate of the planet changes naturally on Earth for three main reasons, called fundamental forcings, one of which is the range of astronomical cycles proposed by Milankovitch in 1941 (Hays et al., 1976). These cycles are a result of the relationship between the position and

orientation of the Earth and the sun, having an impact on the amount of solar energy received by the planet (5 %). Secondly, the distribution of land surface on the planet, which changes over time due to tectonic forces, and through a variety of pathways, including changes to global circulation patterns of the atmosphere and ocean, influences climate (Raymo & Ruddiman, 1992). Finally, the natural variation of solar output, which varies over long periods, results in changes to the energy received at Earth's surface (Friis-Christensen & Lassen, 1991). Further, there are natural variations in the presence of atmospheric carbon and aerosols which have been shown to mirror trends in climate and atmospheric temperature throughout the millennia (Petit et al., 1999). Evidence for the link between the fluctuations in atmospheric carbon and climate are shown in ice cores retrieved from research sites on current ice sheets like Dome C and Vostok, in Antarctica (Lorius et al., 1979; Jouzel et al., 1987; IPCC, 2014). In contrast to the natural changes that occur slowly over time, anthropogenic or human forcings, are rapidly transforming climate (Charlson et al., 1992).

The IPCC provided their 5th Assessment Report in 2014 on the current knowledge base surrounding climate change. The IPCC (2014) identified human influence as the most likely dominant influence on the climate state since the mid-20th century. Further to this, the impact of shifting climates has been observed in increases to global average surface temperatures, both terrestrial and oceanic, on the magnitude of 0.85 °C between 1880 and 2012 (IPCC, 2014). Though the value is averaged across the planet Earth, it illustrates a changing trend that may have long-reaching impacts.

3.3 Asymmetric Climate Change

3.3.1 Seasonal Asymmetry

As climate changes, evidence suggests that the globe is not warming seasonally symmetrically. Analysis of a spatially interpolated temperature record for Canada has shown that there is a significant bifurcation in trends of change between the winter months and the remainder of the year within Alberta **(**Kienzle**,** 2017). The warming trend occurs disproportionately in winter months (**Figure 2**). This evidence of asymmetric change is mirrored in future projections of the CMIP5 global climate model where warming during the winter months is expected to continue through the 2016-2035 period of time (Diffenbaugh & Giorgi, 2012; IPCC, 2014).

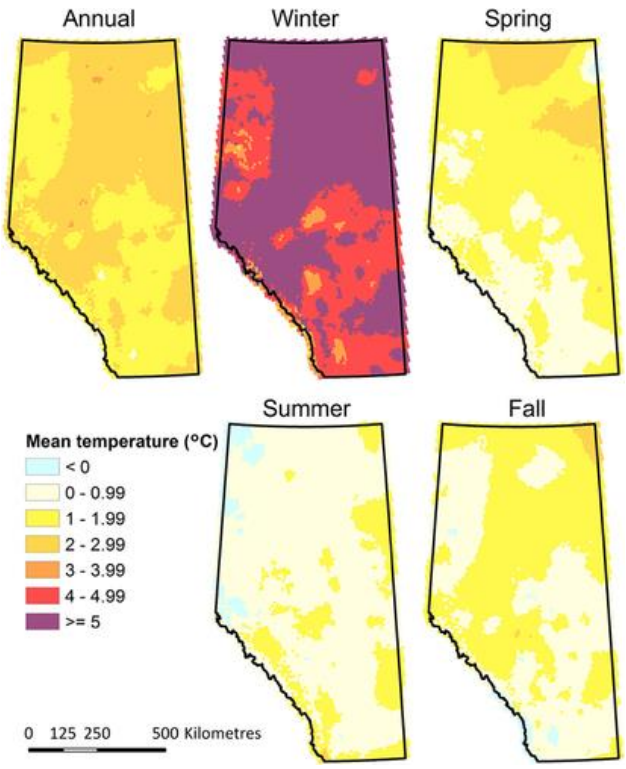

Figure 2: The annual and seasonal change in air temperature occurring across the province of Alberta from 1950-2010 (Kienzle, 2017).

With the growing difference in warming between seasons, potential forcings upon seasonal phenomena such as Arctic sea ice, and snow cover could become more prevalent throughout the years (Deser et al., 2010). It was found that responses in surface air temperature over continents within the northern hemisphere, specifically northern Canada during the winter months of November-December, related to loss of Arctic sea ice, during the future period of 2080-2099, which could result in warming of ~7 ˚C (Deser et al., 2010). The seasonality of sea ice lends itself to the seasonal bias of change with its reduction. A study by Singarayer et al. (2006) found that as sea ice extent is projected to be reduced, surface air temperature, as a result, will rise. This is supported by the earlier

findings of Alexander et al. (2004) showing linear relationships between air temperature and sea ice concentration.

3.3.2 Arctic Amplification

It is widely accepted that Polar Regions are currently warming more rapidly and to a greater degree than the rest of the world, a phenomenon termed Arctic amplification (Serreze & Barry, 2011; Cohen et al., 2014; IPCC, 2014). It has been reported (SWIPA, 2017) that within the Arctic, snow cover, as well as sea ice cover play an instrumental role in the control of climate (Deser et al., 2010). In association with the climatological controls of this, small shifts of warmer temperature impact the spatial and temporal extent of these features and as a result, allow for further warming due to the lowered albedo of the surfaces. The process of Arctic amplification is recognized as a characteristic of the global climate system, and future changes within the Arctic may cause changes to global atmospheric circulation patterns (Serreze & Barry, 2011). As there are similarities between Arctic regions and mountainous terrain, including cryospheric elements, it has been hypothesized that mountains will also be impacted by climate warming asymmetrically and in a more complex manner than adjacent lowland terrain (Giorgi et al., 1997; Pepin et al., 2015).

3.3.3 Elevation Dependent Warming

The unique nature of mountain ranges illustrates the need for and importance of understanding the impacts and changes that will occur in these locations. A recent review (Pepin et al., 2015) on mountain climatological research provided an overview of the

conceptual possibilities and feedbacks that could be seen as a result of climate warming. This review suggests that mountain environments like Arctic environments will also show amplified warming trends. Due to the nature of elements within mountain systems, especially the cryospheric components (e.g. annual snow cover and glaciers), positive feedback loops promoting continued warming are expected to occur (Giorgi et al., 1997; Fyfe & Flato, 1999; Pepin & Lundquist, 2008). Conceptually this is apparent, as a small shift to warmer temperatures will, in turn, reduce snow cover extent, changing albedo, and allow for further heating of the surface (Fyfe & Flato, 1999; Hernández-Henríquez et al., 2015; SWIPA, 2017). Although this is conceptually well understood, quantifying this is still a considerable challenge. Additionally, the impact of a change in albedo, is expected to impact cloud cover dynamics, aerosol concentrations, and relative humidity with substantial impacts expected in the radiative fluxes of the energy balance by raising the altitude of the Lifting Condensation Level (LCL) (**Figure 3**). This is potentially very significant because it means that the release of latent heat at the LCL site will coincide with higher elevations (Held & Soden, 2006). Further to this, the addition of black carbon and particles transferred through the atmosphere and settling on snow in high-elevation regions modifies the albedo regime and alters the radiation budget (Painter et al., 2007; Xu et al., 2009).

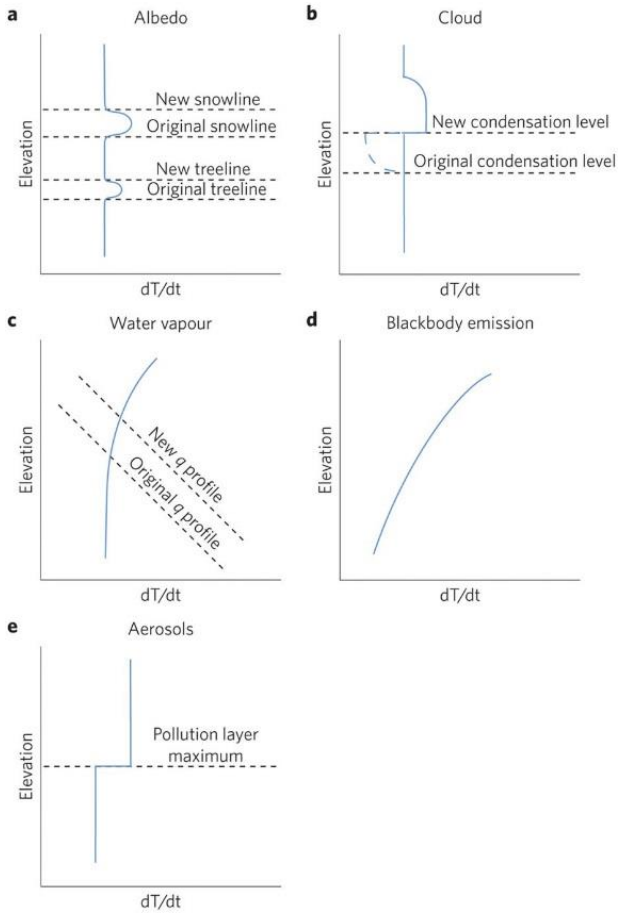

Figure 3: Conceptual changes in various processes with elevation and the change in air temperature over time (Pepin et al., 2015).

The combination of all of these influences implies that the nature of warming in mountain environments is complex and will manifest itself differently than in lowland environments. This is also likely significant for other elements of climate as mountains significantly influence the distribution of precipitation (Daly et al., 1994) and thus modify the timing and amount of discharge as a result of snowpack dynamics and precipitation (Adam et al., 2009). This can be an important mechanism for the water balance and water security of mountains and downstream regions that depend on mountain watersheds for their water needs (Kienzle et al., 2012). Understanding how climate change will impact

precipitation, and water storage within mountain watersheds will be an important tool for natural resource managers and policymakers. Pepin et al. (2015) highlight the lack of long-term monitoring stations in high-elevation locations and draws a contrast between Arctic and mountainous regions by highlighting the relative homogenous nature of the former in comparison to the extreme local variability of the latter. As a result, the understanding of change within these systems is limited, not only due to the bias of sampling but the heterogeneity implicit within montane locales.

3.4 Physical Processes of Air Temperature

The temperature of the parcel of air within the boundary layer is controlled by several processes and at its base is the partitioning and movement of energy within the system (Oke, 1987). The net radiation (Q*) budget is considered crucial to the understanding of Earth-Atmosphere system at the Earth's surface. The surface energy budget can be conceptualized as an equation:

$$\text{Equation 1:} \quad Q^* = K\downarrow - K\uparrow + L\downarrow - L\uparrow$$

where Equation 1 represents the daytime budget including incoming and outgoing shortwave radiation (K↓ and K↑), as well as the influence of incoming and outgoing longwave radiation (L↓ and L↑). Incoming shortwave radiation includes direct and diffuse components, direct being the porting transmitted by the atmosphere and diffuse being the portion refracted and reflected by the atmosphere and other surfaces. Outgoing shortwave radiation is the component of shortwave radiation incident upon a surface that is reflected by the albedo, which is the characteristic of the surface controlling the absorption and

reflection of the electromagnetic energy. Longwave radiation is the component of the radiation budget controlled by the absorption and re-radiation of electromagnetic energy by the Earth, atmosphere, and objects on the surface. The nighttime energy balance does not include shortwave solar radiation as a components as there is no incident shortwave radiation (Oke, 1987).

Energy distribution and movement can be summarized by three processes: Radiation, convection, and conduction. All objects radiate electromagnetic energy, defined by Planck's Law, and thus lose and transfer energy radiating outwards from the object. Convection is the process through which the exchange of air masses and liquids cause energy to be moved from one location to another and can occur due to the properties of the media, or due to mechanical forces such as wind. Conduction is the transmission of energy as a result of collision of molecules in close proximity and thus occur best in solids, and less so in liquid and gasses.

The energy budget accounts for the radiative forcings at the surface, but the discrepancies seen in the balancing of the budget can be explained through the movement of energy in the form of non-radiative fluxes: sensible heat flux, latent heat flux, and soil heat flux. The summation of these various fluxes is equal to that of Q*:

$$\textit{Equation 2:} \quad Q^* = H + E + G$$

where H is sensible heat flux, E is latent heat flux, and G is soil heat flux. Latent heat flux is the movement of energy as it is absorbed and released by water associated with the process of phase change. When water condenses it releases 540 calories/gram to the surrounding environment whereas when it evaporates the same amount of energy is absorbed from the surrounding environment and facilitates a phase change from liquid to

gas. Soil heat flux is the movement of energy within the soil profile controlled by the thermal properties of the soil: thermal conductivity, heat capacity, thermal diffusivity, and thermal admittance. Soil heat flux notably has a pattern by which heat is conducted into the ground during the day, and out at night. Sensible heat flux is the change in temperature of an object or air parcel as a result of the movement of energy between media. This process is not associated with phase change.

While collecting the suite of data involved in surface energy balance is difficult as a result of the cost of instrumentation and the necessary distribution of sampling location within mountainous regions, modelling climate can be done through complementary or stand-alone processes.

3.5 Modelling Climate

Conventionally, near-surface air temperature is estimated through the use of lapse rates based upon the proven and significant relationship between elevation and temperature. Free-air lapse rates can differ significantly from SLRs. SLRs are changes in temperature with elevation rather and altitude, and as such, once an SLR is established for a time period or region, it can be applied to adjacent elevation points.

3.5.1 Small Scale, Broad Coverage

Top-down modelling is the process through which a complex system is broken down systematically into sub-systems (Young, 2003). These sub-systems are then defined

or further broken down to identify base relationships between variables or statistical downscaling techniques are developed, and in association with computer processing, these models can be slowly formed and altered to produce high-quality outputs (Praskievicz, 2018). Top-down modelling takes large observable trends and through a variety of statistical procedures applies transformations to the data as the scale is increased. Some climatological examples of this approach are the PRISM model (Daly et al., 1994), the ANUSPLIN software (Hutchinson et al., 2009), and ClimateNA/WNA (Wang et al., 2012; Wang et al., 2016).

3.5.1.1 PRISM

Parameter-elevation Regressions on Independent Slopes Model (PRISM) is an example of a top-down regression model that performs expert climatological analysis to produce geospatial surfaces. Ground-breaking in its field, PRISM, created by Chris Daly, used data collected between 1961 and 1990 to allow the computer to develop a local statistical relationship for each pixel (Daly et al., 1994). This modelling process was subject to scrutiny by experts in the field of climatology and was determined to produce justifiable results (Daly et al., 2002). As a result of this work, a map and associated spatial data for climatological representations of temperature and precipitation for the contiguous United States was developed at a gridded resolution of 800 m (Daly & Bryant, 2013). After successfully modelling precipitation, Daly focused the model to other climatological factors such as temperature. Since then, the model has been applied to many geographical regions including Canada, Europe, China, and South East Asia (Daly & Bryant, 2013). The process through which this model operates is as follows: estimated

values for daily, monthly, and annual climate parameters are interpolated using point data from a network of weather stations in association with a digital elevation model (DEM) and a computer algorithm. The algorithm weighs and transforms the values of the input point data based on a multitude of well understood geographical climatological controls or sub-systems. Specifically, for PRISM, these include the effect of proximity to coastal areas, the influence of elevation on climate, how effectively terrain produces an orographic impact, as well as the influence of aspect and exposure on climate. The data from this modelling method demonstrate the effects of each of these climatological controls.

3.5.1.2 Canada-Wide Climate Datasets

Through the work of Hutchinson et al. (2009), a model of daily precipitation, and minimum and maximum temperatures for the whole of Canada was derived using a trivariate thin-plate spline interpolation technique using the software ANUSPLIN. This software employs a non-parametric, multi-dimensional curve fitting technique for noisy multi-variate data useful for mapping and analyzing climate. Hutchinson et al. (2009) created, through this process, a gridded climate dataset at a resolution of 300 arc-seconds (~10 km × 10 km). The interpolation applied to the climate data correlated the input data as functions of elevation, longitude, and latitude. The method integrated the adaption to varying station density as well as spatially varying dependence to elevation throughout Canada (Hutchinson et al., 2009). This work excels in creating an essential resource for many industries and research specialists as in many cases the need for the identification of extreme daily temperature values is of greater importance than the muted monthly

averages. The initial work focused on the period of 1961-2003, though Natural Resources Canada has stated that data have been developed for the period of 1950-2010 and this will be updated as new data becomes available (NRCAN, 2019). The utility of this model is continuously subject to improvement, shown through the alignment of data to the climatological day redefined in 1961 to 0600 UTC within Canada (Hopkinson et al., 2011). This model provides researchers, managers, and policymakers with data that covers a wide spatial footprint and a with strong basis for further inquiry.

3.5.1.3 Alberta Climate Records

Work produced by Kienzle (2017) follows closely with Hutchinson et al. (2009). This research builds on the previous work and provides 30 temperature indices for the same grid created by Hutchinson et al. (2009). In the reanalysis of the data, Kienzle (2017) found that within Alberta between 1950 and 2010, annual temperatures increased by 2 -5 °C in northern portions of the province whereas between 1 °C and 2 °C of warming was observed annually across the southern portion of the province. To simplify and aggregate the massive amount of results of this study, a trend analysis was done for the 18 ecoregions present across Alberta. As ecoregions are manifestations of the intimate relationship between climate and vegetation, this is a logical delineation of spatial trends. Kienzle (2017) makes a note of the issues presented by the complex terrain of the Rocky Mountains. Comparison of the average elevation of the 10 km by 10 km grid and an available 1 arc second, or approximately 30 m DEM, highlighted as much as 150 m of variation (Kienzle, 2017). This variation will result in over- and underestimated temperature indices for mountain regions where elevation and is a major determination in

temperature at a location. This issue is compounded with the current infrastructure distribution (**Figure 4**) within mountainous ecoregions of the province, as there is a low density of stations in Albertan mountains (Kienzle (2017), and stations are concentrated in low elevation locations, a trend similarly observed throughout the entire province of British Columbia (**Figure 1**) (Stahl et al., 2006).

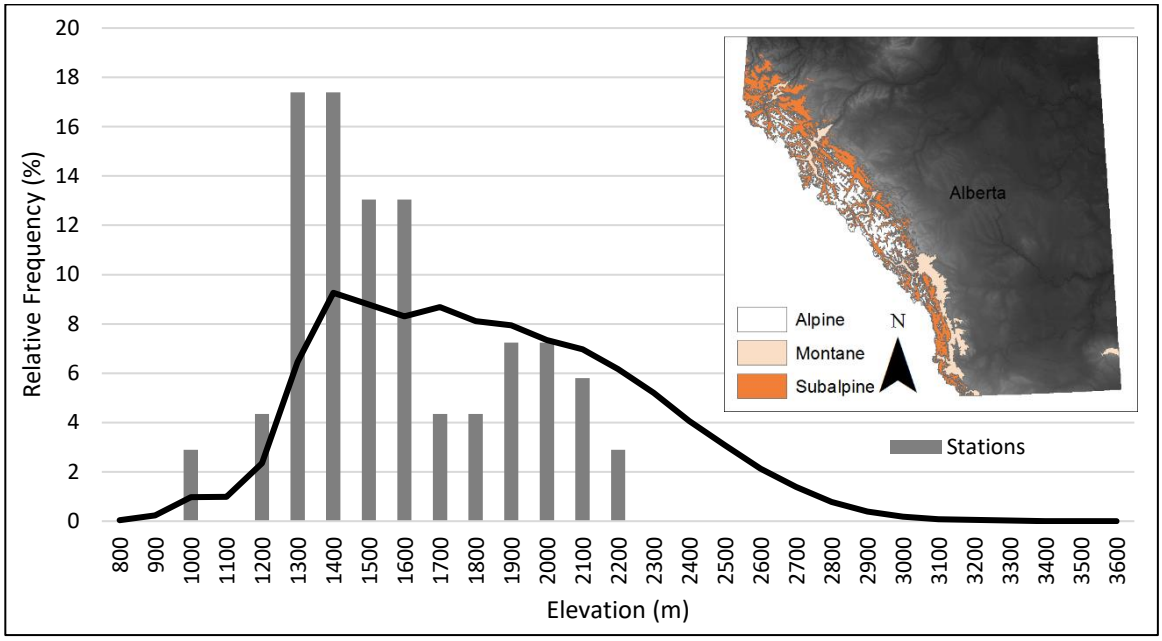

Figure 4: Distribution of 69 government meteorological stations within Alberta's Alpine, Sub-Alpine, and Montane ecoregions in comparison to the elevation distribution within the same spatial extent, the inset highlighting these ecoregions within Alberta.

3.5.2 Large Scale, Narrow Coverage

Bottom-up modelling is a process by which specific elements are studied and modelled and can be used in congruence with other models for the greater understanding of the system as a whole. This process is exemplified by the construction of independent

arrays of monitoring sites from which relationships between various influencing factors can be analyzed with the collected information and then spatially interpolated and modelled. In contrast to small scale models and broad networks, smaller, spatially-constrained networks of stations can allow an increase in resolution, provide higher accuracy in complex terrain, and reduce the errors seen as a result of variable station density.

3.5.2.1 Calgary Foothills Climate Array

A mesoscale observation network called the Calgary Foothills Climate Array (FCA) was installed in 2004, to monitor regional temperature, humidity, and precipitation covering the mountainous terrain, foothills, and prairie region near Calgary, Alberta (Cullen & Marshall, 2011; Wood et al., 2019).. The network was established in such a manner to produce a system of uniform spacing and density within the varying terrain. Cullen and Marshall (2011) sought to explain the influence of synoptic weather systems on regional temperature values. A multivariate regression model was used to account for the influence of elevation, aspect, slope, and surface cover on derived monthly mean temperatures (Cullen & Marshall, 2011). A unique aspect of this work was the relevance of the shifting synoptic weather patterns which include the distinctive Chinook experienced in Southern Alberta.

4.0 Study Area

4.1 The Castle

The study area for this research is the West Castle Watershed (WCW) located on the East slopes of the Southern Canadian Rocky Mountains within Alberta (**Figure 5**). The WCW covers 375.5 km^2 and is comprised of mountainous terrain ranging in elevation from the outlet of the watershed at 1332.5 m to the highest peak (Mount Haig) at 2632 m above sea level (ASL) consisting of variable land cover from montane communities to alpine communities. The dominant land cover present within this watershed is that of coniferous forest communities consisting predominantly of Lodgepole Pine (*Pinus contorta*) White Spruce (*Picea glauca*), Engelmann Spruce (*Picea engelmannii*), and Douglas Fir (*Pseudotsuga menziesii*). The region is also host to a variety of rare and endangered vegetative species including Limber Pine (*Pinus flexilis*) and Whitebark Pine (*Pinus albicalus*) both considered to endangered provincially while Whitebark Pine is also federally endangered (AEP, 2018). The main watercourses within the watershed are the Castle River and the West Castle River. The landscape has a history of anthropogenic use including extensive clear cut logging, petroleum exploration, and recreational uses such as off-highway vehicle use and other outdoor activities. As well as these landscape uses, there is currently an operational alpine ski resort (Castle Mountain Resort, 49°19′6.9″ N 114°24′52.1″ W) located within the WCW. The area encompassed by the WCW as well as the surrounding area was re-designated by the Provincial Government on February 16th, 2017 as Castle Provincial Park and Castle Wildland Provincial Park with the majority of this study area falling within the Castle Wildland Provincial Park. The study area was chosen as it represents a mountainous landscape,

heterogeneous (**Figure 6**) in nature, in both topography and land cover. This area also has the benefit of logistical support due to the presence of the University of Lethbridge Field Station.

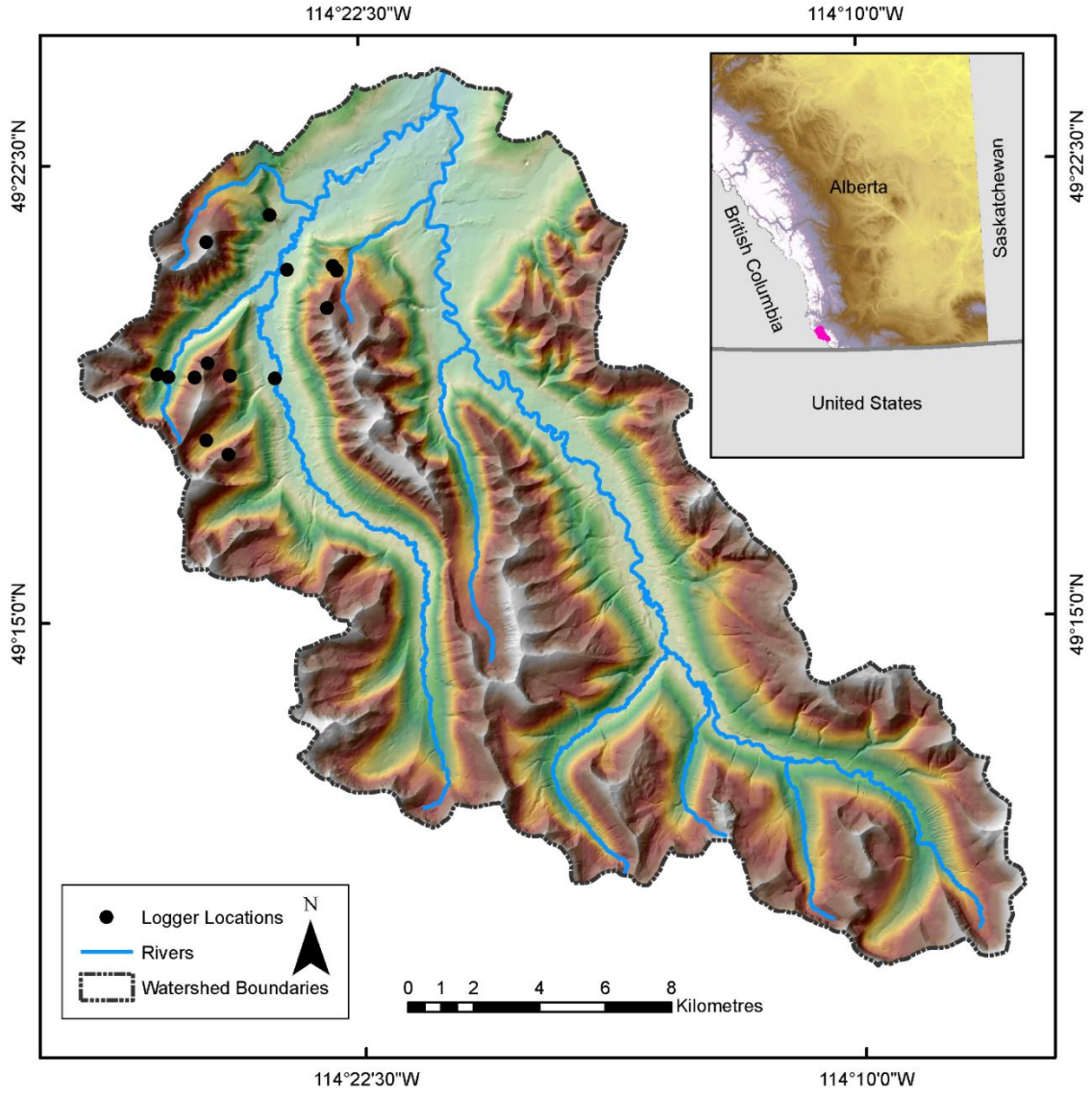

Figure 5: Map of study area watershed which covers 375 km^2 of land including logger locations.

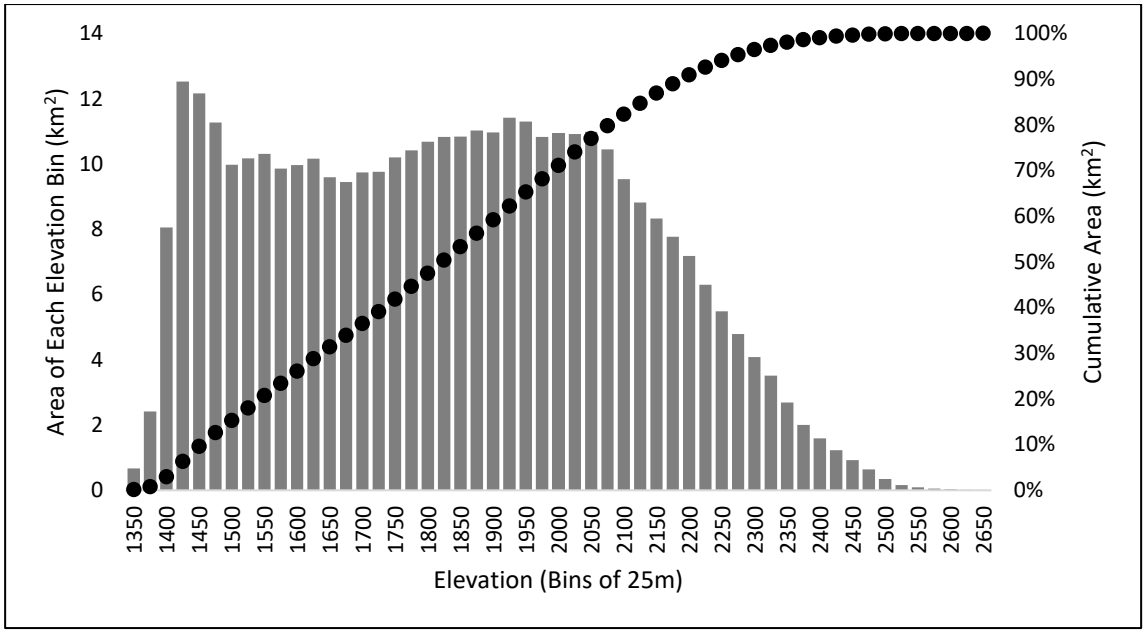

Figure 6: Hypsometry of the WCW, each bin representing a 25 m elevation band and the points representing the percent of total area noting that 50 % of the watershed is above or below the 1825 m bin.

The WCW is a snow dominant, fully humid, and extremely continental climate according to its Koppen-Geiger classification. The extreme continentality of the location, as well as the influence of the westerlies and topography, make this location unique compared to other locations in the Canadian Rockies. Mean annual precipitation (1981-2010) is 679.8 mm in Beaver Mines (1257 m), the nearest Environment Canada Station located 14 km from the study site (Environment Canada, 2018). Three Alberta meteorological stations exist close to the study area named Gardner Headwaters, Castle Auto, and West Castle (**Figure 7**). The region experiences intense chinooks, bringing extreme wind speeds as well as unseasonably warm temperatures. In addition to the chinooks, small-scale weather events such as inversions often occur within mountainous regions. The influence of topography on the fluidity of the atmosphere causes dense,

cooler parcels of air to drain and pool within the U-shaped valleys that occur in the WCW.

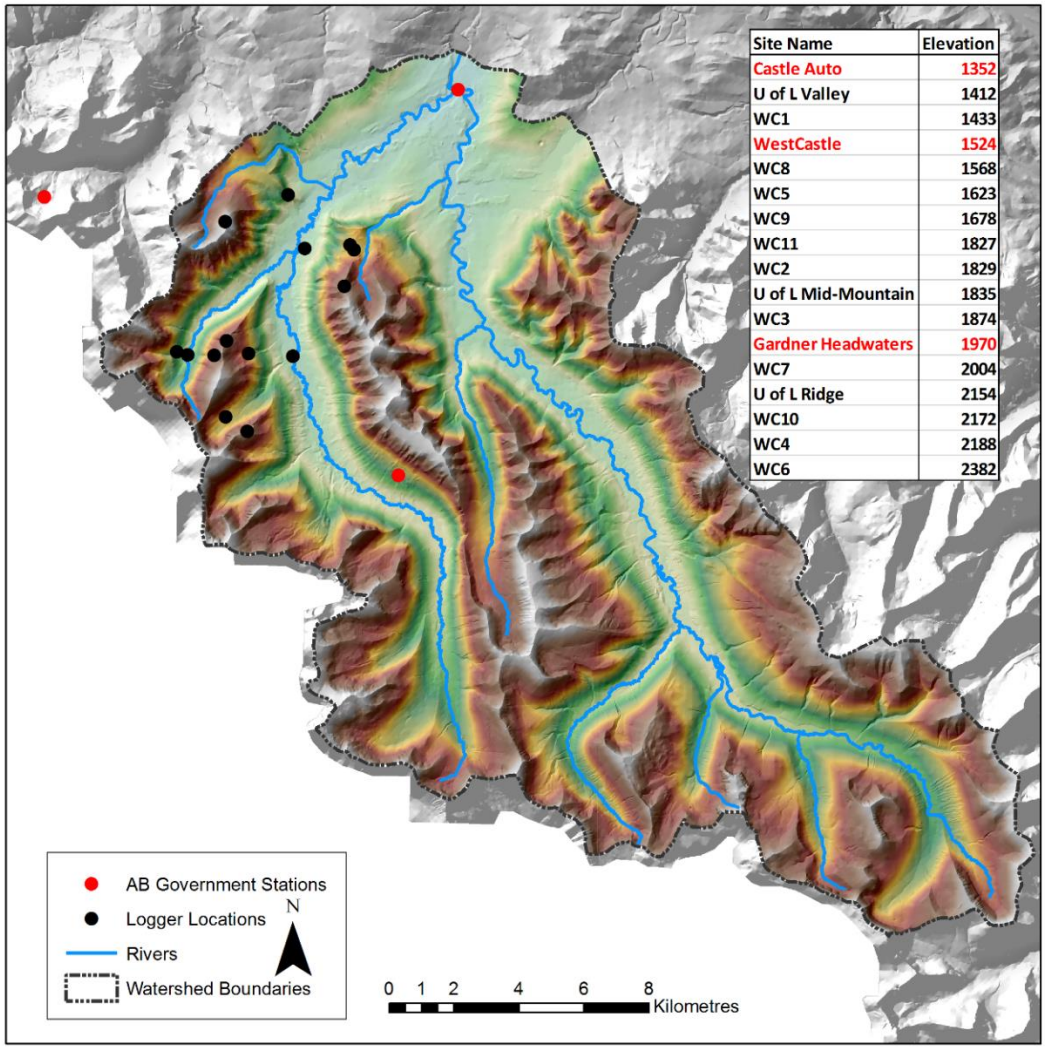

Figure 7: Location of the nearest Alberta Government Meteorological Stations (red) and their associated elevation in comparison to stations implemented for this research (black).

4.2 Regional Context

The Castle watershed is a part of the Crown of the Continent region known for its high biodiversity and a large number of endemic species relative to other temperature continental regions (Hauer et al., 2007). It sits on the leeward side of the Continental divide and is part of the Clark Range of the Rocky Mountains, a subdivision of the Border Ranges. This area lays between the broader Cordilleran region of British Columbia to the west and the great plains to the east and provides a unique opportunity to study a transitional region of geography, ecology, and climate.

4.3 The Current Understanding of Climate in Castle Watershed

The current climate of Southern Alberta can be representative of a continental climate (Cullen & Marshall, 2011; Anderson, 2014). More specifically, the Southern Alberta region is dominated by two major weather systems, the westerlies that blow over and through the mountains, and continental air masses, which are influenced by the position of the polar jet stream and the air masses brought by the prevailing westerlies to the area are maritime and continental polar respectively, and as such these two systems vary greatly in their impact on local climate (Cullen & Marshall, 2011). In regard to precipitation regimes for the Castle Watershed, moisture originating from the Pacific Ocean is deposited during winter months at high rates across the Cordillera and immediately on the leeward side of the Rocky Mountain range, trailing off into a rain shadow on the prairies (Reinelt, 1970; Al-Rawas & Valeo, 2009). With respect to the Castle Watershed, it was determined that precipitation that falls within the Castle Watershed contributes 14.9 % of the total volume of streamflow within the broader Oldman Watershed (Kienzle & Mueller, 2013).

Within the broad region of low relief terrain in Alberta, the temperature is mainly influenced by latitude and decreases south to north, while in the mountainous regions, this gradient is complicated by the influence of elevation (Schneider, 2013). Specifically, for the Castle Watershed, temperature ranges throughout the year from the extremes of 35 °C in the summer to -35 °C in the winter (Anderson, 2014). Generally, the temperature is assumed to change in relation to elevation at a uniform or constant rate (Minder et al., 2010). A typical SLR used in climatic modelling is -6.5 °C km^{-1} and given the broad application of this SLR to climatic modelling, it is generally not clear if the use of this standard SLR is appropriate for temperature field generation (Cullen & Marshall, 2011). In the Castle Watershed, Pigeon and Jiskoot (2008) conducted an in-depth study of SLR at Castle Mountain Ski Resort within the watershed. They determined the pooling of cold air masses has an impact on average lapse rates for the region and as such, they worked to separate inverted SLR from normal SLR to better represent and model temperature in the area over time. Another study elucidated the seasonal and diurnal variations in SLR in complex terrain and the impacts for hydrological modelling (Minder et al., 2010). The concept and derivation of SLR representative of local and regional factors are essential to understanding the spatial extent of isotherms throughout complex terrain (Rolland, 2003; Mattie, 2009; Minder et al., 2010).

4.4 Historical Evidence for a Changing Climate in Alberta

Elements of the cryosphere, such as permafrost and glaciers, are fundamentally associated with climate and therefore can be used as proxies for the general understanding

of historical climates. The extent and influence of glaciation have been recorded and observed through various means; including the use and interpretation of volcanic tephra, pollen, cosmogenic dating, vertebrate fossils, and glacially deposited earth materials (Bobrowsky & Rutter, 1992; Jackson et al., 1997; Dyke et al., 2002). During the Wisconsin glaciation, glaciers flowed out of the large catchment basin of the Castle Watershed and formed piedmont glaciers on the plains and foothills (Stalker, 1969). Specifically, in the Waterton-Castle region, a composite stratigraphic column was compiled by Stalker and Harrison (1977) as cited in Bobrowsky and Rutter (1992).

In association with historical glacial extent evidence, glacial ice cores identifying the global trends in climate and the localized historical changes in the extent of glacial ice sheets, dendrology can be utilized to interpret regional historical climate. Research conducted by Luckman and Wilson (2005) sought the use of tree-ring analogs to interpret recent historical climate accurately. Their work was able to reconstruct the summer temperature for the time period between 950 – 1994 (Luckman & Wilson, 2005). The findings from this work identified historical periods comparable to the current climate while concluding that the period of greatest warming trend was identified from the mid-1800s onward (Luckman & Wilson, 2005).

5.0 Methods

Methods for this research project consisted of a combination of field work, including the creation of a climatic sensor network and data collection, as well as data analysis, interpretation, air temperature modelling, and perturbing current air temperature models for future IPCC scenarios.

5.1 Data Collection and Field Methodology

Deploying sensors that capture the heterogeneity of the landscape was crucial and a distributed network needed to be established (**Figure 9**). Sites were chosen to represent landscape units present within the study area including valley bottoms, mid slopes, upper slopes, and mountain tops (**Table 1**). To accomplish this, elevational transects were placed leading up mountain slopes through the forested landscape to mountain peaks, as well as across topographically constrained valleys (**Figure 8**). Further, topographic position index (TPI), elevation, aspect, potential incoming solar radiation (PISR) and land cover were considered in the selection and placement of sites. TPI is a relative measure of topographic prominence or topographic protection where the average of a defined neighbourhood of cells is looked at in comparison to the cell of note to identify if it is above or below the average of the neighbourhood (Jenness, 2006). A high TPI value represents a cell that is prominent on the landscape and has a value > 0, a TPI value of 0 is a perfectly flat region or a region of uniform change, and a value < 0 is in a depression or hollow in contrast to the surrounding terrain. These metrics were selected as criteria to give insight into the temperature variation observed within the landscape, topographically

but also biologically (e.g. above and below treeline) (**Figure 9**). As site selection was made in a GIS environment, real-world conditions varied slightly, and thus not all sites were able to be placed in the exact position planned within the software.

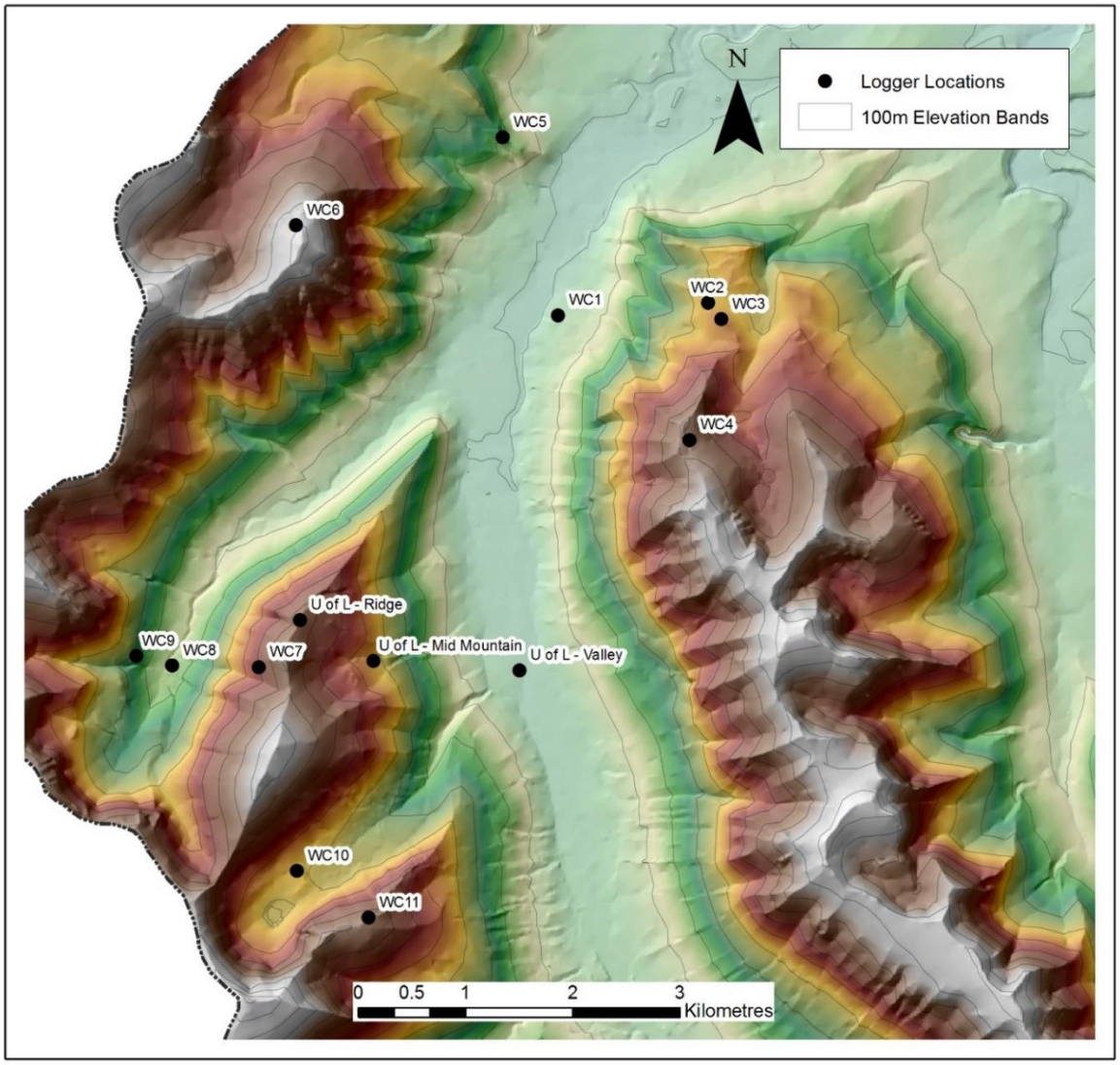

Figure 8: The distribution of research sites across the WCW, WC6 is the highest site in the network with an elevation of 2382 m. ASL, the lowest being U of L – Valley at 1412 m ASL.

Table 1: Topographic variables and position in relation to treeline of each of the stations collecting temperature information.

Site	Elevation	Slope	TPI	Aspect		Treeline
WC1	1433.0	13.3	-6.7	304.5	(West)	Below
WC2	1829.2	11.3	30.3	10.2	(North)	Below
WC3	1874.3	24.4	46.9	27.2	(North)	Above
WC4	2187.5	16.4	115.5	77.1	(East)	Above
WC5	1623.5	26.3	62.8	99.8	(South)	Above
WC6	2381.7	27.8	168.1	303.0	(West)	Above
WC7	2003.8	36.8	13.8	260.3	(West)	Above
WC8	1567.9	9.8	-86.5	304.8	(West)	Below
WC9	1678.4	31.9	-25.3	113.0	(East)	Below
WC10	1826.9	5.1	-56.9	143.4	(South)	Below
WC11	2171.5	33.2	163.7	331.6	(North)	Above
U of L - Mid Mountain	1834.9	19.9	-17.3	101.8	(East)	Below
U of L - Ridge	2154.1	20.9	164.7	100.8	(East)	Above
U of L - Valley	1412.1	4.6	-20.6	70.7	(East)	Below

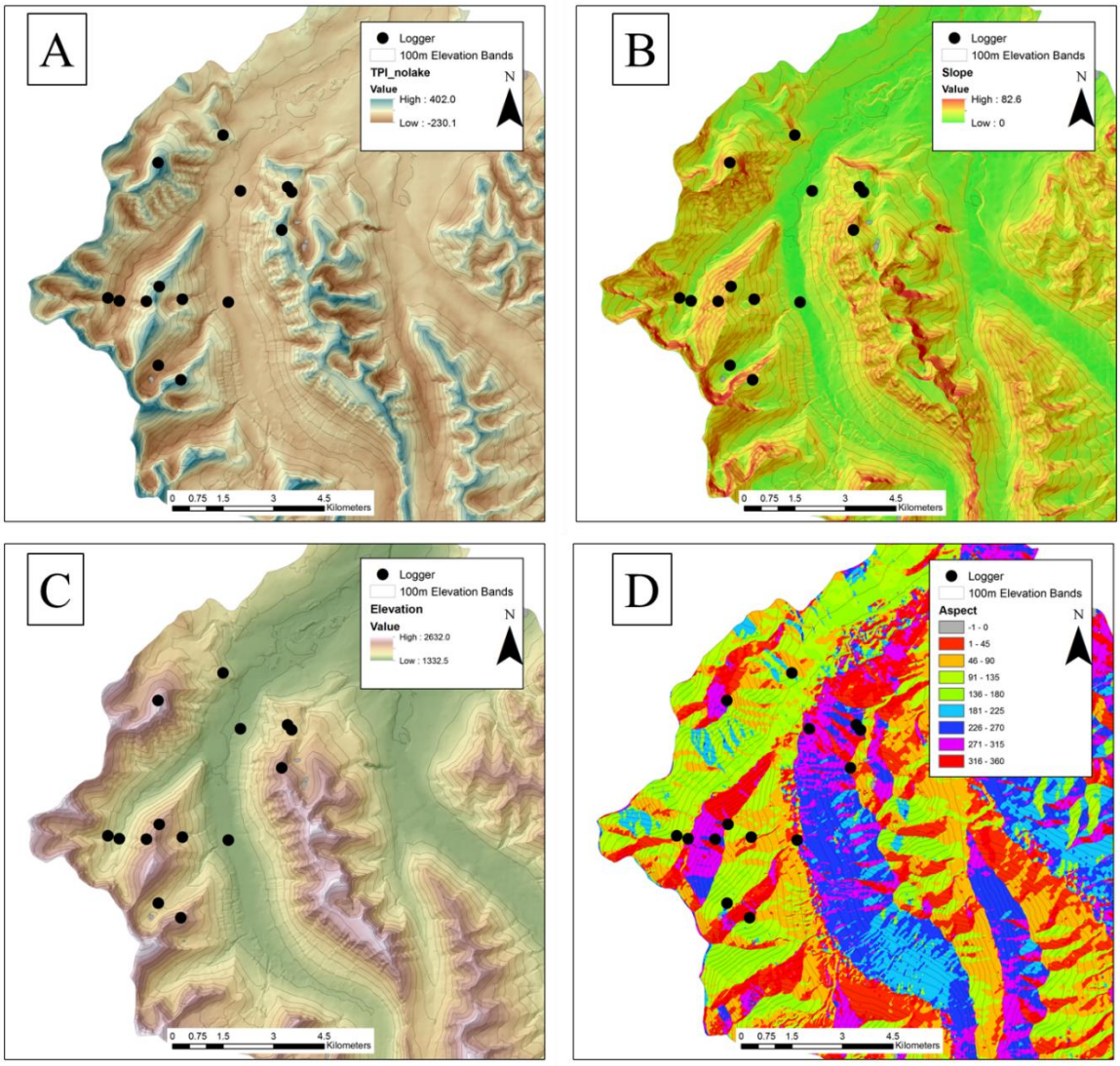

Figure 9: Geographically derived variables used to determine sensor placement. **9A** is representing TPI. **9B** is representing slope. **9C** is representing elevation. **9D** is representing aspect.

Air temperature data were collected hourly using Onset Hobo™ pendant loggers (12 in total) which were launched and deployed throughouttpi the study area, beginning in

August of 2016. This initial array of six sensors were bolstered throughout the summer months of 2017 to a total of 12 locations (**Table 2**). These sites were periodically revisited to ensure data was being collected as well as to retrieve for analysis. After many attempts to re-establish operation of the site titled West Castle Weather Station (WCWS), it was determined that the site inoperative and no data was able to be retrieved from the site during the duration of the study period. These specific logger models were chosen for several reasons including precision, accuracy, durability, functionality under extreme temperatures, as well as cost which was relatively inexpensive (~$70 each). The accuracy and resolution of these sensors, as reported by the manufacturer, is +/- 0.53°C within the range of 0° to 50°C and 0.14°C at 25°C respectively (**Figure 10**). Additionally, these loggers were tested to ensure functionality to extreme temperatures in a -80-degree Celsius freezer (Bonnaventure, *unpublished data*) with drift being considered acceptable for the site conditions.

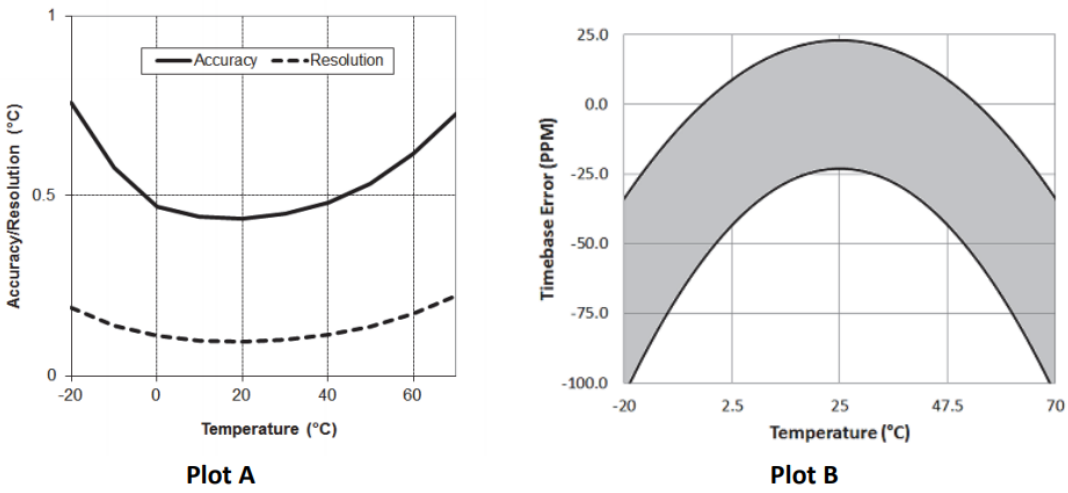

Figure 10: Accuracy, resolution, and timing error of Onset loggers.

At each site, solar radiation shields were mounted at the height of approximately 1.6 m above the ground surface on a steel post or t-bar (**Figure 11**), unless restricted by potential snowpack and infill. Loggers suspected of burial within snowpack were mounted at approximately 2.6 m above the ground surface as a direct counter-measure in order to prevent this. Fitted within solar radiation shields (Onset RS1) were loggers equipped with thermistors and at particular sites relative humidity sensors (UA-001-64, U23-001) (**Table 2**). Loggers were also placed just below the ground surface at four sites as well to collect ground surface temperature. The ground surface temperature recorded was not used in the analysis but served as a comparison for other projects unrelated to this thesis. Furthermore, two sites were outfitted with an array of vertical iButton thermistors at regular intervals above the ground for the identification of snowpack depth and timing for use in correlation with ground surface temperatures in projects unrelated to this thesis. One site was outfitted more exhaustively with additional sensors collecting data including relative humidity, wind speed, and direction, soil moisture, photosynthetic active radiation (PAR), incoming radiation and snow depth stakes for the purpose of collecting additional regional climatic information (**Table 2**).

Table 2: A reference of all equipment used in the collection of environmental data within the WCW, as well as the accuracy, resolution, and locations name where sensors are present. Information retrieved from manufacturers websites.

Manufacturer	ID	Measurement	Accuracy	Resolution	Site Name
Onset	UA-001-64	Air Temperature	+/- 0.53°C	0.14°C	WC2-11
	UA-001-64	Ground Temperature	+/- 0.53°C	0.14°C	WC1,5,11
	U23-001	Air Temperature	+/- 0.21°C	0.02°C	WC5-6
		Relative Humidity	+/- 2.5 %	0.05%	
	UA-002-64	Light Intensity	+/- 2.5 %	0.02%	WC1-4
	S-WCA-M003	Wind Speed	+/- 0.5ms^{-1}	0.19 ms^{-1}	WCWS
		Wind Gust	+/- 0.5ms^{-1}	0.19 ms^{-1}	
		Direction	+/- 5.0°	1.4°	
	S-LIA-M003	PAR	+/- 5.0 $umolm^{-2}s^{-1}$	2.5 $umolm^{-2}s^{-1}$	WCWS
	S-LIB-M003	Solar Radiation	+/- 10 Wm^{-2}	1.25 Wm^{-1}	WCWS
	S-THB-M003	Air Temperature	+/- 0.21°C	0.02°C	WCWS
		Relative Humidity	+/- 2.5 %	0.10%	
	S-TMB-M003	Ground Temperature	+/- 0.2°C	0.03°C	WCWS
	S-SMC-M003	Soil Moisture	+/- 0.031 m^3m^{-3}	0.0007 m^3m^{-3}	WCWS
Maxim Integrated	DS1921G	Temperature (Snow Depth)	+/- 0.53°C	+/- 0.53°C	WCWS, WC11

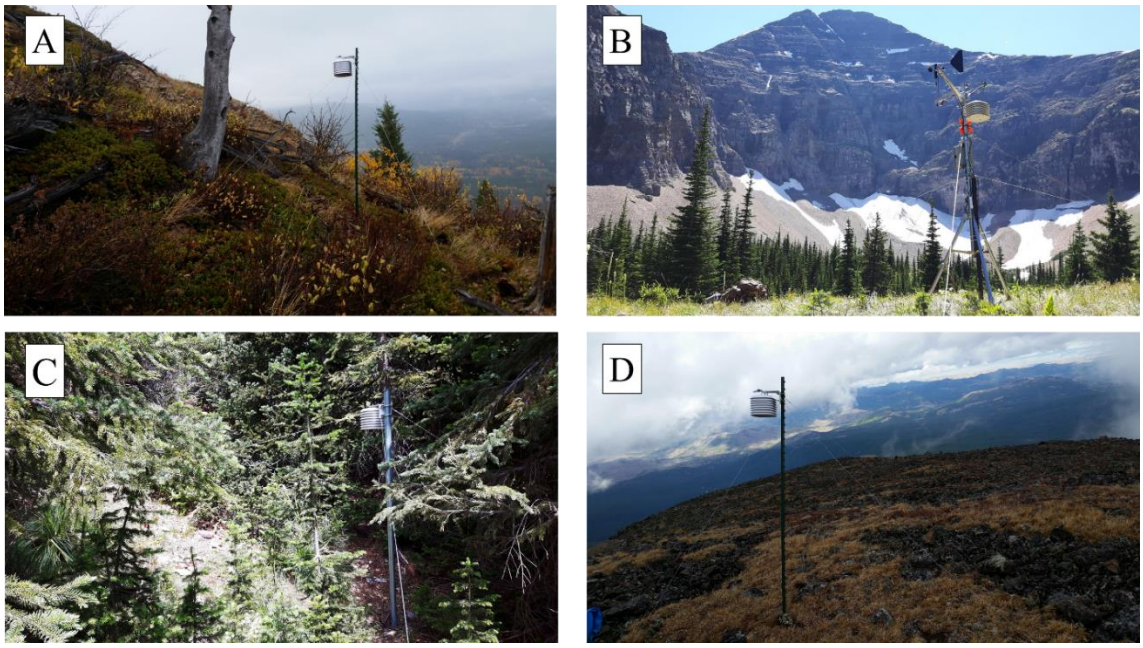

Figure 11: Examples of 4 sites within the WCW. **Figure 11A** is of WC5 and an example of a station above treeline. **11B** is of the WCWS-BB station which is outfitted with

supplemental loggers. **11C** is of WC10 and an example of a station below treeline. **11D** is WC6 and is the logger at the highest elevation within the WCW (2382m).

5.2 Data Processing and Input Variable Collection and Derivation

Data were collected during this study over the outlined time periods from a total of 11 stations (**Figure 12**). This network of stations was reinforced by the addition of three stations with a near-continuous data record for the study period from the Dr. Chris Hopkinson's ARTEMIS lab at the University of Lethbridge named U of L-Valley, U of L-Mid-mountain, and U of L-Ridge (**Figure 8**).

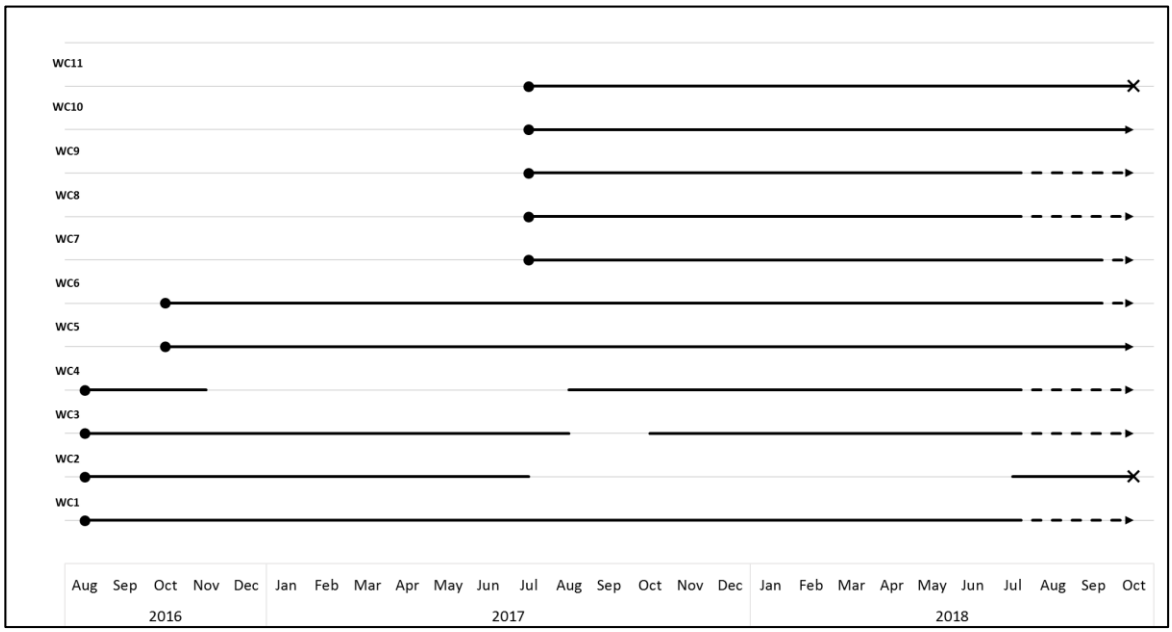

Figure 12: Temporal coverage of data collection for this research, beginning in August of 2016 and ending in the summer and fall of 2018. Circles indicate logging inception, crosses indicate loggers being removed or rendered inoperable, dashed lines indicating data that has been collected and yet to be retrieved, arrows indicate loggers continued logging.

Using the collected data, temperature averages were calculated on daily, monthly and annual scales. Also, both daily max and daily minimum temperatures were

determined. For any sensors that malfunctioned, were not correctly recording, or were buried in snow, the data wereinfilled. A total of 16.8 % of the data were infilled using this process. This method was applied using the three nearest Alberta Government meteorological stations, Castle Auto, WestCastle, and Gardner Headwater (**Figure 7**) collecting air temperature data. A linear relationship was established between the average daily temperature of the data successfully collected from sites from this study and the data acquired from Environment Canada stations similar to the process by Wood et al. (2019) (**Figure 13**). The linear equation was used to fill gaps within the data from each station.

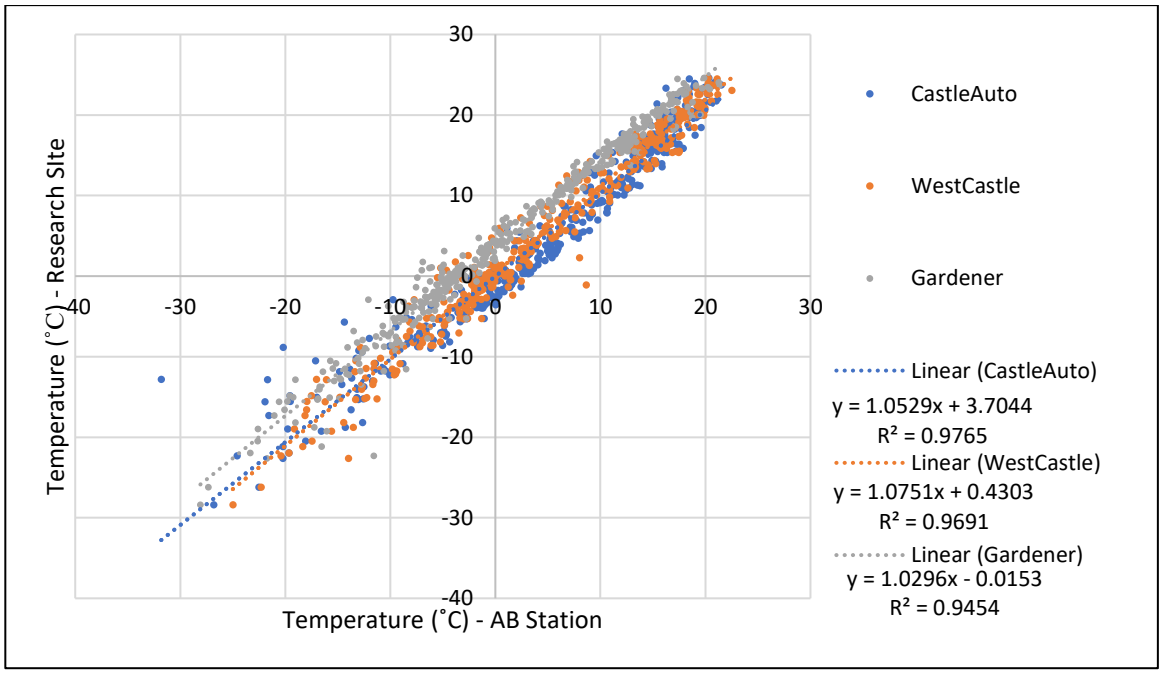

Figure 13: An example regression curve where the temperature at the research site is a function of temperature at the independent station, used to infill data between research sites and Environment Canada and the Government of Alberta stations within the region.

To reduce the potential compounding of error, the data was divided into two unique datasets. One dataset containing temporally gap-filled data, and one dataset that did not contain infilled data. The temporally gap-filled dataset (Set A), as described above, was used in analyzing the seasonality and temporal events such as inversions and

chinooks within the watershed as well as future projections. The non-gap-filled dataset (Set B) was used solely for spatial modelling and comparison between models.

5.3 Air temperature General Linear Model

Multivariate linear regression and linear regression were used to analyze the relationships between temperature, topographic, and land cover characteristics. The monthly average temperature (MAT) for each site was regressed against assemblages of explanatory variables in order to determine those that had the most influential and most robust explanatory ability. Variables such as elevation, TPI, slope, aspect, PISR, equivalent elevation, and albedo, similar to the method of studies of Cullen and Marshall (2011) and Wood et al. (2019), were all considered and used in multiple iterations and variations as explanatory factors. Equivalent elevation is a variable pioneered by Lewkowicz and Bonnaventure (2011) to express surface air temperature lapse rates in regions above and below treeline. Furthermore, the delineation of the treeline, a seemingly significant influence on local microclimate and boundary layer climate conditions (Lewkowicz & Bonnaventure, 2011; Ross, 2017), had to be spatially represented. Therefore, stations that existed above and below treeline were separated in order to run the model upon each region independently.

Each iteration of the regression model was reviewed to determine if the values that were being produced by the equation were logical and within the realistic range for the time of year (i.e. the model was not producing negative relationships where it is expected positive ones should exist as with solar radiation). Explanatory variables that

resulted in erroneous values being predicted or illogical relationships were removed from consideration within the model. As a result, only elevation was the selected regression variable for modelling temperature. Variables that did not produce consistent statistically significant relationships were not considered for use in the final model.

5.4 Cross-Validation

The spatial model generated was validated through the use of the leave-one-out cross-validation (LOOCV) technique. LOOCV is accomplished by the iterative removal of individual stations and the re-computation of the general linear regression models on the new set of data missing one location. These new models were then used to derive the temperature at the location that had been left out and the difference between the model containing the totality of the locations and the network of stations with one missing was determined. This technique was applied for all stations across all months within the study period.

5.5 Pre-Modelling

Treeline for this region was determined using a supervised classification operation within ENVI software. Using a 0.5 m resolution image mosaic of Southern Alberta, the study area was isolated and ran through the classification process (**Figure 14**). Locations representing exposed rocky and sparsely vegetated areas were manually identified as above treeline, whereas locations with dense forest and prominently present vegetation were identified as below treeline. These manually identified regions were used to train the program to identify similar regions with spectral responses that matched the input regions. Once the program had identified all pixels within the study area to its closest

matching the supervised input data, they were quality controlled through on-site visual inspection, and the use of clumping and sieving algorithms within ENVI. Areas like roads and rivers were manually reclassified as below treeline locations. Classified treeline varied in the study region (1471-2459 m) but was generally found at a mean elevation of 1980 m. As modelling over lakes could potentially cause substantial error in the calculation of surface air temperature, and there were no logging locations placed on the landscape in order to capture the variations there, they were artificially removed from the study area through the process of manual identification and delineation using 0.5 m image mosaic.

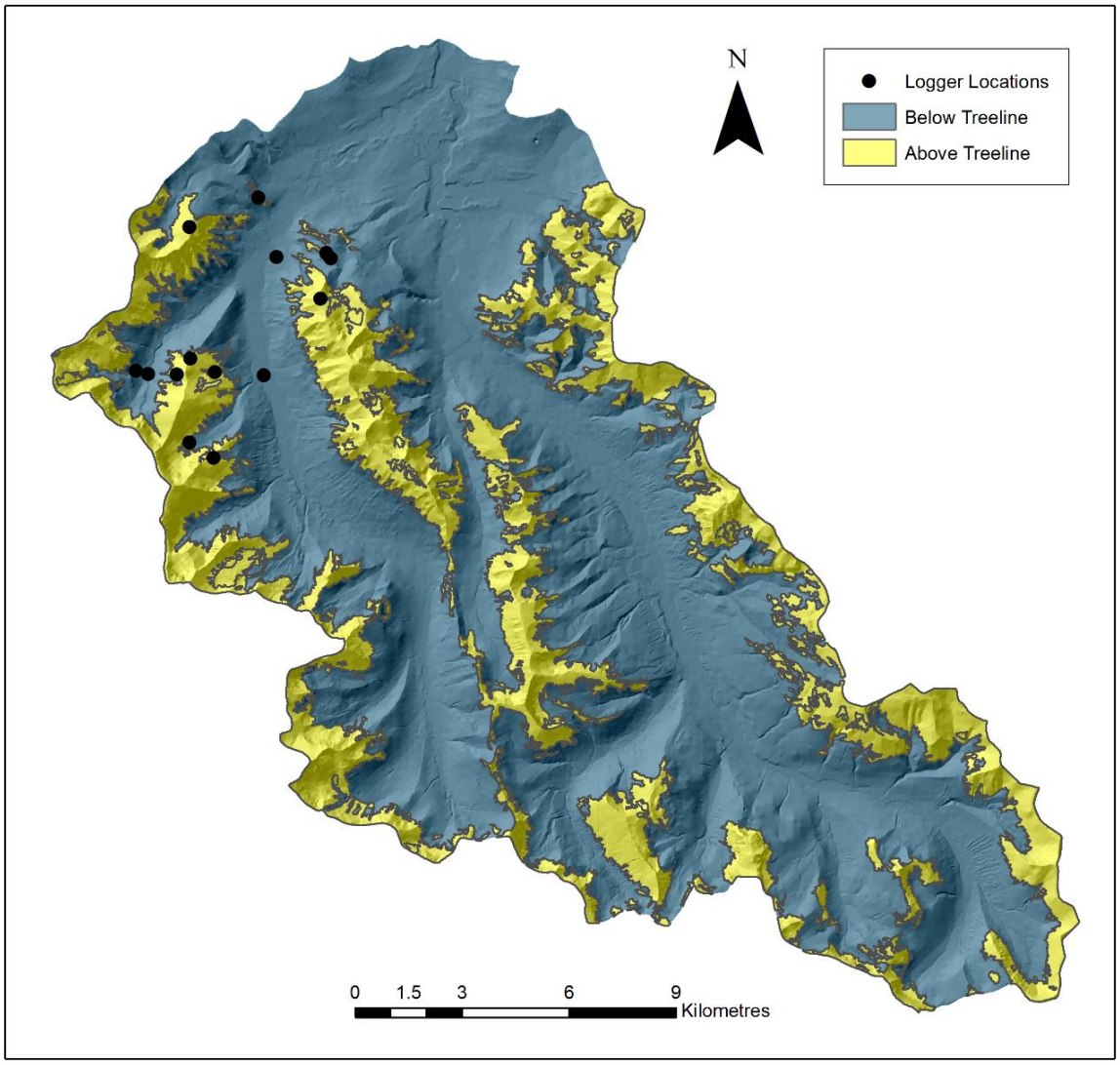

Figure 14: Regions within the WCW determined to be above or below treeline through supervised classification of aerial imagery.

5.6 Modelling

Once all input grids were prepared for the modelling process, the surface temperature at a location was determined by implementing the linear regression equation for each grid cell (10 m × 10 m) within the study area. Surface air temperature models were produced for all months, using **Set B**, over the time period selected for analysis as well as one representing a predicted annual mean air temperature (AMAT). To ensure

realistic surface air temperatures were being modelled, these generated raster files were manually capped to remove extreme values well outside the norm. This process was achieved through identification of values that were three times greater than the standard deviation of the data, above and below the mean value, and the subsequent replacement of these values with the value that was equal to three times the standard deviation above or below the mean. This resulted in a hard cap for values within the model that consisted of air temperature values within a 99 % confidence interval.

5.7 Future Models

Using the software ClimateNA (Wang et al., 2016), three future climate normals were predicted along three RCP scenarios that were set out by the IPCC. This was done for each month over which the study period extended. For each sensor location, the coordinates and elevation were seeded into the software which then drew from an archive of precalculated models. The model within the software that was selected for use is the CanESM2, the second generation of a Canadian earth system model (Wang et al., 2016). The average surface air temperature provided through ClimateNA for the 1981-2010 climate normal was used in association with future scenario IPCC RCP models to derive the difference in magnitude between the two.

Equation 3: $$M_{dif} = \left|Ta(CNA)_{prj} - Ta(CNA)_{ave}\right|$$

Equation 4: $$Ta_{future} = M_{dif} + Ta(WCW)_{ave}$$

where M_{dif} is the difference in magnitude between $Ta(CNA)_{prj}$ and $Ta(CNA)_{ave}$, the average temperatures from both ClimateNA and the WCW (**Set A)** respectively. M_{dif}

is then applied to the WCW model derived, $Ta(WCW)_{ave}$, to generate a regionally corrected future air temperature, Ta_{future}.

The magnitude of air temperature change was applied to the predicted mean air temperature surfaces for the July 2017 to June 2018 period (Bonnaventure & Lamoureux, 2013). This is done as it is assumed that the local climate that had been determined through this research would be more representative of the region whereas the CanESM2 and IPCC RCP models were more able to represent change into the future and at a global scale, thus combining top-down global circulation models and bottom-up local models.

5.8 Model Comparison

Models generated (**Set B**) for this research are compared to several other published models which share a spatial extent with the study area. Direct comparisons are made between the average surface air temperatures modelled within this work with the lower resolution models for the spatially coincident areas. As the model created by Hutchinson et al. (2009) and later further analyzed by Kienzle (2017) for the climate period of 1970-2010 is coincident with this study, it was used as a comparator for both annual air temperature as well as seasonal temperatures. Also used as a comparison is the ClimateNA model by Wang et al. (2016). This model utilizes and expands from previous models such as PRISM and ANUSPLIN topographically corrected surfaces (Wang et al., 2016). This model is compared on an annual basis. The models were compared in all cases by subtracting the results of the generated models from the comparison models to form difference grids using raster calculator in ArcGIS.

Equation 5: $$MAAT_{Comparative} - AMAT_{WCW\ Model} = Difference\ Grid$$

As the resolution for the models created for the Castle study area was of higher resolution than the comparison models, the comparative models were resampled to the same cell size using the Nearest Neighbor interpolation as the comparative models are discrete areas. The Alberta Climate Records dataset was resampled from a resolution of 10 km × 10 km to a cell size of 10 m × 10 m. The ClimateNA dataset was resampled from a cell size of 4.65 km × 3 km to 10 m × 10 m, the rectangular cell size is a result of the dataset using angular units. This process did not serve to increase the resolution of the data but rather just to make the models numerically comparable on a pixel level (Bonnaventure & Lewkowicz, 2013).

5.9 Surface Lapse Rate Derivation

The average monthly temperature recorded at each site (**Set A**) is regressed against the elevation of each site to determine the rate of change in temperature as a purely elevational driven variable. The monthly average SLRs were calculated using the best-fit linear trend through the least squares method with input from all sites within the study area (Cullen & Marshall, 2011). To determine hourly SLR hourly temperature measurements were regressed again against elevation. SLRs calculated for above and below treeline were done through using the same methods with only stations above or below the classified treeline being used to determine lapse rates.

6.0 Results

6.1 Observed Air Temperature

6.1.1 Daily

Daily Air temperature varied seasonally across the watershed from the coldest daily average temperature –31.2 °C on January 13th, 2018 to the warmest of 24.6 °C on July 7th, 2017 (**Table 3**). The monthly range of daily air temperature observed at each of the stations is presented in **Figure 15**.

Table 3: Maximum and Minimum daily averages observed at each sensor location from July 2017 and June 2018

Station	Maximum (˚C)	Minimum (˚C)
WC1	20.5 (September 2)	-26.9 (December 30)
WC2	22.1 (July 7)	-26.5 (December 30)
WC3	23.1 (July 8)	-29.0 (December 30)
WC4	20.2 (August 19)	-30.4 (December 19)
WC5	24.5 (August 28)	-28.4 (December 30)
WC6	19.6 (July 7)	-22.3 (December 22)
WC7	23.3 (July 7)	-28.6 (December 29)
WC8	21.2 (September 2)	-27.8 (December 30)
WC9	24.6 (July 7)	-27.9 (December 31)
WC10	21.2 (July 7)	-31.2 (January 13)
WC11	18.3 (July 8)	-29.2 (December 30)
Valley	23.1 (July 8)	-26.4 (December 30)
MidMtn	22.6 (July 8)	-29.3 (December 30)
Ridge	20.6 (August 29)	-29.6 (December 29)

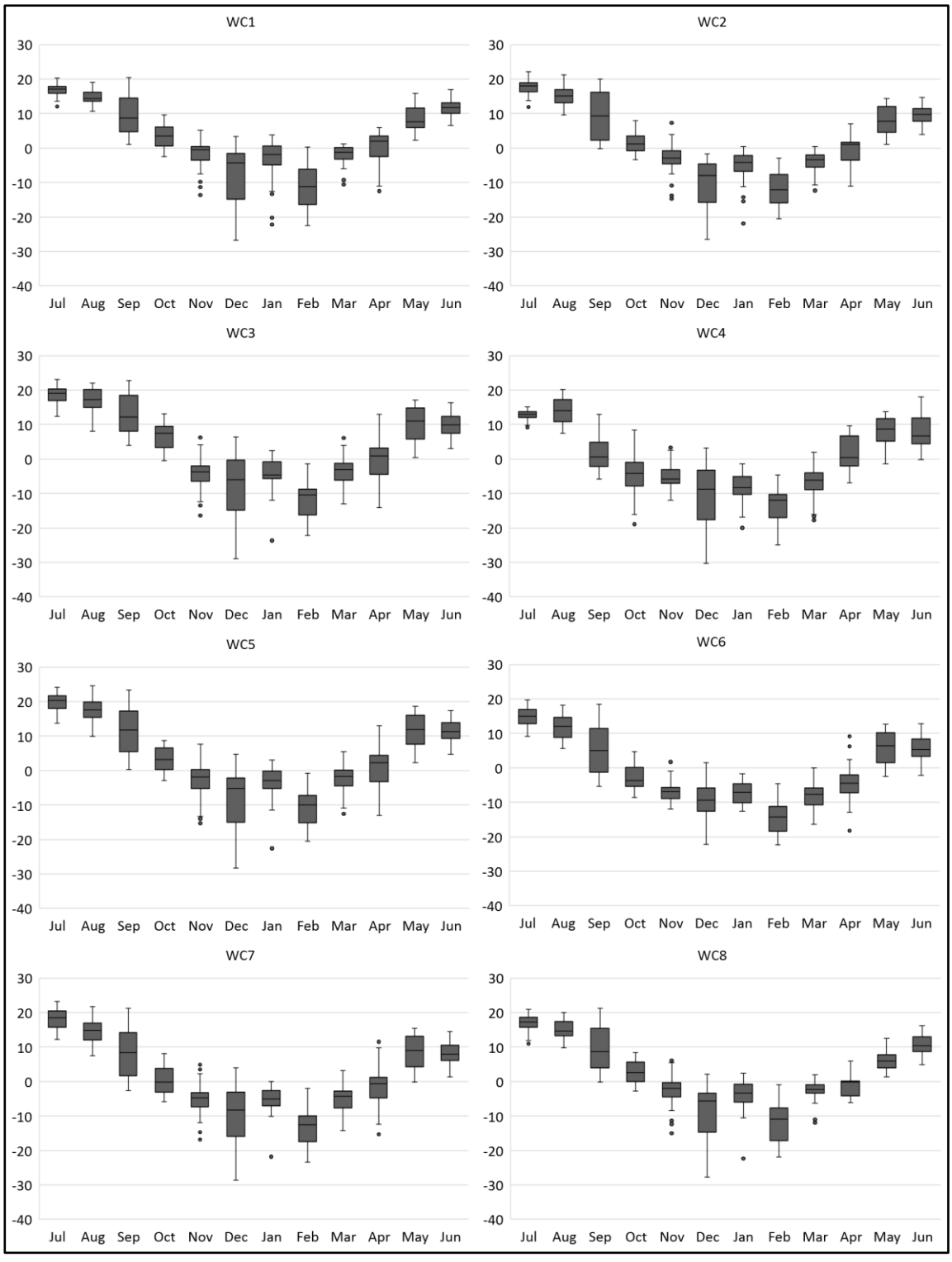
WC1
WC2
WC3
WC4
WC5
WC6
WC7
WC8
30
20
10
0
-10
-20
-30
-40
Jul
Aug
Sep
Oct
Nov
Dec
Jan
Feb
Mar
Apr
May
Jun

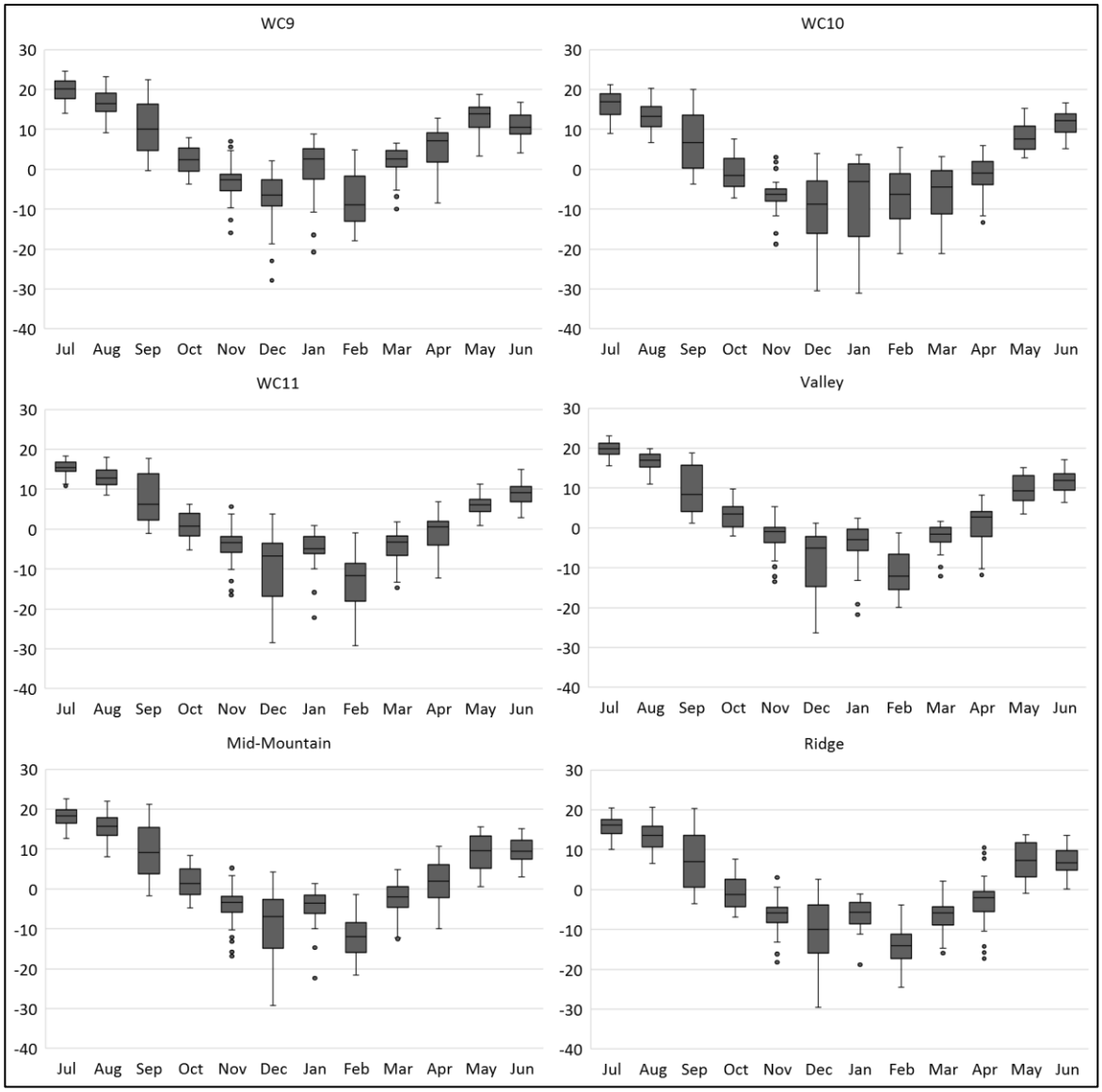

Figure 15: Box and whisker plots for daily average air temperature in ˚C observed at each station indicating the mean, median, quartiles, standard error, and outlying data separated into monthly collections.

6.1.2 Monthly

The month with the broadest range of MAT between sensors observed was September with monthly averages of 13.0 °C observed at site WC3 and 1.76 °C observed at site WC4. December observed MAT ranged from -7.48 °C at site WC9 to -10.4 °C at site WC4. The average range of monthly average air temperature observed within the study period was 7.78 °C throughout the year. The coldest average monthly temperature observed was February at -11.6 °C and the warmest month of July with a temperature of 16.9 °C (**Table 4**).

Table 4: Monthly average air temperature measured at each sensor location between July 2017 and June 2018 inclusive. Italics denotes months that have had data infilled.

Station	**Monthly Average Air Temperature (°C)**											
	Jul	**Aug**	**Sep**	**Oct**	**Nov**	**Dec**	**Jan**	**Feb**	**Mar**	**Apr**	**May**	**Jun**
WC1	16.6	14.8	9.7	3.4	-2.3	-8.1	-3.6	-11.3	-2.6	-0.1	9.0	11.4
WC2	*17.7*	*15.3*	*9.1*	*1.7*	*-3.8*	*-10.3*	*-5.4*	*-12.0*	*-4.3*	*-1.0*	*8.1*	*9.4*
WC3	18.5	*16.8*	*13.0*	6.8	-4.5	-7.7	-3.9	-11.9	-3.7	0.0	10.1	10.1
WC4	*12.7*	14.0	1.8	-4.5	-4.3	-10.4	-8.3	-13.5	-6.5	1.5	7.7	7.9
WC5	20.0	17.9	11.4	3.3	-3.1	-8.0	-4.0	-11.2	-2.5	0.9	11.5	*11.6*
WC6	*14.7*	11.8	5.2	-2.8	-6.8	-9.5	-7.2	-14.7	-7.9	-4.7	6.1	5.8
WC7	*18.0*	14.8	8.3	0.4	-5.8	-9.5	-5.3	-13.3	-5.0	-1.6	8.7	8.4
WC8	*16.7*	15.1	9.7	2.7	-3.1	-9.0	-4.4	-11.8	-2.9	-1.0	6.1	10.4
WC9	*19.8*	16.9	10.5	2.6	-3.8	-7.5	*0.1*	*-7.7*	*1.4*	*4.8*	*12.9*	11.0
WC10	*16.3*	13.4	7.1	-1.0	-7.2	-10.1	*-7.4*	*-6.9*	*-6.1*	*-1.7*	*8.1*	*11.6*
WC11	*15.3*	13.1	7.7	0.9	-4.7	-9.7	-5.1	-13.4	-4.6	-1.0	6.0	8.8
Valley	19.6	16.7	9.7	3.3	-2.7	-8.6	-4.2	-11.3	-2.5	0.5	9.5	11.6
MidMtn	18.0	15.8	9.5	1.7	-4.6	-8.8	-4.6	-12.2	*-2.6*	*1.3*	9.3	9.7
Ridge	15.8	13.6	7.2	-0.9	-7.0	-10.4	-6.2	-14.5	-6.3	-3.0	7.3	7.2
Average	17.1	15.0	8.6	1.2	-4.5	-9.1	-5.0	-11.8	-4.0	-0.4	8.6	9.7

6.1.3 Seasonal and Annual

The seasonal temperatures varied throughout the WCW from an average across the network of 13.9 ˚C during the summer months of June, July, and August to – 8.4 ˚C during the winter months of December, January, and February. The AMAT as recorded from the sensor network over the study period was 2.2 °C (**Table 5**). The station with the coldest AMAT was WC6 at -0.7 ˚C while the warmest AMAT was recorded at WC9 at 5.2 ˚C.

Table 5: Average seasonal daily mean temperature observed at each sensor location in °C.

Station	AMAT	JJA_{ave}	SON_{ave}	DJF_{ave}	MAM_{ave}
WC1	3.2	14.3	3.6	-7.5	2.1
WC2	2.1	14.2	2.3	-9.1	0.9
WC3	3.8	15.2	5.1	-7.7	2.2
WC4	-0.1	11.6	-2.4	-10.6	0.9
WC5	4.1	16.5	3.9	-7.6	3.3
WC6	-0.7	10.8	-1.5	-10.3	-2.1
WC7	1.6	13.8	1.0	-9.3	0.7
WC8	2.5	14.1	3.1	-8.3	0.8
WC9	5.2	16.0	3.1	-4.9	6.4
WC10	1.4	13.8	-0.4	-8.2	0.1
WC11	1.2	12.4	1.3	-9.2	0.1
Valley	3.6	16.0	3.4	-8.1	2.5
MidMtn	2.8	14.5	2.2	-8.5	2.7
Ridge	0.4	12.2	-0.2	-10.4	-0.7
Average	2.2	13.9	1.8	-8.4	1.4

6.2 Surface Lapse Rates and Inversions

The monthly average SLRs observed and calculated using the best-fit linear trend through the least squares method varied from –8.0 °C km^{-1} in October to –2.2 °C km^{-1} in

February (**Table 6**). Hourly average annual SLRs ranged from –2.3 °C km^{-1} at 5 AM to -8.1 °C km^{-1} at 2 PM (**Figure 16**)

Table 6: Average monthly surface lapse rates calculated using best-fit linear regression (n=14).

Year	Month	Average Monthly Surface Lapse Rate (°C km^{-1})	The difference from Standard Surface Lapse Rate (°C km^{-1})
2017	July	-4.2	2.3
	August	-4.0	2.5
	September	-7.3	-0.8
	October	-8.0	-1.5
	November	-4.6	1.9
	December	-2.3	4.2
2018	January	-5.8	0.7
	February	-2.2	4.3
	March	-6.9	-0.4
	April	-3.9	2.6
	May	-2.9	3.6
	June	-4.5	2.0

Within the WCW, inverted SLRs were found to be present in the watershed for 18.5 % of the time (**Figure 17**). A total of 163 distinct inversion events were observed, and the average length was 9 hours and 55 minutes. Average inversion strength was 4.8 °C km^{-1}. The strongest hourly inversion was 21.2 °C km^{-1} and occurred on December 31st, 2017 at 2:00 AM. The most extensive inversion lasted for 71 hours from December 6th to December 9th of 2017. While inversions occurred most frequently (62.6 %) during the warmer periods of the year (April – September) compared to 37.4 % in October – March, there were more stable inversions present for more extended periods of time (e.g. 11 hours and 42 minutes) during the colder months (October – March).

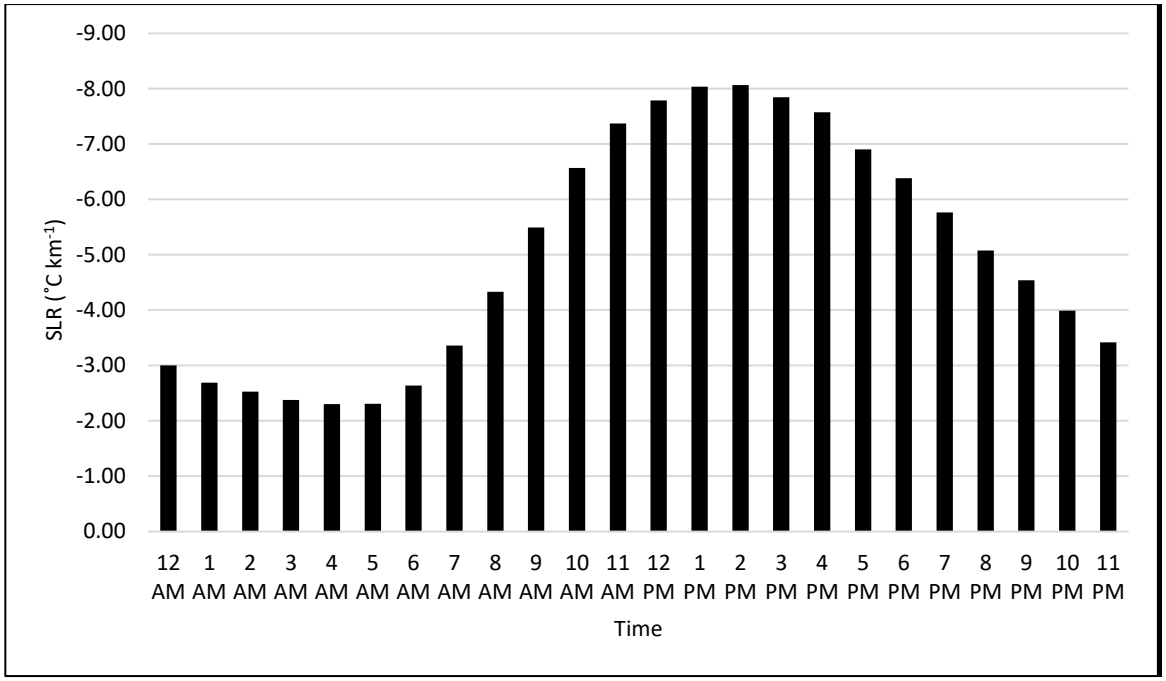

Figure 16: Observed annual averages of hourly surface lapse rate for the period of the study showing the presence of a diurnal signal.

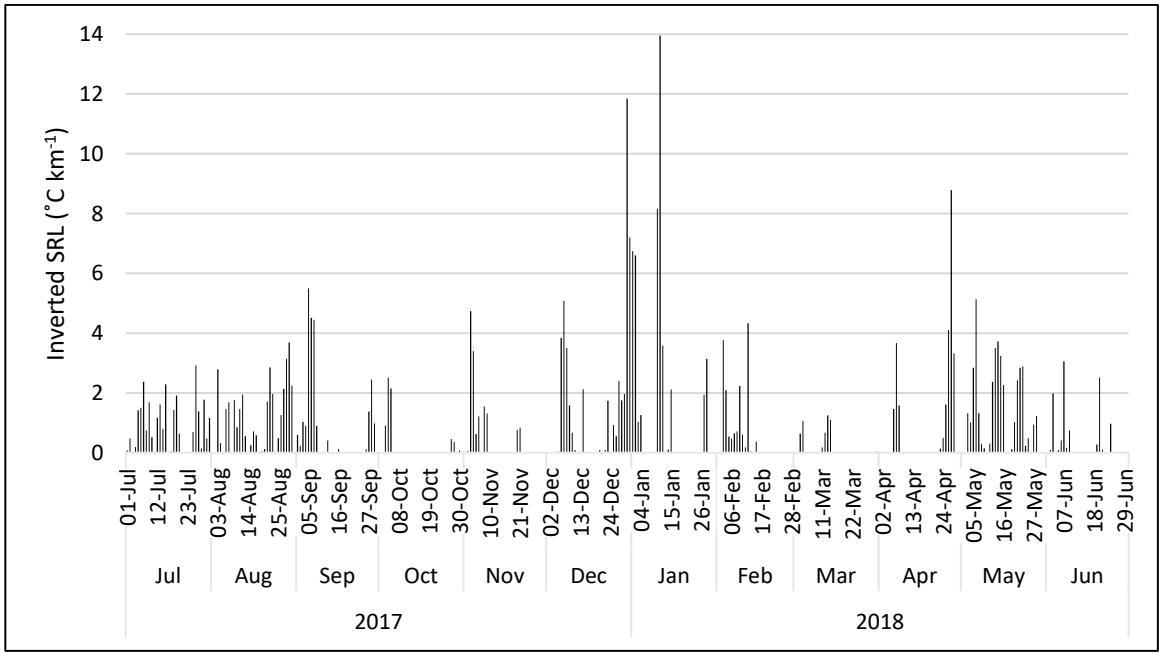

Figure 17: The strength and seasonal timing of daily inverted surface lapse rates.

6.3 Regression Models

The models and statistics for each of the surfaces created are presented below (**Table 7-8**). The selected variable for the final model was exclusively elevation though statistics for the other models will also be presented in **Table 9 and Table 10** including slope, TPI, aspect, PISR, and treeline. Treeline was used as a device to partition the study area and derive separate models for elevation within these regions and found to not be consistenly significant both above and below the deliniation. Cross-validation statistics of the regression models are also presented here **(Table 11)** showing the difference determined as a result of an individual station being removed from the modelling process, thus highlighting the ability of the rest of the network of sites to predict the value of the removed location.

Table 7: Monthly linear regression model statistics that were generated between July 2017 and June 2018 where monthly average temperature was a function of elevation. Months where elevation did not have a statistically significant p-value of 0.05 are indicated by bold and italicized p-values.

	July (n=7)			**August (n=11)**		
	Coefficients	*Standard Error*	*P-value*	*Coefficients*	*Standard Error*	*P-value*
Intercept	24.685	3.13008	0.00053	22.7098	2.36505	$5.0*10^{-6}$
Elevation	-0.0039	0.00169	***0.0697***	-0.0043	0.00128	0.00855
	September (n=12)			**October (n=12)**		
	Coefficients	*Standard Error*	*P-value*	*Coefficients*	*Standard Error*	*P-value*
Intercept	19.894	3.09856	$7.6*10^{-5}$	14.5655	1.91002	$1.8*10^{-5}$
Elevation	-0.0063	0.00165	0.00324	-0.0074	0.00102	$2.5*10^{-5}$
	November (n=13)			**December (n=13)**		
	Coefficients	*Standard Error*	*P-value*	*Coefficients*	*Standard Error*	*P-value*
Intercept	4.30949	1.34634	0.00844	-4.2148	1.864	0.045
Elevation	-0.0048	0.00072	$3.4*10^{-5}$	-0.0025	0.00099	0.02748
	January (n=11)			**February (n=11)**		
	Coefficients	*Standard Error*	*P-value*	*Coefficients*	*Standard Error*	*P-value*
Intercept	2.12522	1.56372	0.2072	-5.8446	1.01199	0.00027
Elevation	-0.0039	0.00084	0.0011	-0.0037	0.00054	$7.9*10^{-5}$
	March (n=10)			**April (n=10)**		
	Coefficients	*Standard Error*	*P-value*	*Coefficients*	*Standard Error*	*P-value*
Intercept	5.97932	0.98514	0.0003	5.02038	3.02826	0.13594
Elevation	-0.0056	0.00053	$5.0*10^{-6}$	-0.0032	0.00162	***0.08436***
	May (n=11)			**June (n=11)**		
	Coefficients	*Standard Error*	*P-value*	*Coefficients*	*Standard Error*	*P-value*
Intercept	12.7834	3.23709	0.00336	19.7844	1.08195	$2.0*10^{-8}$
Elevation	-0.0024	0.00173	***0.1943***	-0.0057	0.00058	$4.2*10^{-6}$

Table 8: Monthly r^2 values of the elevation and temperature models generated for the WCW between July 2017 and June 2018.

Month	**r^2**
July	0.51
August	0.55
September	0.60
October	0.84
November	0.80
December	0.37
January	0.71
February	0.84
March	0.94
April	0.33
May	0.18
June	0.91

Table 9: The P-value and R^2 value of Aspect, slope, TPI, and PISR in relation to temperature. Significant P-values in bold and italics.

		Aspect		**Slope**		**TPI**		**PISR**	
Month	*n*	*R^2*	*P-value*	*R^2*	*P-value*	*R^2*	*P-value*	*R^2*	*P-value*
July	7	0.51	0.07	0.00	0.92	0.44	0.11	0.12	0.46
August	11	0.32	0.07	0.01	0.79	0.23	0.13	0.01	0.77
September	12	0.00	0.92	0.00	0.83	0.35	***0.04***	0.00	0.90
October	12	0.00	0.86	0.03	0.60	0.53	***0.01***	0.00	0.96
November	13	0.06	0.43	0.20	0.13	0.53	$\boldsymbol{4.7\times10^{-3}}$	0.00	1.00
December	13	0.06	0.42	0.03	0.56	0.24	0.09	0.00	0.87
January	11	0.00	0.97	0.01	0.74	0.45	***0.02***	0.13	0.28
February	11	0.02	0.72	0.04	0.56	0.42	***0.03***	0.04	0.57
March	10	0.01	0.81	0.07	0.47	0.56	***0.01***	0.11	0.35
April	10	0.26	0.13	0.04	0.57	0.16	0.26	0.00	0.88
May	11	0.25	0.12	0.18	0.19	0.00	0.94	0.17	0.20
June	11	0.02	0.68	0.12	0.29	0.60	$\boldsymbol{5.0\times10^{-3}}$	0.13	0.28

Table 10: The P-value and R^2 value of elevation in relation to temperature partitioned by presence above or below treeline. Significant P-values in bold and italics.

	Treeline - Above			Treeline - Below		
Month	*n*	R^2	*P-value*	*n*	R^2	*P-value*
July	4	0.96	***0.02***	3	0.26	0.66
August	4	1.00	$\boldsymbol{1.1\times10^{-3}}$	7	0.15	0.39
September	5	0.39	0.26	7	0.30	0.21
October	5	0.59	0.13	7	0.86	$\boldsymbol{2.6\times10^{-3}}$
November	6	0.42	0.17	7	0.96	$\boldsymbol{1.3\times10^{-5}}$
December	6	0.49	0.12	7	0.10	0.49
January	5	0.71	0.07	6	0.80	***0.02***
February	5	0.85	***0.03***	6	0.81	***0.01***
March	4	0.99	$\boldsymbol{3.2\times10^{-3}}$	6	0.87	***0.01***
April	4	0.36	0.40	6	0.49	0.12
May	5	0.93	***0.01***	6	0.06	0.64
June	5	0.95	***0.01***	6	0.88	***0.01***

Table 11: Leave-one-out Cross-Validation results showing the difference (˚C) between the model run using all points and the model with one of the points left out. Each data entry is the result of that location being removed for that particular month. Blanks indicate months without complete data coverage and have thus been left out.

Name	**Jul**	**Aug**	**Sep**	**Oct**	**Nov**	**Dec**	**Jan**	**Feb**	**Mar**	**Apr**	**May**	**Jun**
WC1	1.24	0.56	0.37	0.15	0.07	0.08	0.04	0.05	0.17	3.53	0.12	0.09
WC3	0.20			0.00	0.02	0.10	0.14	0.08	0.10	1.73	0.19	0.10
WC4			0.94	0.62	0.40	0.13	0.46	0.11	0.04	1.04	0.06	0.12
WC5	0.37	0.32	0.26	0.12	0.05	0.04	0.04	0.10	0.12	3.01	0.44	
WC6	0.88	0.49	0.18	0.14	0.12	0.31	0.03	0.04	0.31	2.18	0.52	0.30
WC7		0.10	0.12	0.08	0.05	0.03	0.06	0.01	0.05	0.95	0.11	0.01
WC8		0.17	0.07	0.05	0.01	0.14	0.07	0.04	0.01	2.87	0.58	0.11
WC9		0.17	0.16	0.07	0.01	0.31						0.10
WC10		1.46	2.37	2.68	1.44	0.79						
WC11		1.65	2.24	2.57	1.67	0.94	1.36	1.35	1.97	0.95	1.08	2.02
Valley	0.23	0.01	0.42	0.28	0.09	0.29	0.29	0.11	0.21	3.83	0.07	0.08
Mid Mtn	0.08	0.09	0.11	0.07	0.01	0.00	0.05	0.04			0.10	0.03
Ridge	0.19	0.03	0.18	0.11	0.18	0.14	0.05	0.16	0.03	0.02	0.07	0.09
Average	0.45	0.46	0.62	0.53	0.32	0.25	0.24	0.19	0.30	2.01	0.30	0.28

Table 12: Averages of the Leave-one-out Cross-Validation results showing the difference (˚C) between the model run using all points and the model with one of the points left out. Each data entry is the result of that location being removed for that particular month.

Name	Average
WC1	0.54
WC3	0.26
WC4	0.39
WC5	0.44
WC6	0.46
WC7	0.14
WC8	0.37
WC9	0.13
WC10	1.75
WC11	1.62
Valley	0.49
Mid Mtn	0.06
Ridge	0.10

6.4 Modelled Air Temperature Surfaces

The air temperature surfaces created using the models outlined above (**Table 7)** are presented below (**Figure 18-27**). The modelled AMAT temperature across the entire study area ranged from -1.8 to 4.5 °C with an average modelled temperature of 2.1 °C.

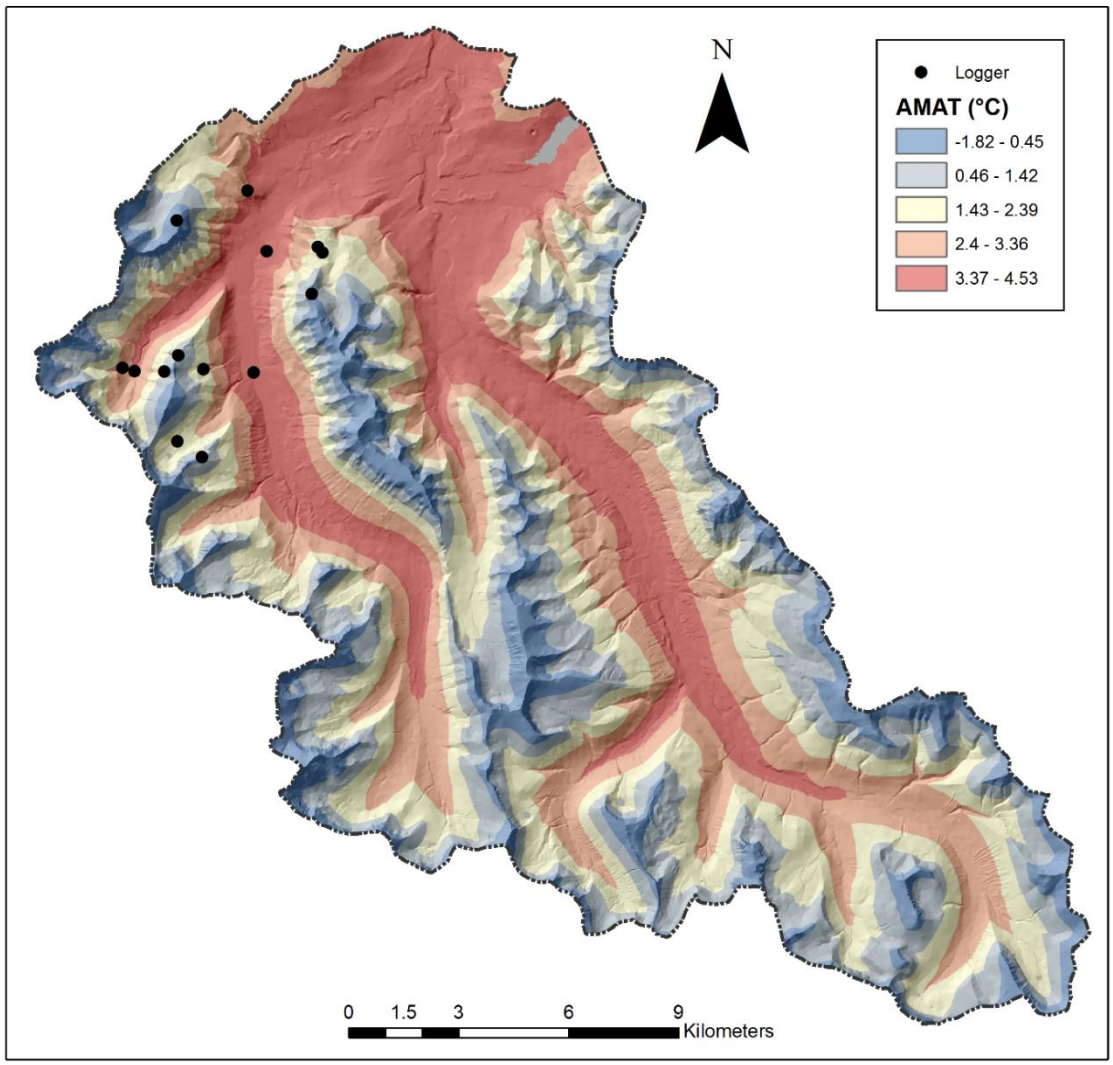

Figure 18: Annual mean air temperature modelled across the WCW between the months of July 2017 and June 2018.

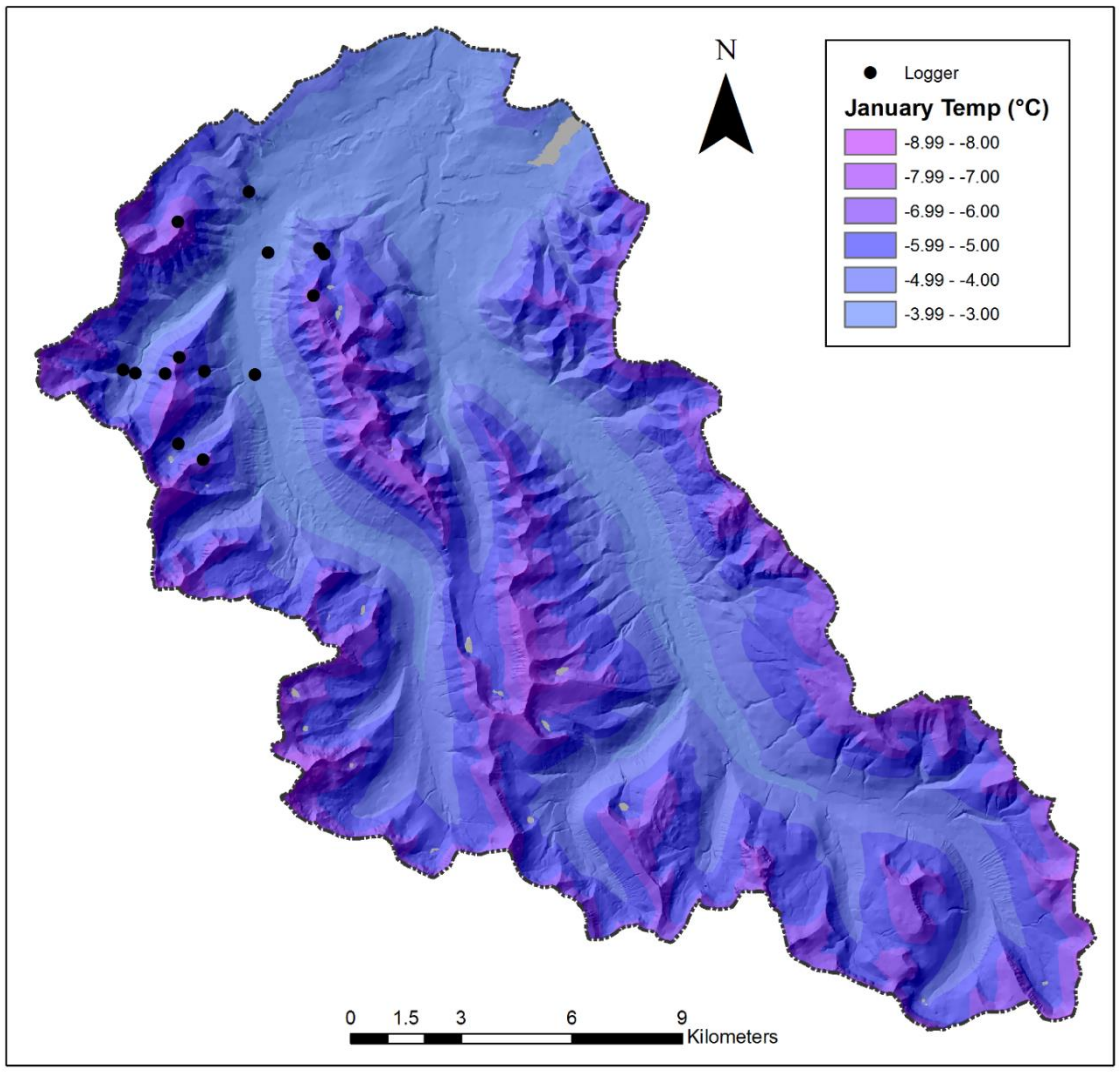

Figure 19: Average January temperature modelled across the WCW, ranging from the maximum modelled temperature of -3.13 °C and the minimum of -8.25 °C.

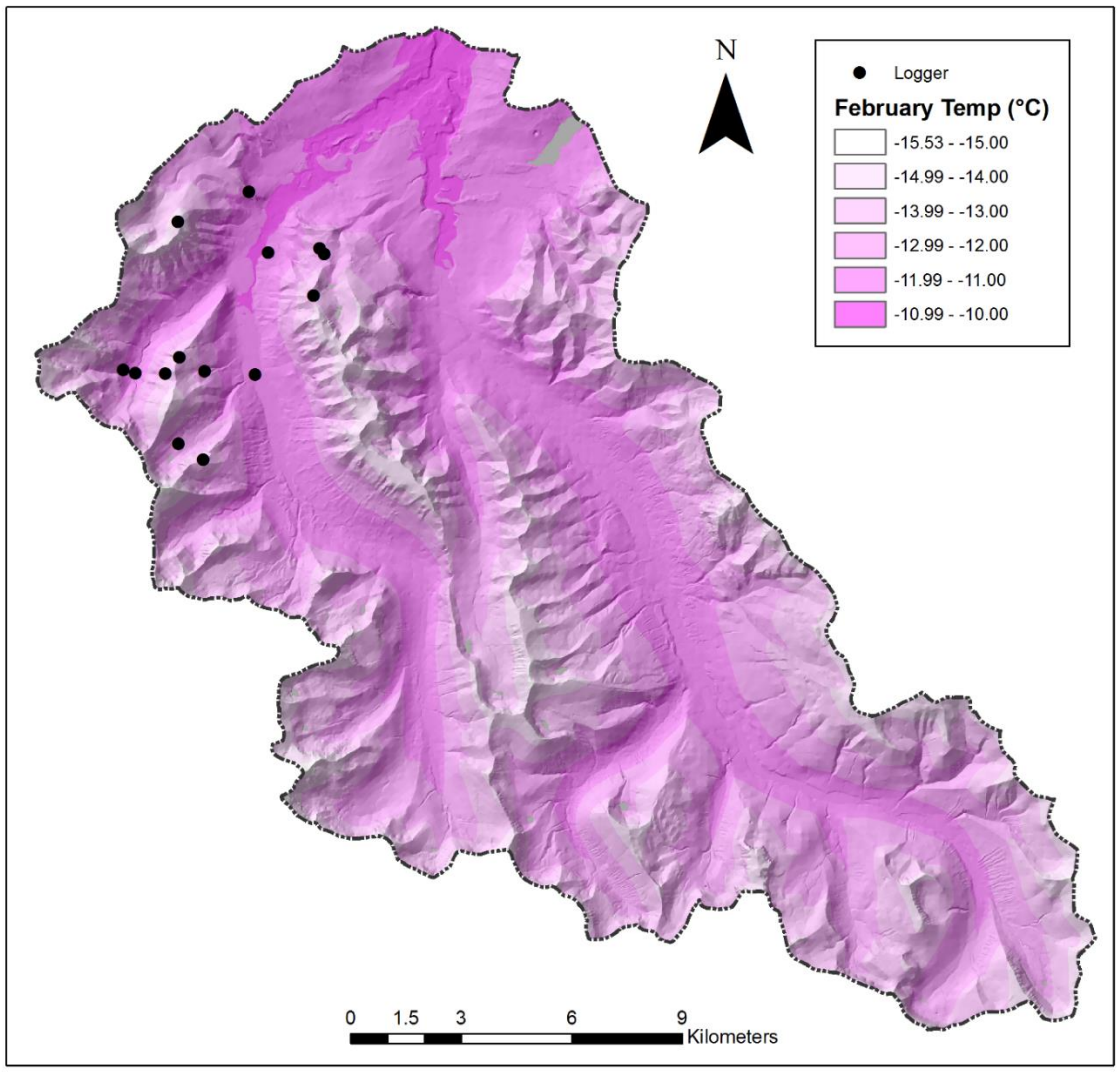

Figure 20: Average February temperature modelled across the WCW, ranging from the maximum modelled temperature of -10.75 °C to the minimum of -15.53 °C.

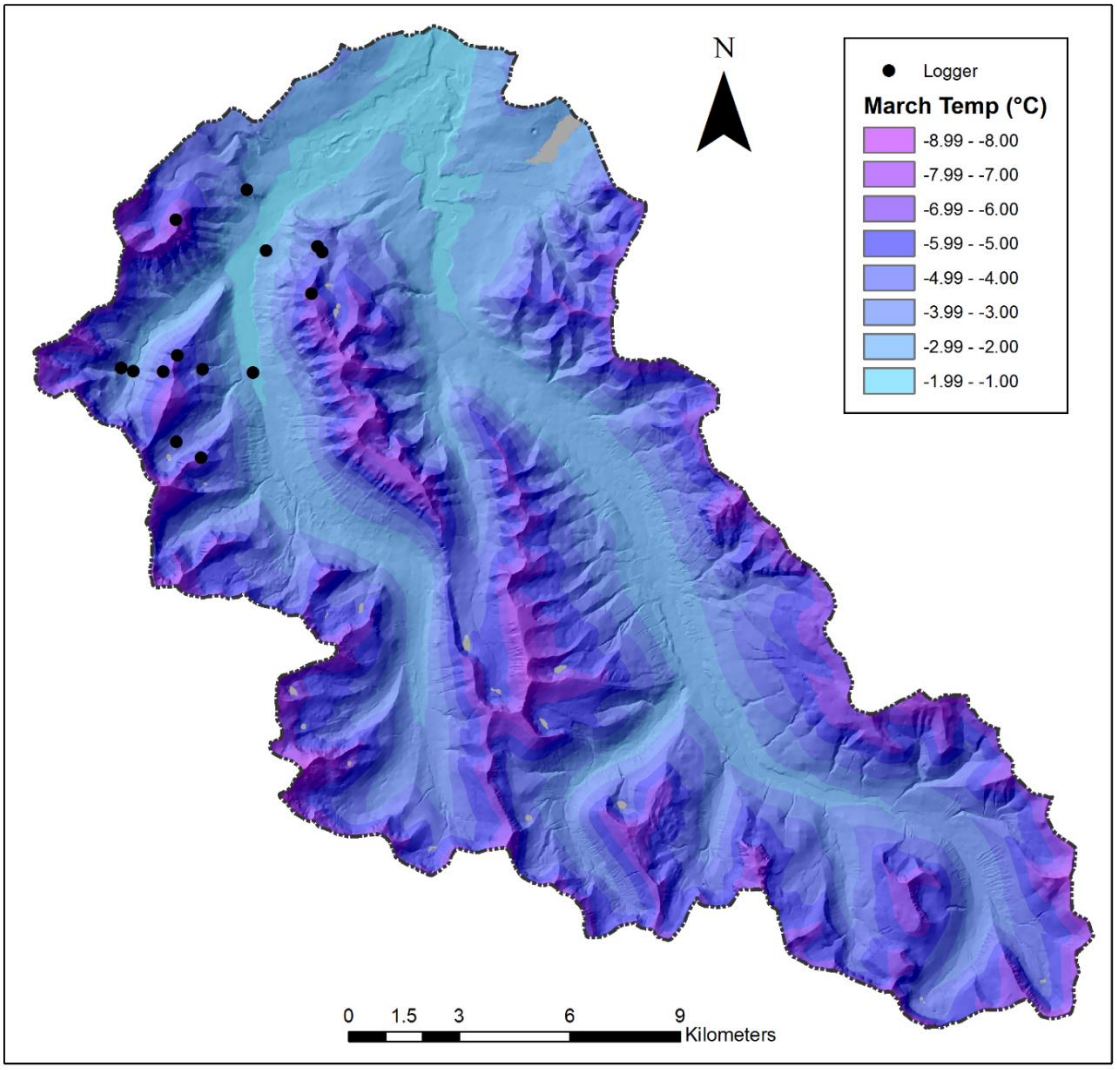

Figure 21: Average March temperature modelled across the WCW, ranging from the maximum modelled temperature of -1.54 °C to the minimum of -8.87 °C.

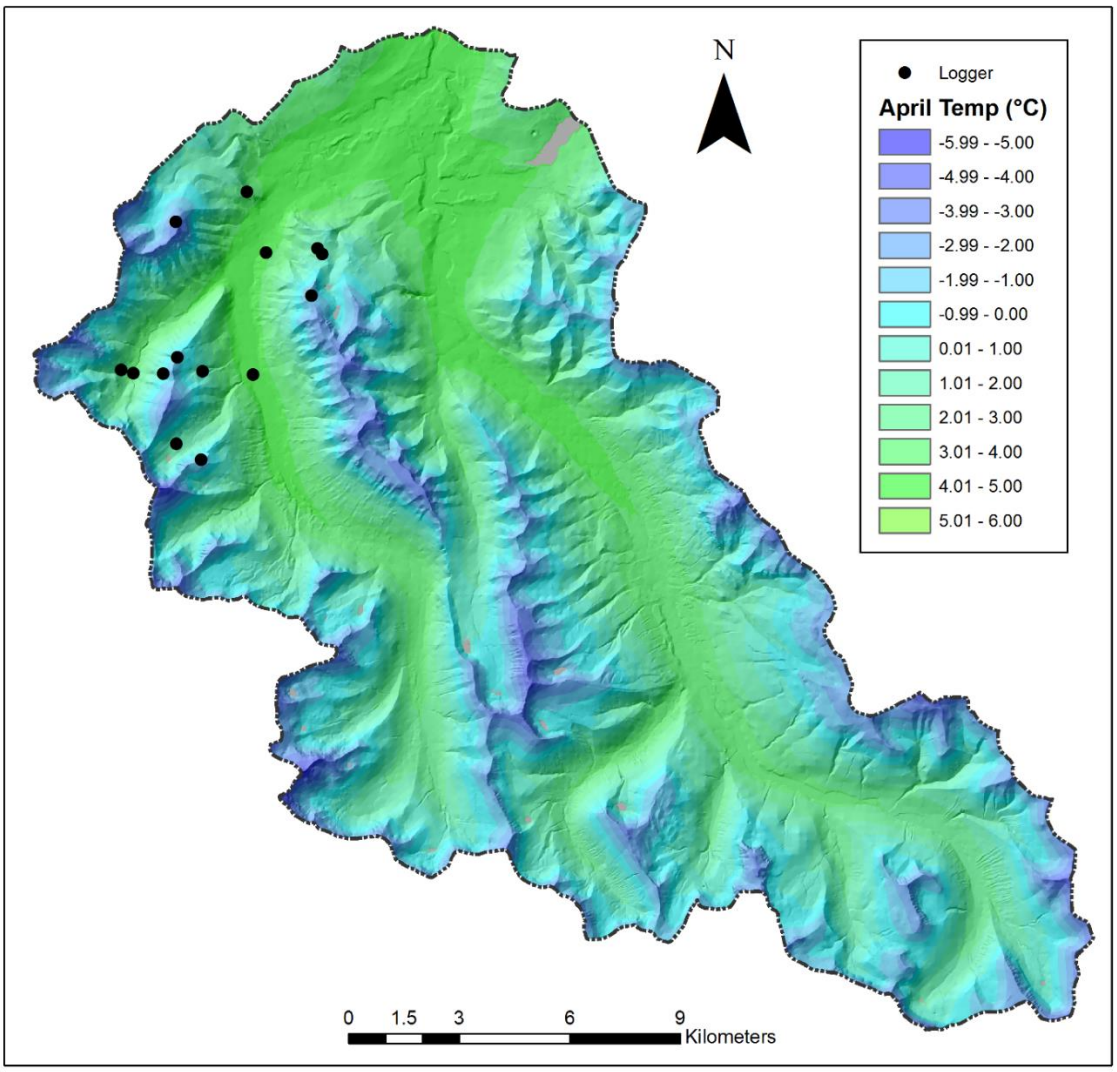

Figure 22: Average April temperature modelled across the WCW, ranging from the maximum modelled temperature of 5.02 °C to the minimum of -5.42 °C.

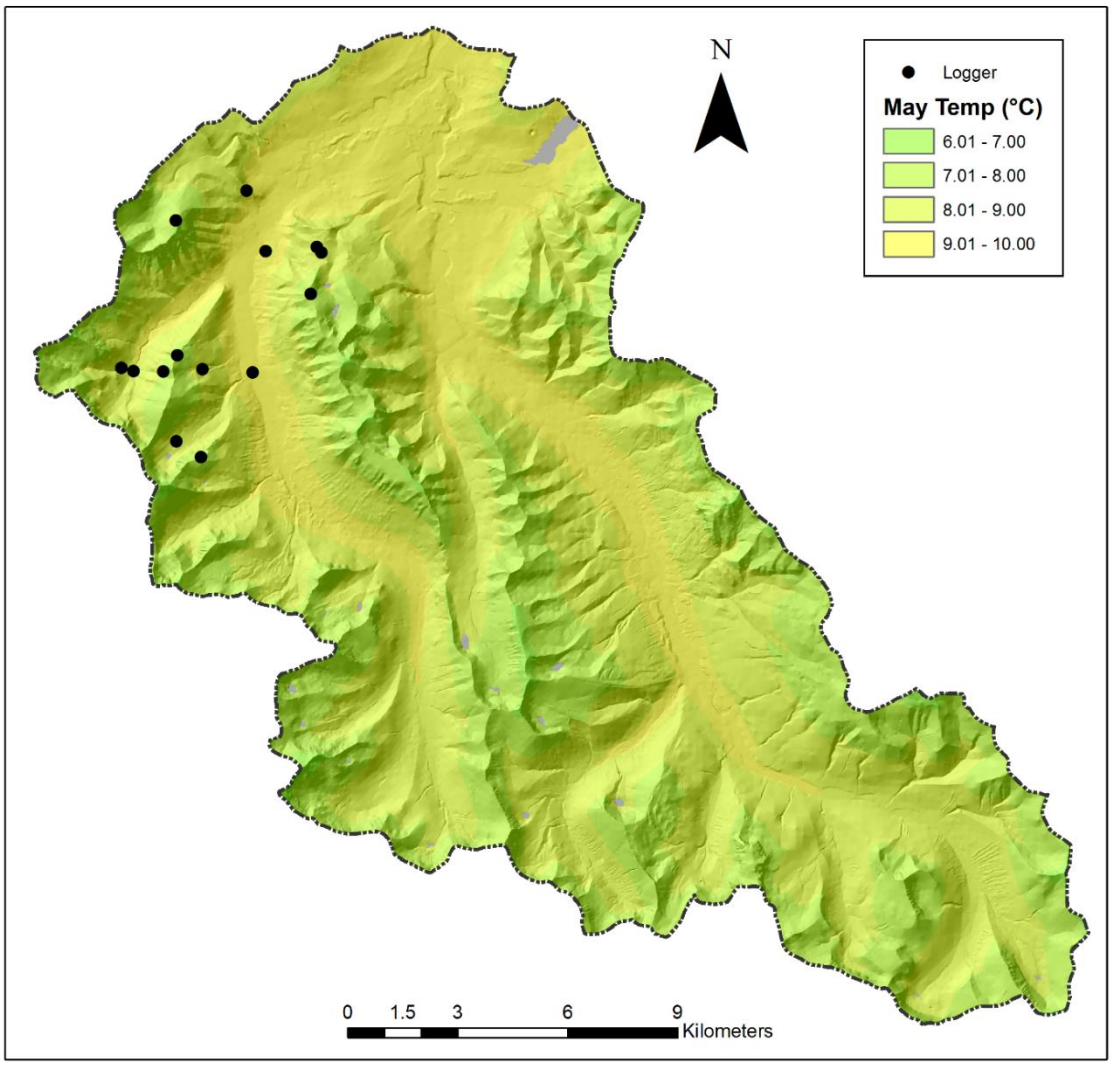

Figure 23: Average May temperature modelled across the WCW, ranging from the maximum modelled temperature of 9.55 °C to the minimum of 6.39 °C.

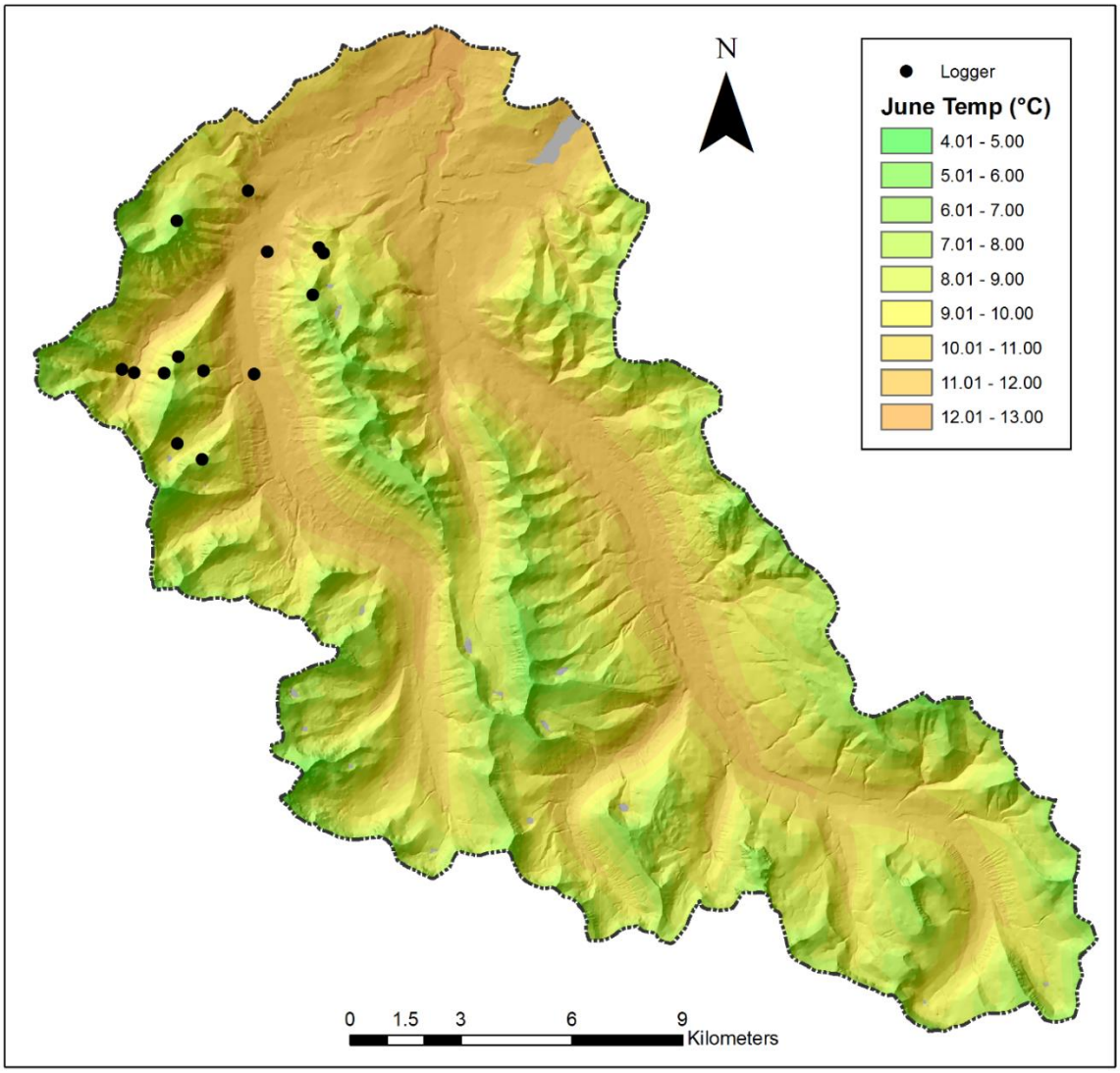

Figure 24: Average June temperature modelled across the WCW, ranging from the maximum modelled temperature of 12.25 °C to the minimum of 4.89 °C.

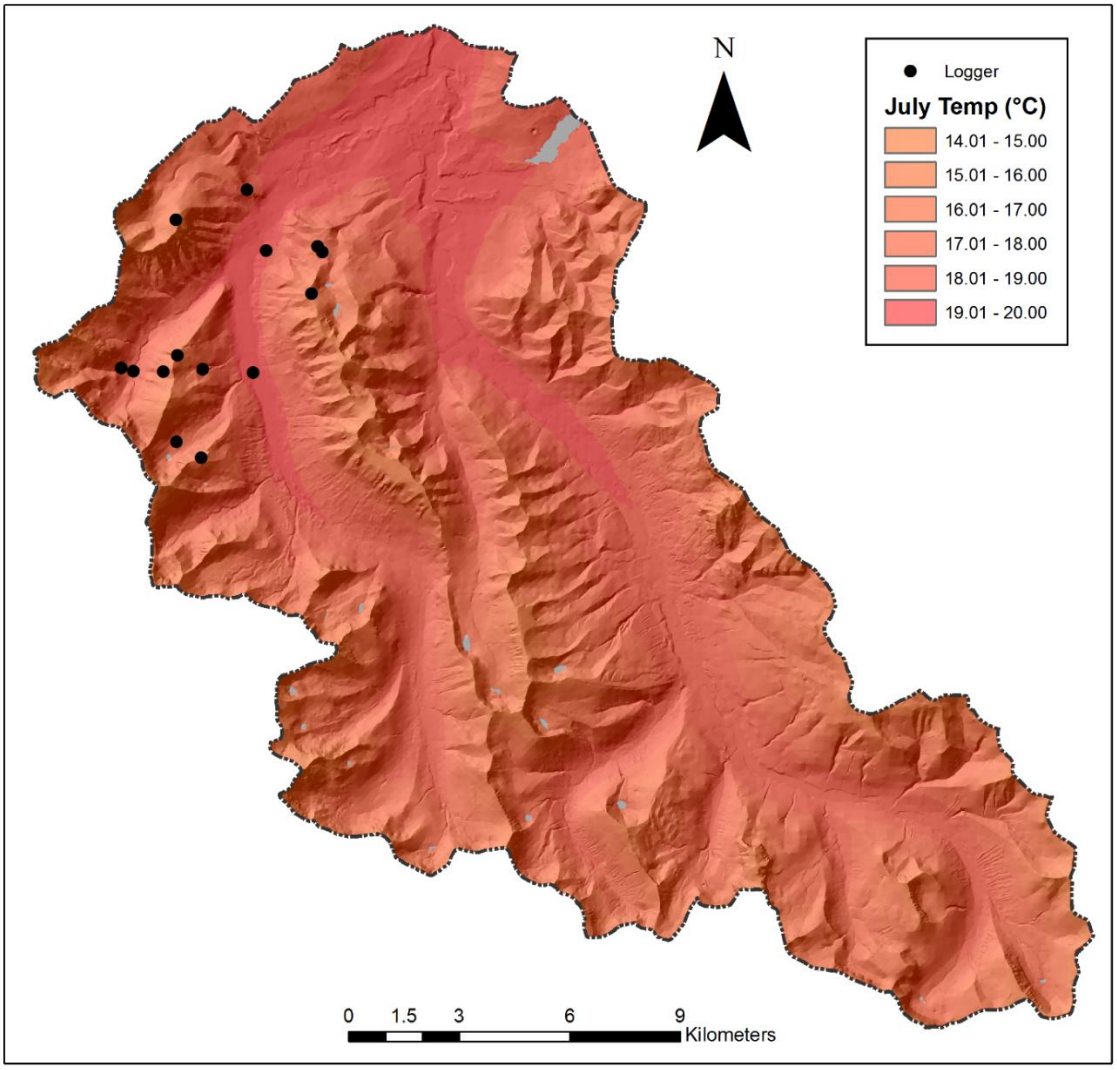

Figure 25: Average July temperature modelled across the WCW, ranging from the maximum modelled temperature of 19.49 °C to the minimum of 14.42 °C.

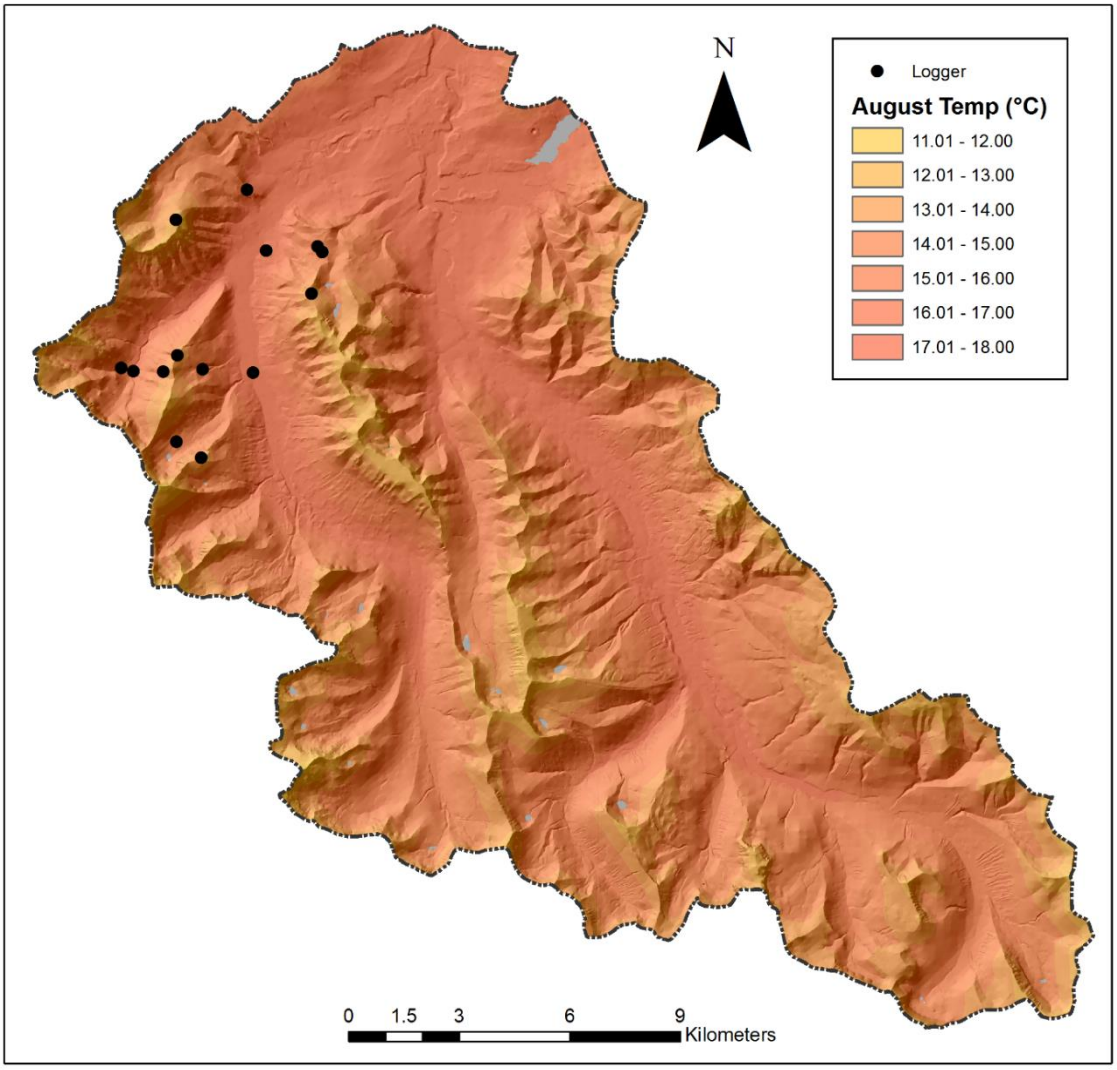

Figure 26: Average August temperature modelled across the WCW, ranging from the maximum modelled temperature of 17.01 °C to the minimum of 11.45 °C.

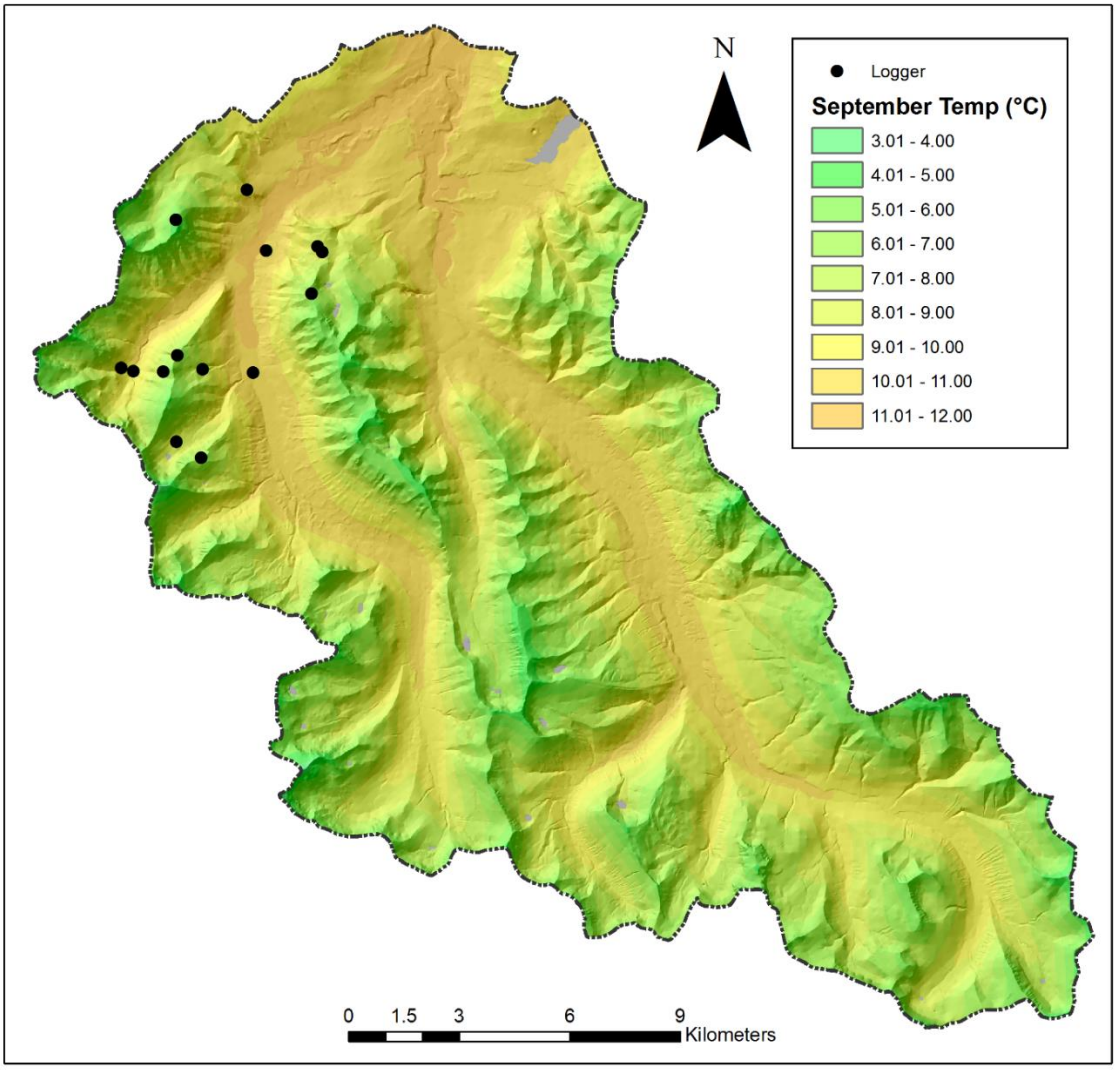

Figure 27: Average September temperature modelled across the WCW, ranging from the maximum modelled temperature of 11.46 °C to the minimum of 3.24 °C.

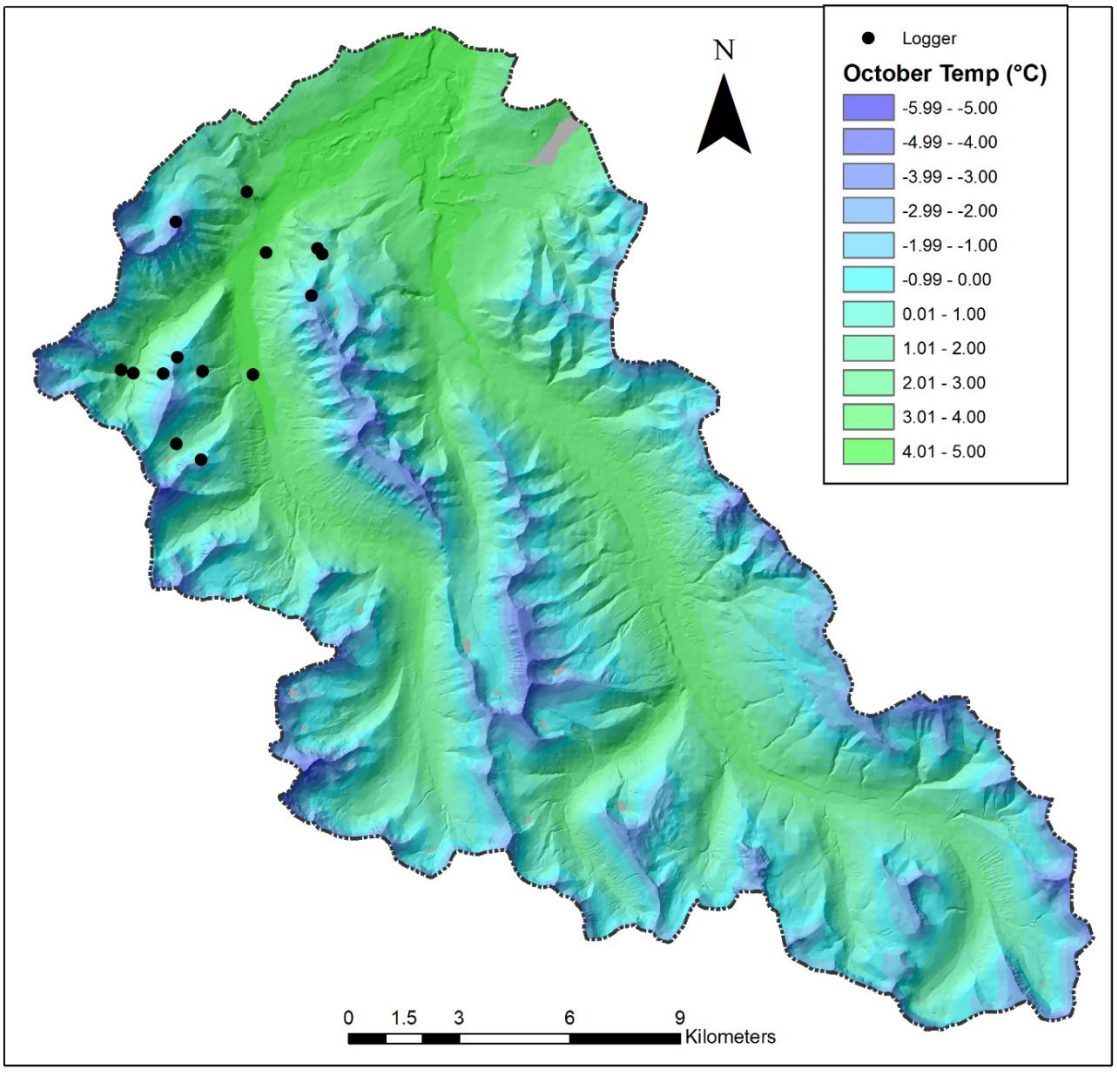

Figure 28: Average October temperature modelled across the WCW, ranging from the maximum modelled temperature of 4.65 °C to the minimum of -5.02 °C.

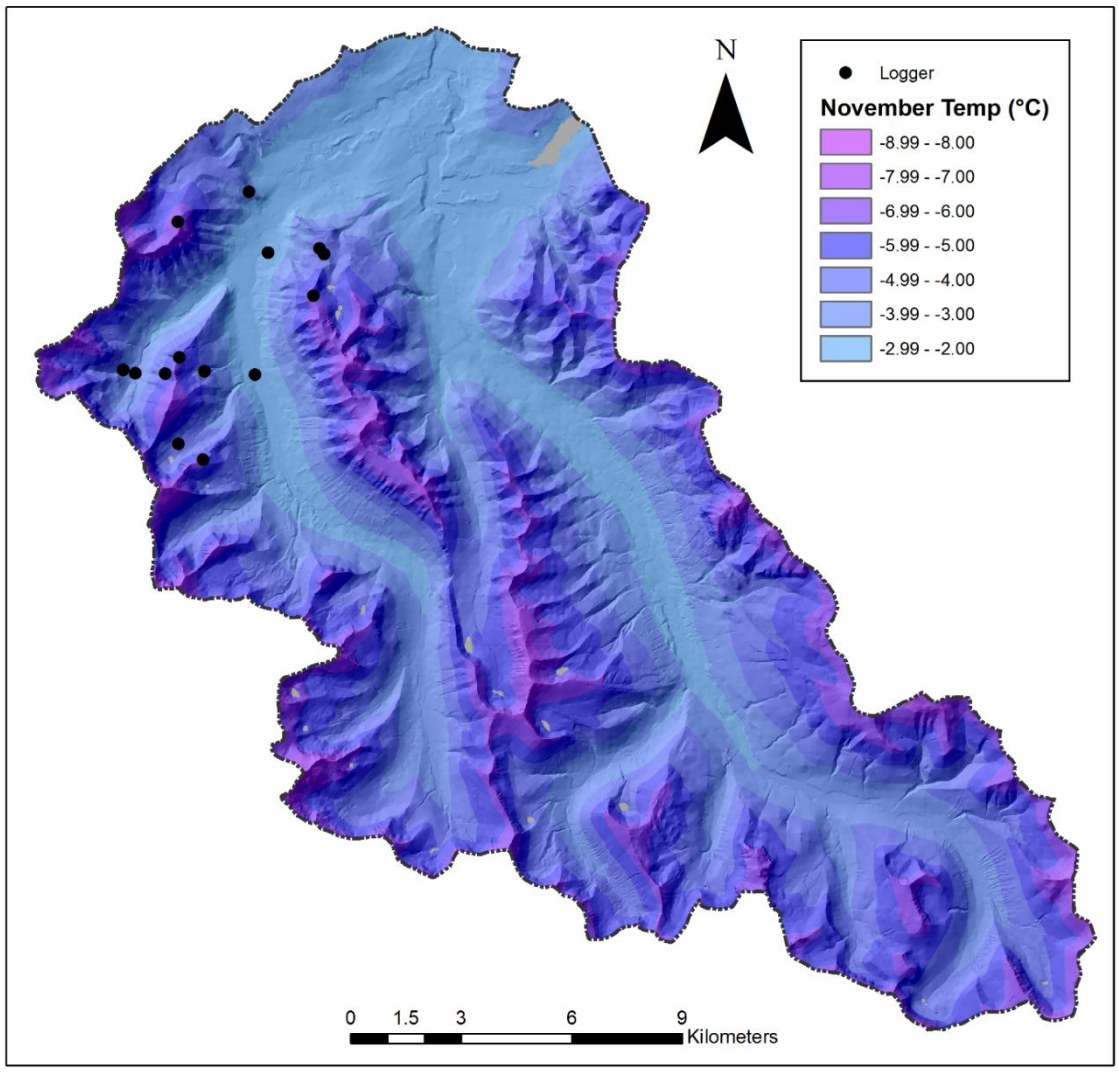

Figure 29: Average November temperature modelled across the WCW, ranging from the maximum modelled temperature of -2.08 °C to the minimum of -8.30 °C.

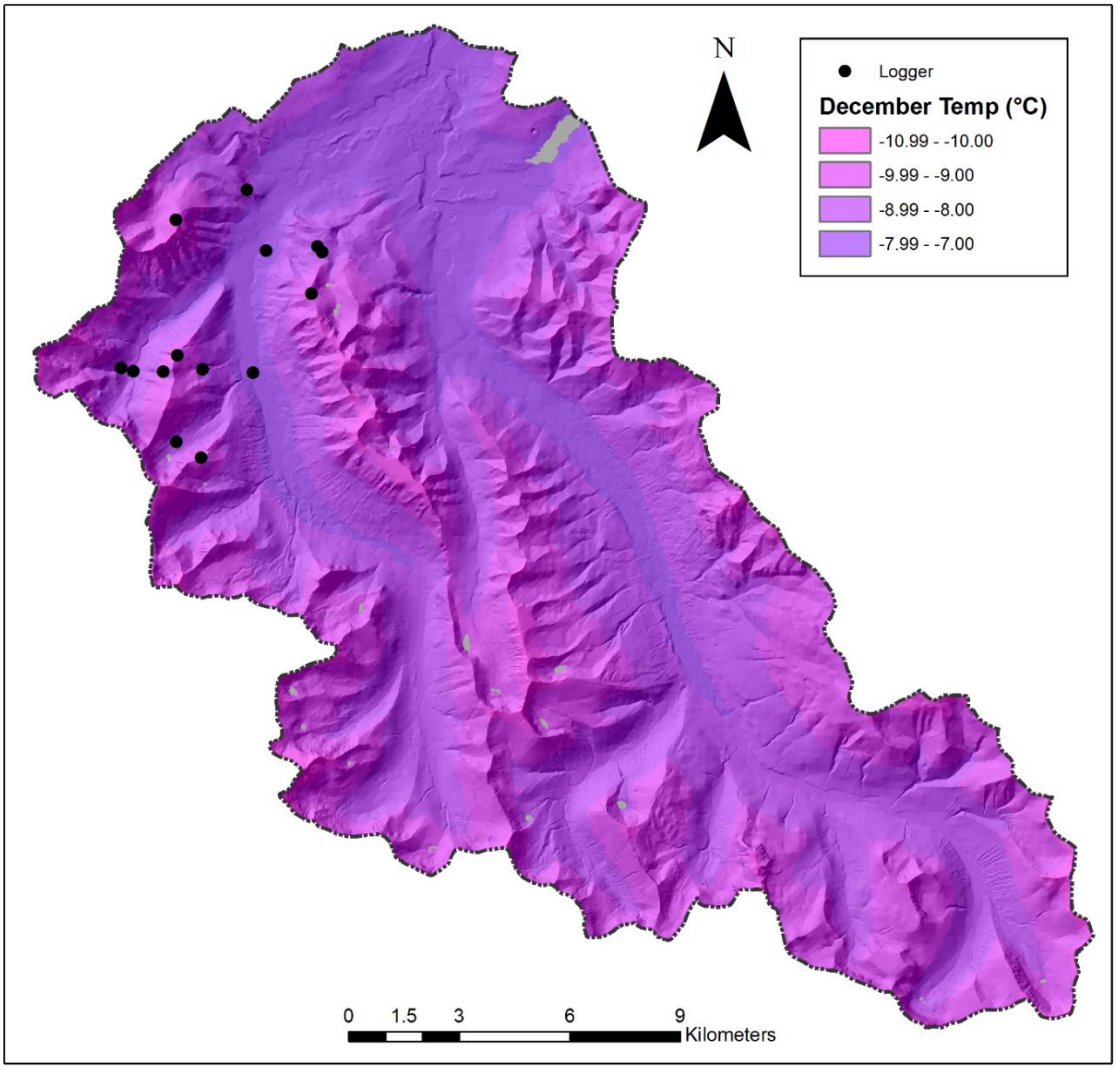

Figure 30: Average December temperature modelled across the WCW, ranging from the maximum modelled temperature of -7.57 °C to the minimum of -10.84 °C.

6.5 Perturbed Climate Models

Three IPCC climate perturbation models, RPC 2.6, 4.5, and 8.5 are presented below for three future climate normal periods (**Figure 31-33**). These models were chosen to be used because they represent three potential future radiative forcing scenarios associated with greenhouse gases emissions for low, middle, and high temperature change scenarios. The average change throughout a calendar year at each future interval for RCP 2.6 is 2.3 ˚C, 2.9 ˚C, and 2.9 ˚C for the respective climate normals of 2011-2040, 2041-2070, and 2071-2100. For RCP 4.5 the average change throughout the year is 2.2 ˚C, 3.5 ˚C, and 4.4 ˚C for the same respective climate normal periods. For RCP 8.5 the average change throughout the year is 2.4 ˚C, 4.4 ˚C, and 7.1 ˚C for the same respective climate normal periods.

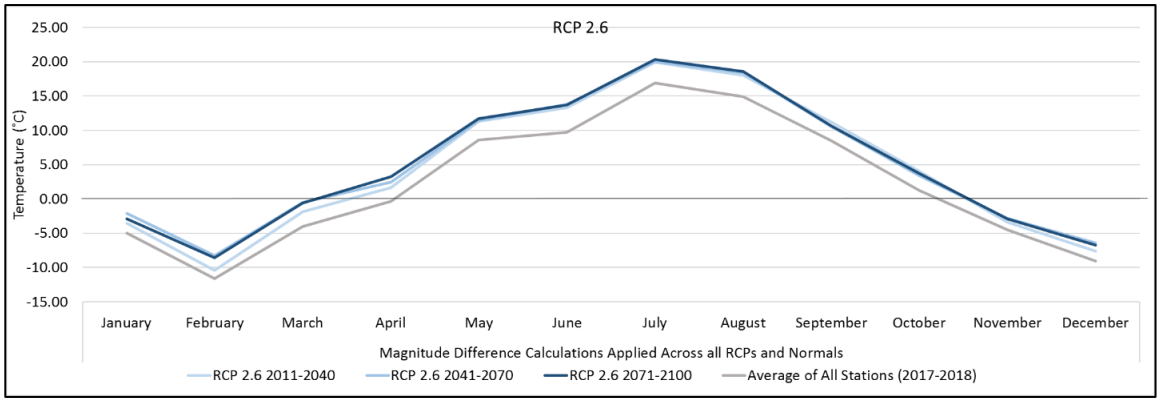

Figure 31: Measured average monthly surface air temperature perturbed along IPCC RCP 2.6 pathway to 3 future climate normals including 2011-2040, 2041-2070, and 2071-2100.

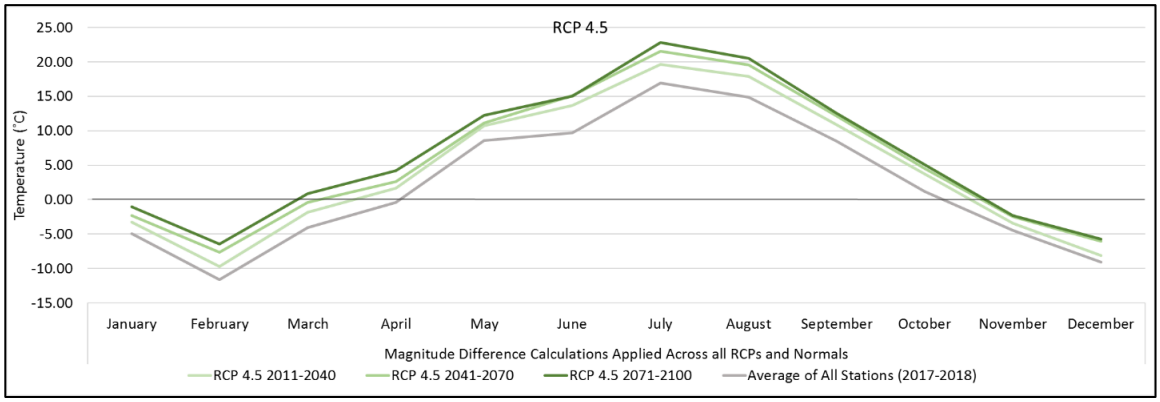

Figure 32: Measured average monthly surface air temperature perturbed along IPCC RCP 4.5 pathway to 3 future climate normals including 2011-2040, 2041-2070, and 2071-2100.

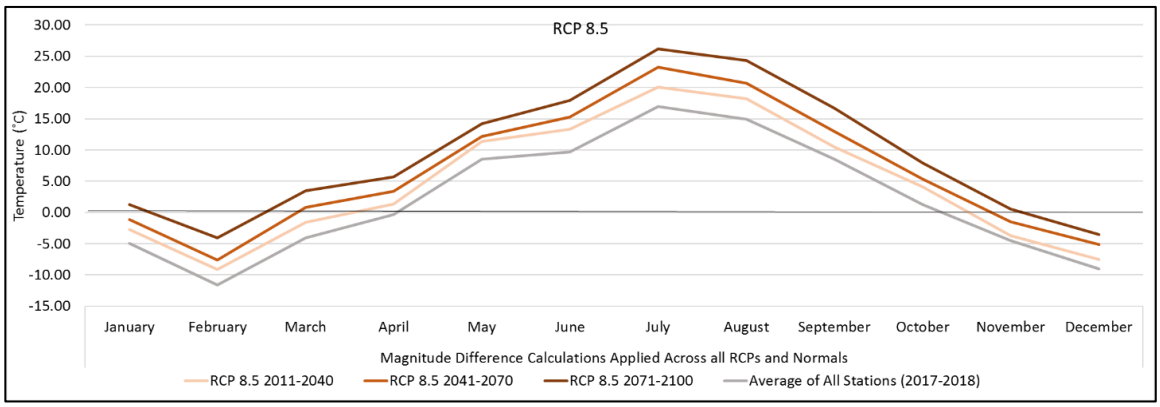

Figure 33: Measured average monthly surface air temperature perturbed along IPCC RCP 8.5 pathway to 3 future climate normals including 2011-2040, 2041-2070, and 2071-2100.

7.0 Discussion

7.1 Observed Temperature

The surface air temperature within the WCW varied daily, monthly and seasonally. Daily variability in temperature observed in the WCW presented in **Figure 15** and an average representation in **Figure 34** show temperature trends as a result of synoptic climate conditions modified by weather events, site conditions and seasonality causing daily variability. A clear distinction in variability is the difference between the maximum and minimum daily average temperature. Minimum average daily air temperatures were mostly recorded during an arctic air mass intrusion from December 29th-31st, 2017, while the coldest temperatures recorded outside of this time period were from sensors at mountain peaks and high ridge tops (WC4, WC6, WC10) (**Table 3**). The occurrence of maximum daily averages was temporally sporadic through the warmer months, though predominantly encircling an individual weather event around July 7th-8th, 2017.

Air temperature at a location may be influenced by the contributing upslope area, similar to water drainage regarding cold-air pooling, as well as the orientation of the surrounding topography (Dobrowski et al., 2009). In mountainous regions, especially within the valley bottoms, the idea of canyon geography plays a role in the redistribution of longwave radiative energy (Oke, 1987) which can influence the energy budget of a location. At mountain peaks the influence of surface area is reduced as there is minimal influential surrounding surface area that will contribute to temperature at a site, whereas, within valley bottoms, the inverse is true.

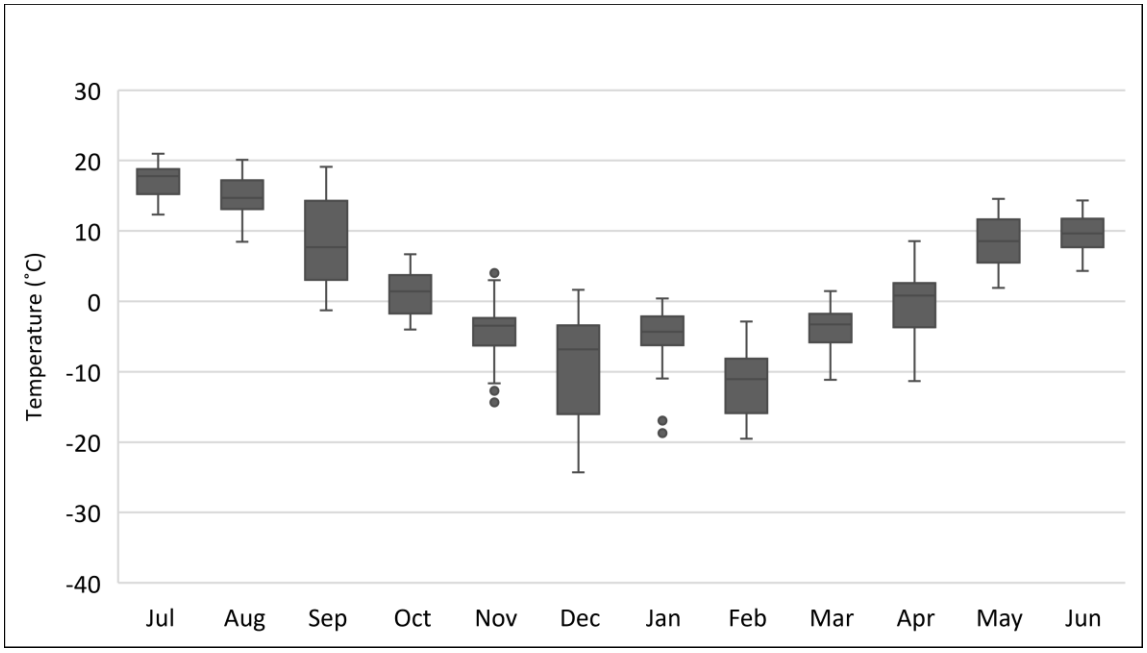

Figure 34: Box and whisker plot for the daily average air temperature throughout the study period averaged across all sensors within the watershed including mean, median quartiles, standard error, and outlying data.

A comparison drawn between the climate normal from an Environment Canada meteorological station in Beaver Mines, Alberta, and the WCW monthly temperature can give insight into typicality of the study period (**Table 13**). As January temperatures are comparable between locations (0.3 ˚C difference), both December and February deviate substantially with a difference of 4.5 ˚C and 8.0 ˚C respectively. Further, April, October, March, and November differ from Beaver Mines differ in excess of 3.0 ˚C while May – September vary 3.0 ˚C or less. This indicates colder seasons within the region as being a highly variable period of the year whereas warmer seasons vary less substantially though more data collection and observation is needed to support this further.

Table 13: Monthly average temperatures (˚C) of the WCW for the 2017-2018 study period and climate normals from an Environment Canada meteorological station in Beaver Mines, Alberta for the climate period of 1981-2010.

Month	WCW	Beaver Mines	Difference
January	-5.0	-4.7	0.3
February	-11.8	-3.8	8.0
March	-4.0	-0.5	3.5
April	-0.4	4.4	4.8
May	8.6	8.9	0.3
June	9.7	12.7	3.0
July	17.1	16	1.1
August	15.0	15.4	0.4
September	8.6	10.8	2.2
October	1.2	5.7	4.5
November	-4.5	-1.2	3.3
December	-9.1	-4.6	4.5

7.2 Surface Lapse Rates

7.2.1 SLR and Inversions

The WCW region of the Rocky Mountains is characterized by unique weather events such as chinooks and cold-air pooling (Pigeon & Jiskoot, 2008). While the influences of chinooks in the region have been studied in detail (Nkemdirim, 1986; Nkemdirim, 1996; Nkemdirim, 1997) the presence, characteristics, and nature of inversions and inverted SLRs have had significantly less attention. Studies farther to the north have examined the significance of inversions within high-latitude mountainous regions of western Canada concerning permafrost distribution (Lewkowicz & Bonnaventure, 2011). The characterization of inversions in lower-latitude regions is necessary to properly understand and draw a comparison between the SLRs in mountains of both mid-latitude and higher-latitude regions, as well as providing data for local and regional climate models focusing on similarly affected complex terrain. Inversion prone landscapes may also influence the current distribution of flora and fauna sensitive to

extreme minimum temperatures, exemplified by species such as the Mountain Pine Beetle (*Dendroctonus ponderosae*) as regions prone to inversions may, more frequently, experience limiting temperatures to sensitive species (Safranyik, 1978). In contrast, these landscapes may impact the future distribution of species in the form of a climatological refugia as a result of consistent cold-air drainage into valleys providing a climatological niche for species buffered against the warming surrounding landscape (Lundquist et al., 2008).

Within the WCW, it was found that there were no inversion events that were frequent enough or persisted long enough to invert the SLR at the monthly scale, as seen farther to the north, although inversions were still present throughout all months in the study period. While the influence of inversions on average monthly temperatures was minimal, as the time step of interest is increased in resolution the importance of the influence of inversions also increases. This is not true for northern regions where inversions are extremely stable during the dominant winter season (Bonnaventure & Lewkowicz, 2013). While inversions are not stable, nor persistent on the landscape of the WCW for long enough to outweigh the influence of a normal SLR, they may contribute to the modification of recreation (skiing/snowshoeing) and faunal behaviour including habitat selection and migration corridors of temperature sensitive species.

The SLRs observed through the work of Cullen and Marshall (2011) using the Foothills Climate Array (FCA) are compared in **Table 14** against SLRs observed within

the WCW. The FCA extends from regions East of Calgary, Alberta into the Rocky Mountains to the Continental Divide to the west, encapsulating similar topography and experiencing similar weather and climate as the WCW.

Table 14: Average monthly SLRs observed in the WCW for the year 2017-18 compared against the average monthly SLRs observed at the FCA for the time period of 2005-09 (Cullen & Marshall, 2011).

Month	**Average Monthly SLR (°C km^{-1})**	**Monthly SLR (FCA) (°C km^{-1})**	**Difference (°C km^{-1})**
January	-5.8	-2.3	-3.5
February	-2.2	-1.5	-0.7
March	-6.9	-4.1	-2.8
April	-3.9	-5.6	1.7
May	-2.9	-6.6	3.7
June	-4.5	-5.8	1.3
July	-4.2	-4.6	0.4
August	-4.0	-4.5	0.5
September	-7.3	-4.9	-2.4
October	-8.0	-3.7	-4.3
November	-4.6	-3.7	-0.9
December	-2.3	-2.6	0.3
Average	-4.7	-4.2	-0.6

The difference in observed SLRs between the two study areas is most notable in the month of October where there is a difference of -4.3 °C km^{-1} followed closely by May and January, with a departure of 3.7 °C km^{-1} and -3.5 °C km^{-1} respectively. These differences could be as a result of weather extremes occurring during the WCW study period and the moderating effect of the FCA data being an average of four years. Further, the difference could be also be attributable to, in part, chinooks that occur with more frequency in southern Alberta compared to more northern regions (Nkemdirim, 1996).

Daily SLR signals were also compared monthly to observe if seasonal patterns were apparent in the winter months (**Figure 35**).There are no periods of time that are on average inverted, though the observed SLRs are substantially lower than the often assumed SLR of -6.5 ˚C km^{-1} (Minder et al., 2010) (**Table 6**). This highlights potential drivers and controls on inversions between seasons where in the summer they are driven by the diurnal cycle and solar heating whereas during the winter they are more driven by regional or synoptic weather conditions in addition to solar influences. This leads to the dissimilar average January SLR observed as a result of frequent chinooks.

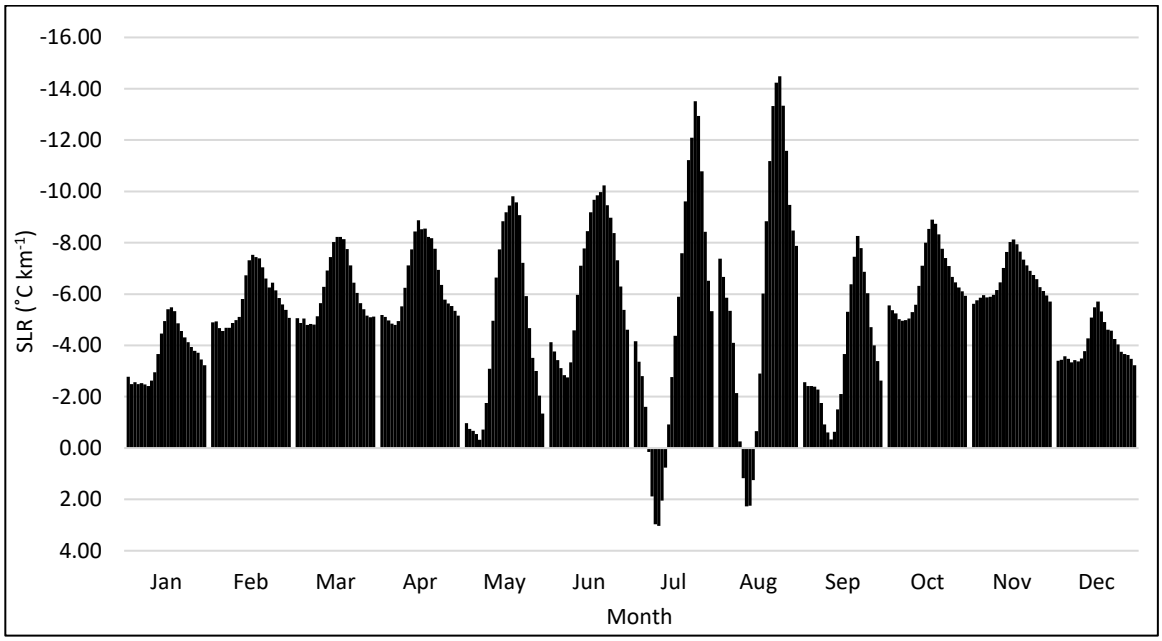

Figure 35: Hourly surface lapse rates of WCW throughout the period of the study separated into monthly averages.

SLRs were also derived for above and below treeline following studies that highlight the different SLRs exhibit in these regions (Lewkowicz & Bonnaventure, 2011).

The average daily SLR signal shown between above and below treeline regions exhibits an opposing relationship (**Figure 36**). On average, regions below treeline only experienced a normal SLR during periods of the day with strong solar radiation. At the same time, above treeline SLRs experience two hours of slightly inverted lapse rates, potentially as a result of solar radiation only being cast upon the exposed upper portion of the topography. This difference in SLRs at treeline has been noted in research by Bonnaventure and Lewkowicz (2013) citing the difference in mixing capabilities in these two regions as a possible explanation.

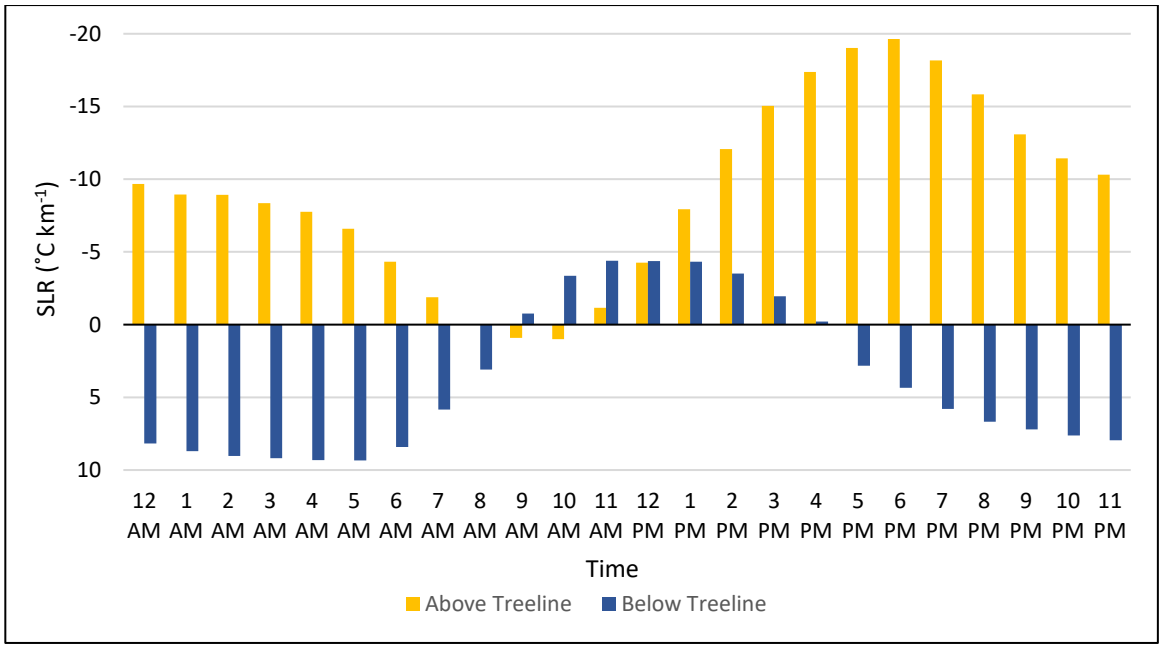

Figure 36: The average hourly SLR observed for each hour within a day throughout the year differentiated between above and below treeline regions within the WCW.

Daily inversion frequency showed a seasonal signal (**Figure 17**, **Figure 37**) where the period of April – September displayed a strong diurnal cycle where inverted SLRs occurred most frequently in the early morning hours, contrasted by the period October –

March that showed a muted diurnal signal and are more consistently present throughout the day. April – September saw 904 hours (10.3 % of the year) of inverted SLRs within the WCW sensor network whereas the October – March period only 715 hours (8.2 % of the year) consisted of inverted SLRs representing a total of 18.5 % of the year within the WCW. This differs substantially from locations in the far north where inverted winter SLRs have been observed to occur more than 50 % of the time (Smith & Bonnaventure, 2017).

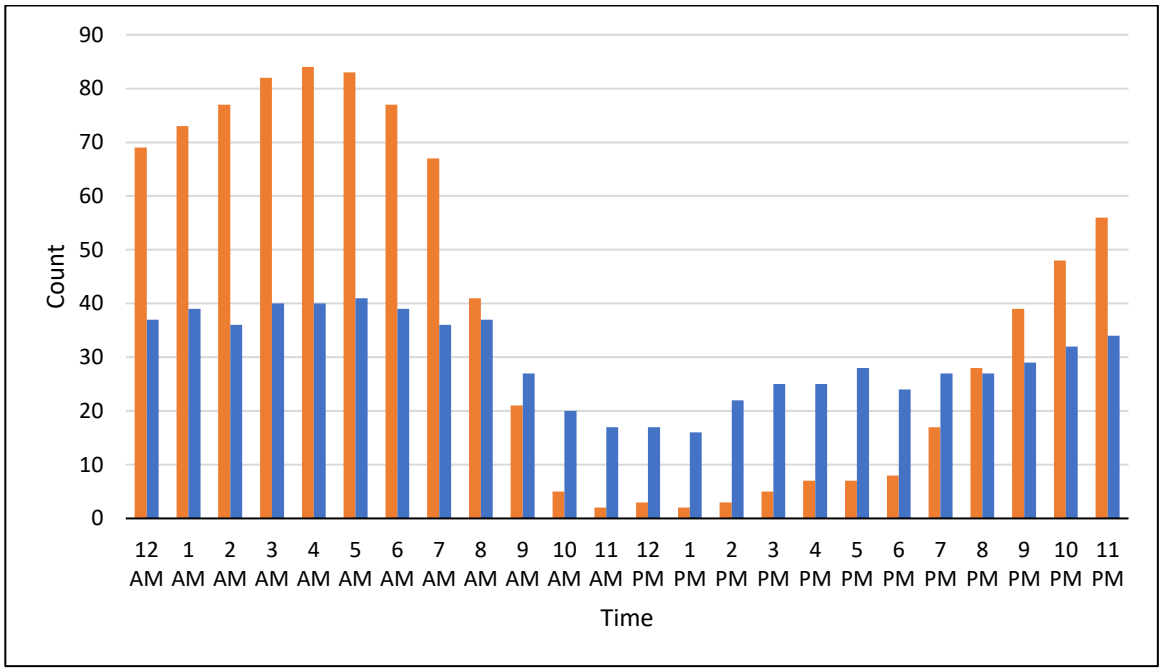

Figure 37: Frequency of inverted surface lapse rate presence binned hourly over a day compared between the warm season months of April to September (orange) and cold season months of October to March (blue) within the WCW.

7.2.2 Chinooks

A common meteorological event in Southern Alberta is the Chinook related to other winds in other parts of the world such as the Foehn, North-wester, and Berg of Europe, New Zealand, and South Africa respectively (Nkemdirim, 1986; Nkemdirim, 1996). These events are driven by the relationship between prevailing winds such as the Westerlies, and the topography of a region that generally is perpendicular to the flow of air (Nkemdirim, 1996). Chinooks events are commonly associated with a sharp increase in air temperature to an unseasonably warm high followed by an equally sharp return to a cooler temperature (Nkemdirim, 1996). For the WCW study region, these patterns were observed frequently (**Figure 38**-**39**). Accompanying this pattern, there is an increase in gusty westerly winds, and a drop in relative humidity level (62 % to 47 %) (Brinkmann, 1970; Nkemdirim, 1996; Cullen & Marshall, 2011). To assess the unique SLR observed in January of 2018 (**Table 6**) in contrast to the adjacent winter months of December 2017 and February 2018 chinooks were identified as a possible explanatory mechanism (**Figure 41**).

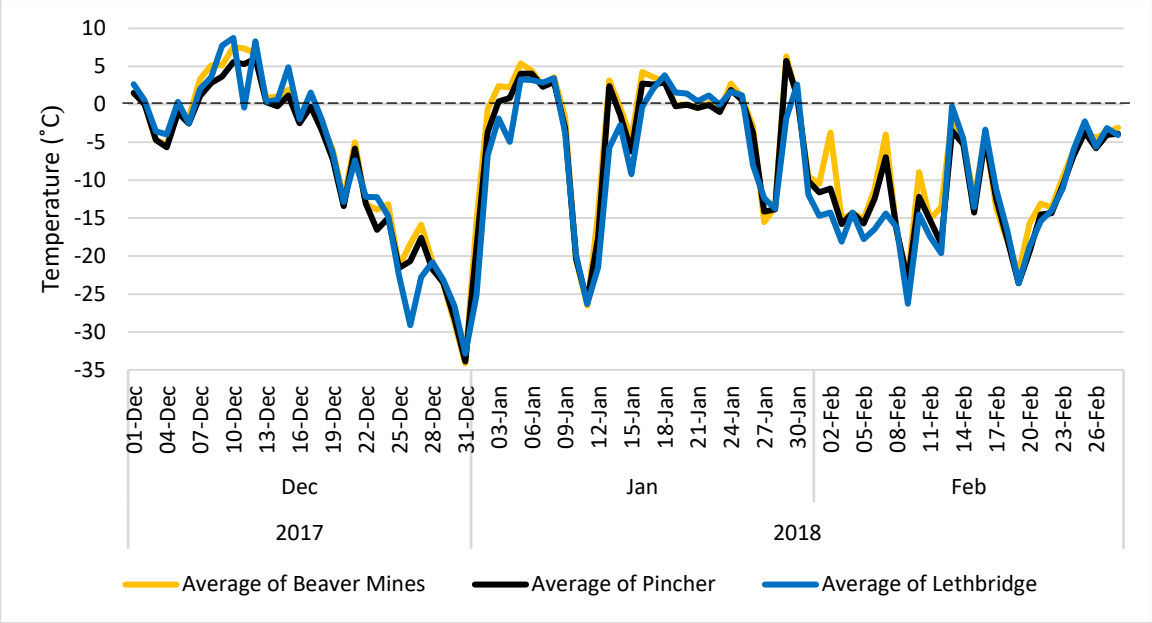

Figure 38: Average daily air temperature of an East-West transect of government climate stations adjacent to the study area throughout December 1st, 2017 to February 28th, 2018.

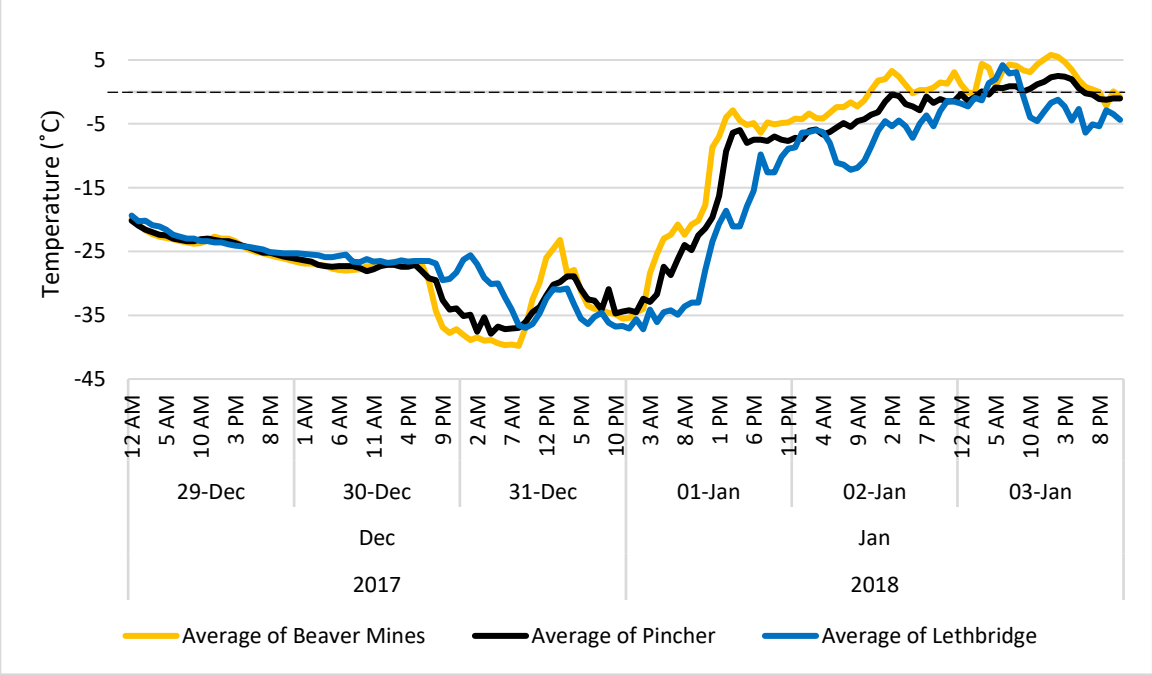

Figure 39: Inception of a singular chinook event in the morning of January 1st, 2018 in a region adjacent to the WCW study area showing the lag period between chinook onset in this East-West transect as well as highlighting the spike in temperature associated with chinooks.

In January 2018, four chinook events were subjectively identified based on several characteristics. These included indicative chinook patterns such as: 1) periods of a sharp temperature increase, 2) a commensurate decrease in relative humidity, 3) an increase in wind speed, as well as, 4) a change in wind direction towards predominantly gusting from the west. These identified events encompassed 77.4 % of the month of January (**Figure 41**) bringing the average daily air temperatures in the WCW above 0 ˚C at times. This is substantiated by the monthly temperatures of the WCW sensors (**Table 4**) where the average surface air temperature is was observed to be -5.0 ˚C in January in comparison to December and February at -9.1 ˚C and -11.8 ˚C respectively. Nkemdirim (1996) found that chinook-rich winter seasonal averages had temperatures greater than -5.0 ˚C, and while the seasonal average does not exceed -5.0 ˚C, the January average does. Accompanying chinook events are high wind and turbulent air masses that are channelled down and through the East-West trending valley of the Rocky Mountains (Nkemdirim, 1986; Nkemdirim, 1996). This event coupled with the winter prevalence of inverted SLRs can lead to a unique interaction where the turbulence of chinook winds may result in the break-up and sequestration of cold-air pooling and drainage.

December and February show little to no change in SLR across topography within the WCW while in January, influenced by chinooks, shows a seemingly normal SLR development (-5.8 °C km^{-1}). The influence of chinooks not only modifies the average air temperature within the watershed, but changes the relationship between temperature and elevation away from what might be expected in a chinook-weak winter. In the past 113 years, there have only been ten instances where the monthly average temperature of

January is above -5.0 ˚C, and only two instances where the seasonal winter average is greater than or equal to -5.0 ˚C in the WCW (**Figure 40**). These data were derived from ClimateNA records (Wang et al., 2016). This means that, while it is showing a temperature anomaly, it also represents a substantial shift towards a normal SLR.

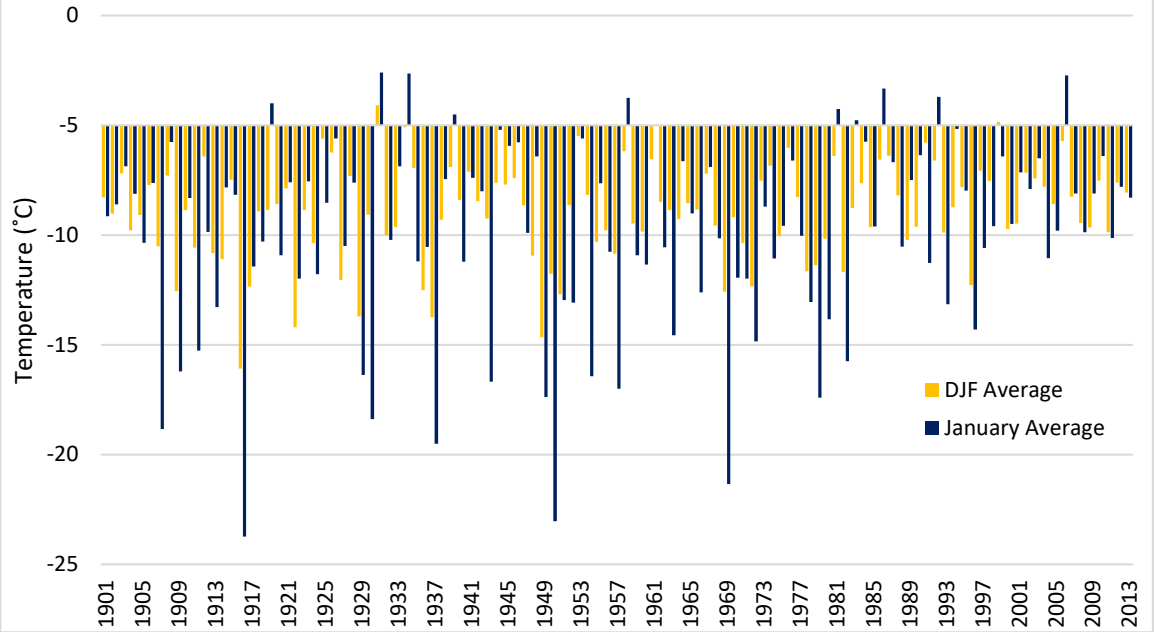

Figure 40: Winter average and January average temperatures over from 1901 to 2013 derived from ClimateNA (Wang et al., 2016) for the WCW region.

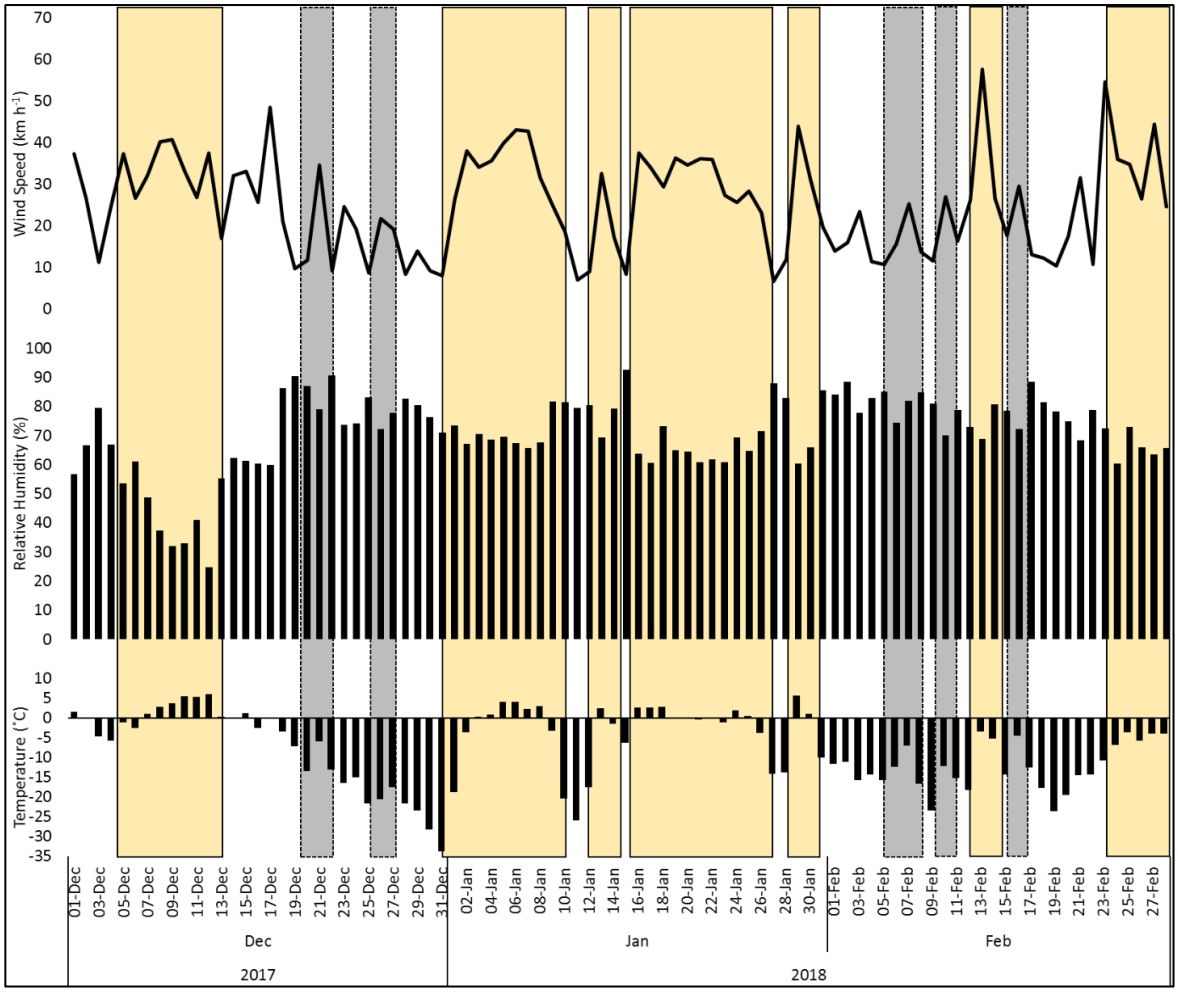

Figure 41: Identification of potential chinook events using daily average wind speed and direction, relative humidity, and temperature between December 1st, 2017 and February 28th, 2018 where solid yellow boxes denote discernable chinook events and dashed grey boxes denote chinook events with a less observable unique signal lasting for a short period. Data from Pincher Creek Climate Station, data provided through Alberta Climate Information Service.

7.3 Regression Models

The statistical significance of the models generated for this research is inconsistent and variable (**Table 7-9**). Only when temperature was regressed against elevation was the statistical significance of the relationship consistent **(Table 7)** where only the months of July, April, and May were found to have P-values greater than 0.05. This indicates that during these warm summer months there are other explanatory variables that can be used in conjunction with elevation to appropriately model temperature within the watershed. Aspect, TPI, PISR, and slope proved to be poor predictors of temperature **(Table 9)** and only TPI yielded any statistically significant relationships, though inconsistent. Treeline, in conjunction with elevation, also was significant throughout much of the study period though it was inconsistent for both above and below treeline, as well as temporally **(Table 10).** With such a small number of stations within the region and only one season of data being analyzed, the variability of the data collected may influence the significance of the explanatory variables as a result of weather events. Continued collection of data in concert with additional sites and an improved sampling distribution within the network would serve to reduce the variability in model performance and significance as well as improve statistical significance. Analysis and inclusion of further potential explanatory variables such as potential solar radiation, albedo, and evapotranspiration would be appropriate and potentially improve the spatial models. This is especially true with concern to solar radiation, as it was found that the placement of stations had an intrinsic bias where the relationship between temperature and PISR was found to decrease with increasing PISR.

7.4 Spatial Models

To gain further insight into the interpolated surfaces, the mean surface air temperature was calculated for elevational bands of 100 m within the watershed. By doing this, the noise of the surface is muted and relationships between elevation, time of year, and temperature can be observed specifically in regards to slope of the lapse rate (**Figure 42**). The expected signal of a seasonal shift in air temperature is observed, but so too is the elevational influence especially during the cold dominant months. The chinooks occurring during the winter months (**Figure 41**) seem to be a substantial driver in the SLRs regionally, represented not only in the SLRs observed (**Table 6**) but also the elevational shift in modelled SLRs derived for the WCW (**Figure 42**). It is to be noted that December and February have very little change and no definite pattern of cooling in average temperature with elevation whereas January exhibits a strong, normal elevational SLR (**Figure 42**) in response to the presence of chinooks. January through April all show a slight average cooling effect being modelled at the lowest elevations, potentially indicating inverted lapse rates present within this 200 m elevation region.

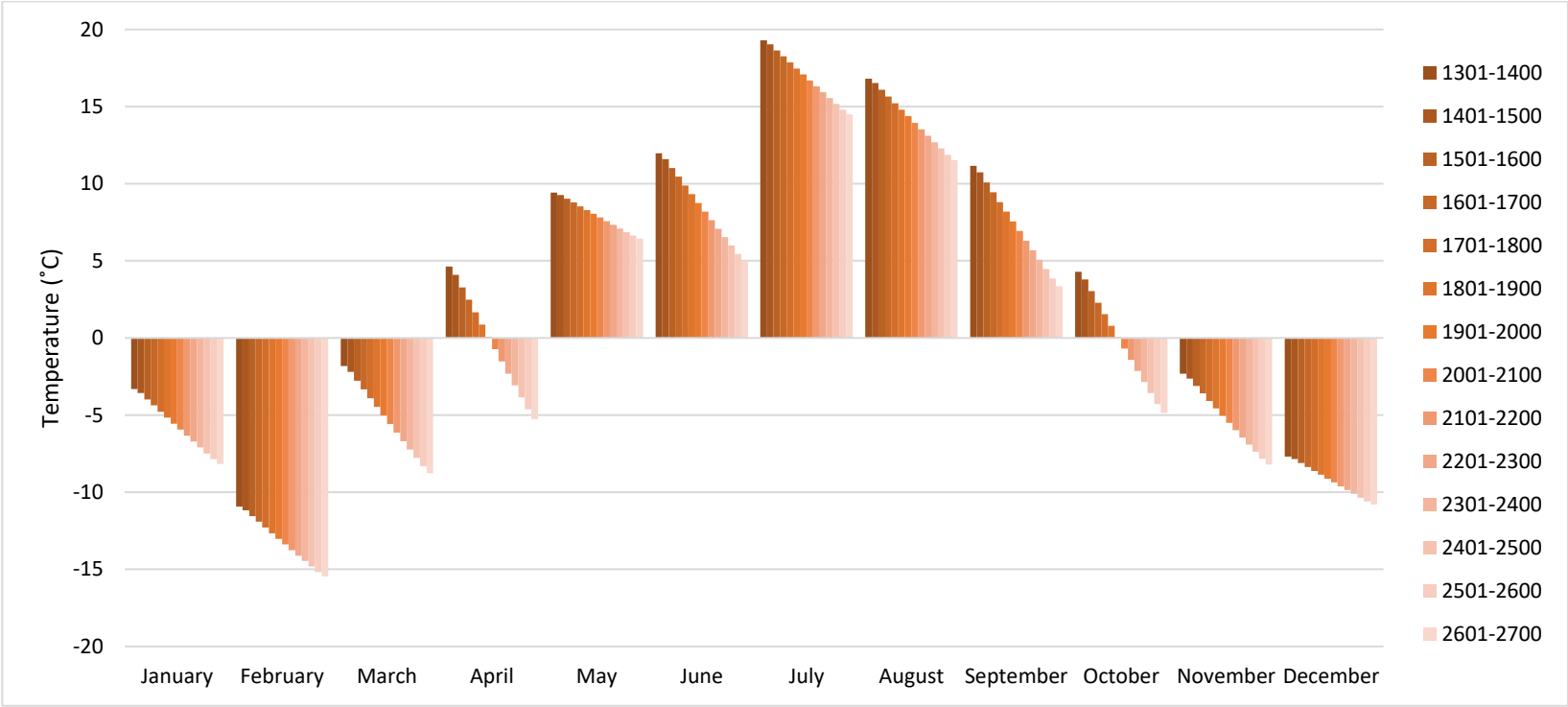

Figure 42: Modeled air temperature averaged within 100 m elevational bands across the WCW exhibiting the variable slope of the modelled lapse rates.

7.5 Model Comparison

To draw attention to potential oversight when modelling, especially as a result of large and unrepresentative cell sizes within regions of complex topography, a comparative analysis was done by determining the difference between small-scale models against the models generated through this research (**Figure 43-45**). It is to be noted that while there is only one year of data being compared to models that are derived from multiple years of data, this analysis still provides insight into seasonal or annual over or underestimation of temperature as a result of the complex topography not being represented within the cell size of broader models. Further, the differences seen between models may be also as a result of error or uncertainty in the models derived through this research.

The statistics drawn from the differential surfaces, presented in **Table 15**, provide insight into where the larger models are the furthest away from the spatial models specifically generated for WCW. The Alberta specific model by Kienzle (2017) aligns well, on average, with the WCW model when compared annually where the mean difference between models is 0.42 ˚C. Seasonally this is not true, where in summer and fall the mean was -1.51 ˚C and -2.74 ˚C respectively while in winter and spring the mean was 2.90 ˚C and 2.47 ˚C respectively. This shows that there is a seasonally biased difference between models. In winter and spring, Alberta Climate Records modelled warmer temperatures while in summer and fall cooler temperature were modelled. Differential surfaces comparing ClimateNA to the WCW models, showed a bias to cooler

temperatures as the mean difference was -0.95 ˚C. In summer and fall seasons, models for this research derived temperatures at mountain tops that were cooler than Alberta Climate records modelled while also modelling warmer valleys, though mid-slope regions were within one degree of difference. The foremost deviation between the two models for these months is the valley temperature being underestimated. The discrepancy for winter and spring seasons is the inverse where Alberta Climate Records model predicted warmer temperatures across the WCW in comparison to the WCW specific models. Mid slopes and valley bottoms in specific cells were within one degree of difference while the remainder predominantly overestimated temperatures in the watershed. ClimateNA model difference surfaces are predominantly underestimating temperature throughout the watershed. Underestimated temperatures are constrained to valleys for the most part while temperatures are overestimates at mountain tops. The model aligns well in mid-slope regions as well as relatively flat topographic regions of the watershed. As ClimateNA data used to derive these difference surfaces is from the climate normal of 1961-1990, the differences observed could be an indication of climate change or the variability of a single year compared to an average of 30.

The spatial surface air temperature models presented within this work contain orders of magnitude more data in contrast to both the Alberta Climate Records dataset and ClimateNA as a result of modelling at a resolution of 10 m × 10 m. Both Alberta Climate Records and ClimateNA datasets lack in their ability to describe the variability present within mountainous regions as a result of size of cells (**Table 15**). For example in a single cell of ClimateNA, the elevation range present is 1459 m - 2502 m and the

modeled temperature is 1.0 ˚C whereas the models for this research provided an expected range in AMAT of -1.2 ˚C – 3.9 ˚C. In a single cell of Alberta Climate Records elevation ranges from 1385 m – 2613 m, modeled an AMAT temperature of 1.1 ˚C, while the expected range of temperature modeled through this research was -1.7 ˚C – 4.3 ˚C.

Table 15: Differential surface statistics between ClimateNA (Wang et al., 2016) and Alberta Climate Records (Kienzle, 2017) and spatial models derived for this research.

	Max	**Min**	**Mean**	**Standard Deviation**
Alberta Climate Records				
Annual	4.90	-3.14	0.42	1.52
DJF	6.18	0.12	2.90	1.18
MAM	7.44	-1.50	2.47	1.70
JJA	2.67	-4.76	-1.51	1.40
SON	2.75	-6.98	-2.74	1.82
ClimateNA				
Annual	2.91	-3.16	-0.95	1.17

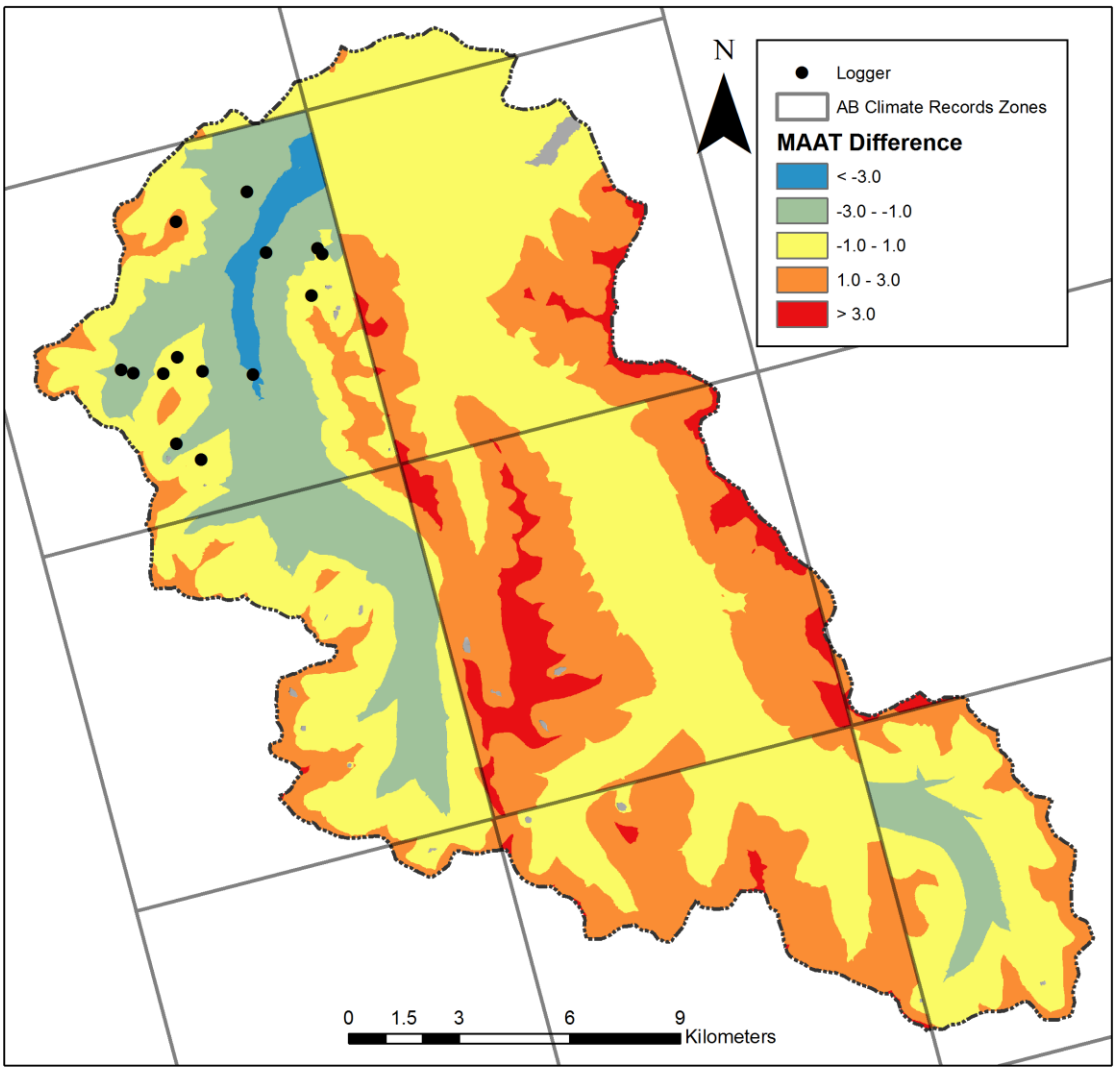

Figure 43: Difference of AMAT derived for this study area and MAAT for the 1970-2010 climate period prepared by Kienzle (2017) following the work of Hutchinson et al. (2009), blue indicates regions where Alberta Climate Records modelled a cooler temperature, and red regions show places modelled to be warmer in contrast to surface air temperature derived for this research. Yellow indicates places within one degree (°C) of difference. The grid shows the cell size of the comparison model (10 km by 10 km).

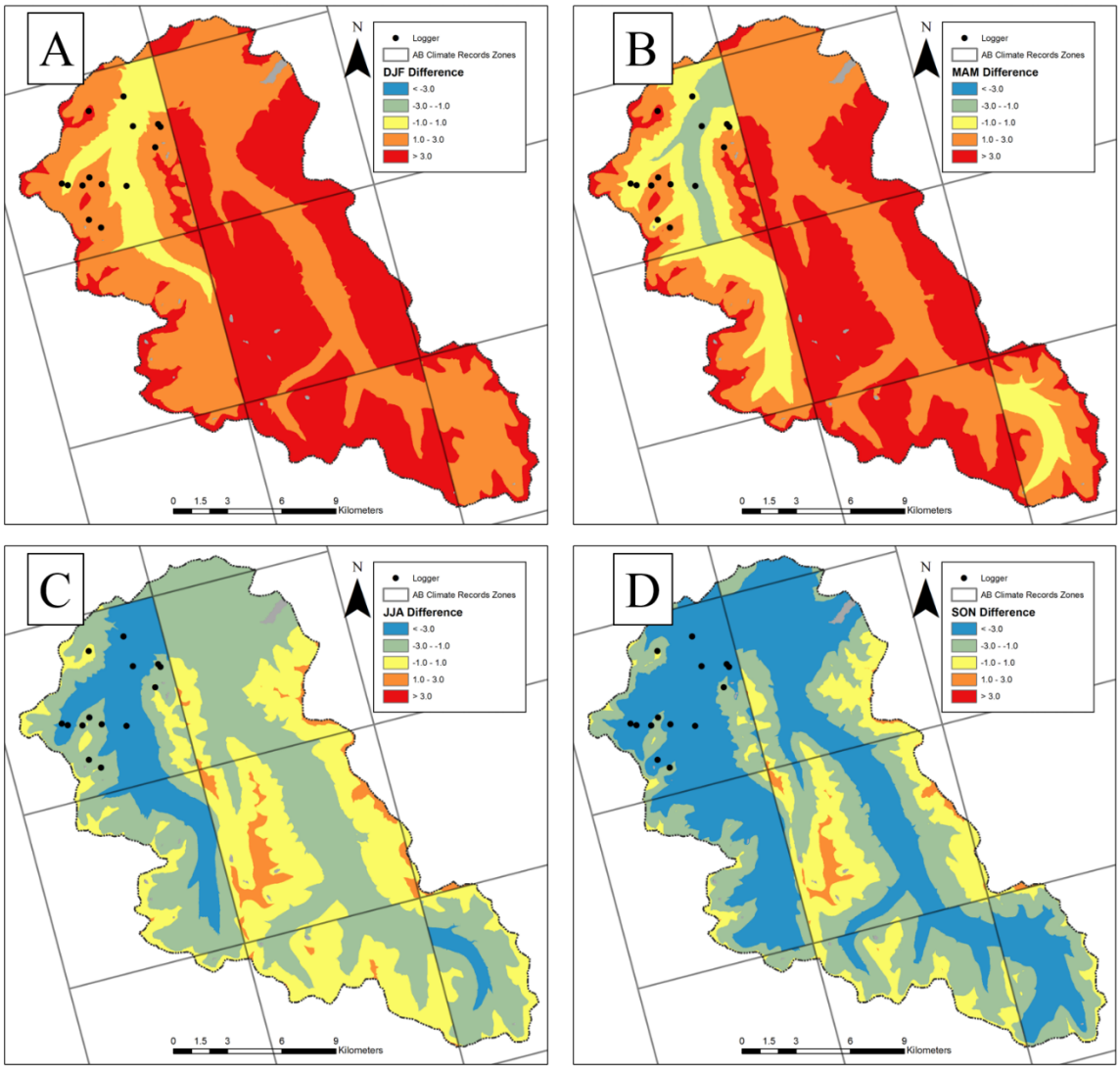

Figure 44: Difference of seasonal mean temperature derived for this study area and seasonal mean temperature for the 1970-2010 climate period prepared by Kienzle (2017) following the work of Hutchinson et al. (2009). **44A)** Winter: DJF, **44B)** Spring: MAM, **44C)** Summer: JJA, **44D)** Fall: SON. Blue colours indicate regions where Alberta Climate Records modelled a cooler temperature, and red regions show places modelled to be warmer in contrast to surface air temperature derived for this research. Yellow indicates places within one degree (˚C) of difference. The grid shows the cell size of the comparison model (10 km by 10 km).

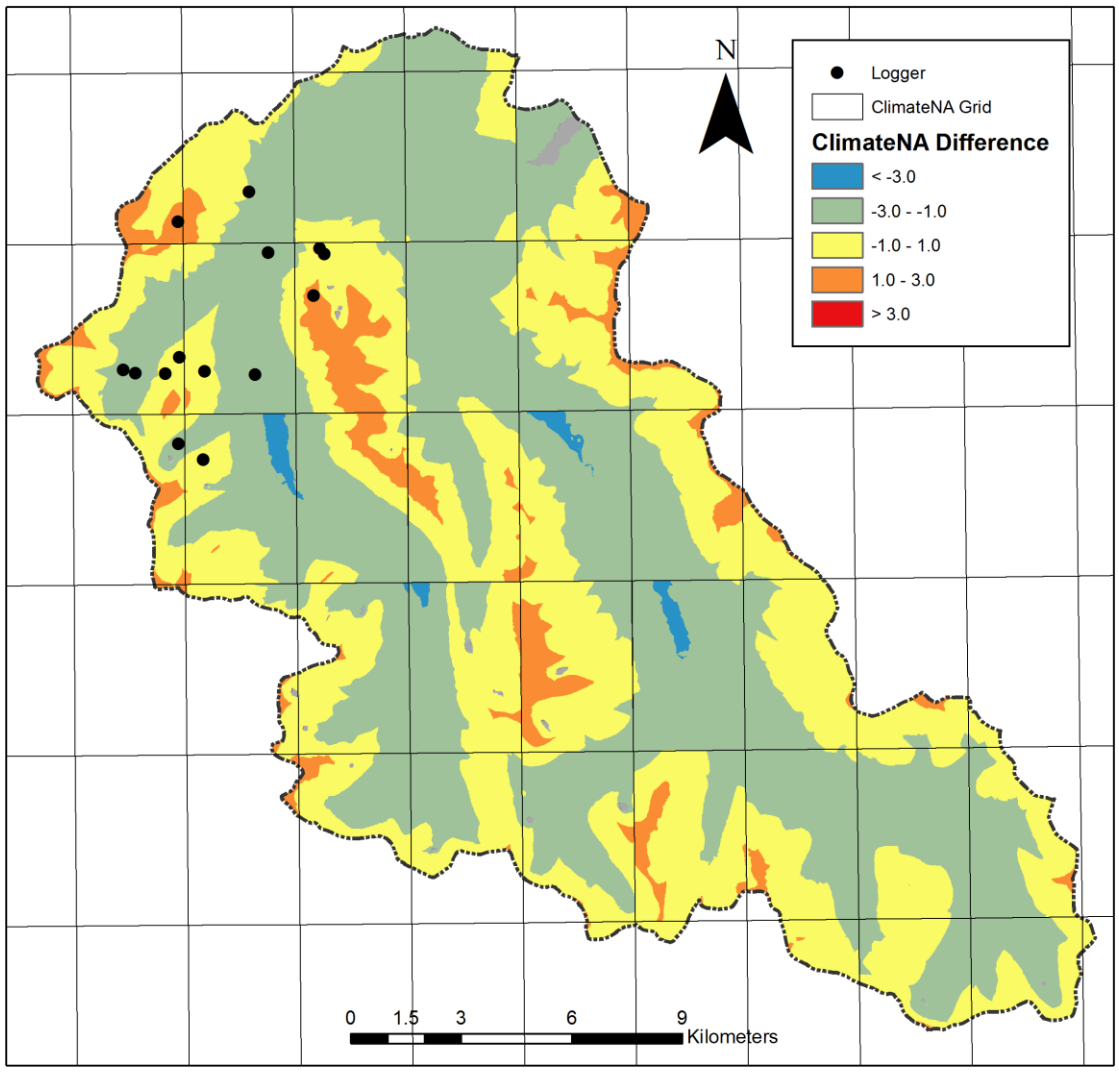

Figure 45: Difference of AMAT derived for this study area and MAAT for the 1961-1990 climate period prepared by Wang et al. (2016) blue colours indicate regions where ClimateNA modelled a cooler temperature, and red regions show places modelled to be warmer in contrast to surface air temperature derived for this research. Yellow indicates places within one degree (˚C) of difference. The grid shows the cell size of the comparison model (4.65 km by 3 km).

7.6 Perturbed Models

The rate of change along the three RCP models is variable both between months as well as between models (**Figure 31-33, Table 16**) with an expected average temperature change of 7.10 ˚C by the 2071-2100 climate normal along RCP 8.5 in contrast to the 1981-2010 climate normal. RCP 2.6 shows slight cooling trends by the same period where the expected average change is 2.89 ˚C from the 1981-2010 climate normal. This is a slight improvement over the expected average change of 2.92 ˚C for the climate normal of 2041-2070. For future models, the change does not occur equally throughout the year, where some months experience accelerated, or decelerated warning based upon the RCP model (**Table 19**). RCP 2.6 and 4.5 models exhibit a reduction in their potential rate of change between the climate normal of 2041-2070 and 2071-2100 while the rate of change for RCP 8.5 continues to increase (**Table 19**).

Table 16: Difference in air temperature between the 1981-2010 climate normal and various future RCP model perturbations (Wang et al., 2016).

Climate Normal	Jan	Feb	Mar	Apr	May	Jun	Jul	Aug	Sep	Oct	Nov	Dec	Ave
RCP 2.6													
2011-2040	1.37	1.15	2.17	2.00	2.77	3.63	2.98	3.08	2.76	2.84	1.06	1.46	2.27
2041-2070	2.05	3.04	3.44	3.58	3.15	4.05	3.38	3.70	2.21	2.54	1.61	2.30	2.92
2071-2100	2.88	3.32	3.57	2.80	2.88	4.09	3.12	3.47	2.13	2.20	1.64	2.61	2.89
RCP 4.5													
2011-2040	1.69	1.93	2.18	2.03	2.18	3.95	2.68	2.95	2.39	2.52	1.05	0.95	2.21
2041-2070	2.62	3.97	3.66	3.01	2.53	5.43	4.65	4.63	3.70	3.29	2.02	2.99	3.54
2071-2100	3.88	5.15	4.94	4.54	3.65	5.34	5.89	5.57	4.04	3.86	2.19	3.33	4.36
RCP 8.5													
2011-2040	2.24	2.45	2.42	1.71	2.80	3.66	3.15	3.33	1.98	2.88	0.80	1.57	2.42
2041-2070	3.79	4.00	4.81	3.73	3.62	5.55	6.35	5.74	4.45	4.13	2.94	3.96	4.42
2071-2100	6.17	7.54	7.49	6.04	5.66	8.24	9.24	9.37	8.17	6.70	5.03	5.55	7.10

7.6.1 Movement of the 0 °C Isotherm

In association with the perturbation of climate models, the identification of regional isotherms of importance and their change into the future offers valuable insight for further research. Currently, there are regions within the WCW with annual temperatures modeled at below 0 ˚C. The 0 °C isotherm is potentially important for understanding if permafrost could be present in the WCW and how this could influence the landscape morphology and processes as climate warms. In association with climate change, these regions will disappear from the landscape as a result of the warming. Currently areas with AMAT temperatures modeled below 0 ˚C represent 5.43 % of the WCW **Figure 46**. All future RCP scenarios have no expected regions within the WCW with an AMAT at or below 0 ˚C. With expected climate change, it can be posited that these regions will cease to exist in this landscape in the future.

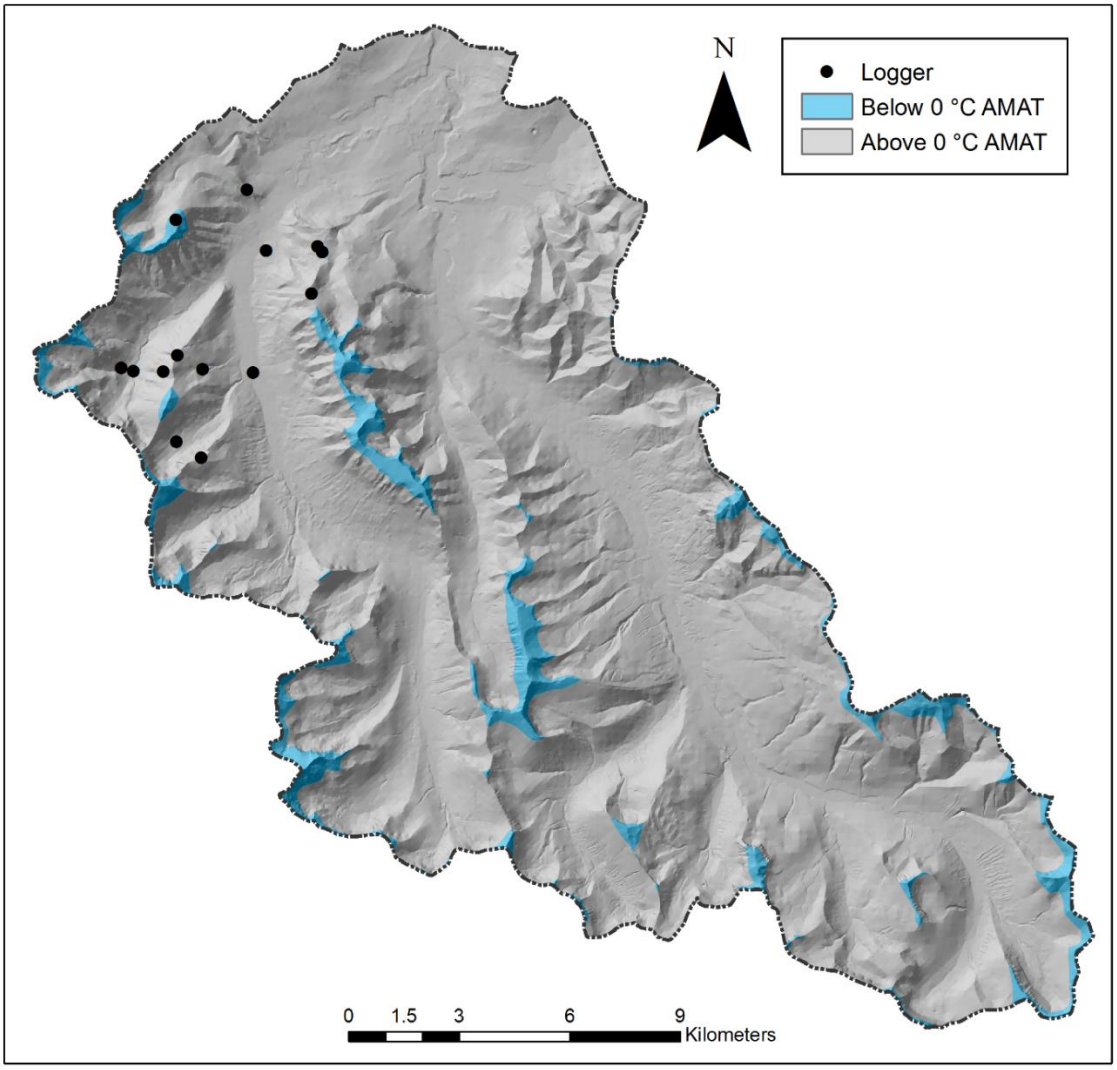

Figure 46: Areas of the WCW modeled as having an AMAT at or below 0 ˚C, depicted in blue, for the 2017-2018 study period covering 5.43 % of the landscape.

7.7 Gaps and Uncertainties

To assess the relationship between the observed and predicted values and quantify potential error inherent within the model an RSME value for each monthly model was determined to quantify uncertainty within the models. (**Table 17**).

Table 17: Root mean square error for each of the monthly models.

Year	Month	RMSE
2017	Jul	1.34
	Aug	1.14
	Sep	1.68
	Oct	1.34
	Nov	1.06
	Dec	1.00
2018	Jan	2.04
	Feb	0.45
	Mar	0.71
	Apr	2.67
	May	1.47
	Jun	0.62
AMAT		1.29

As it was assumed that the sensor placement is representative of the landscape, an error would be introduced as a result of inherent spatial bias. Distribution of sensors is a significant source of potential gaps within this research. The analysis of the data collected showed that the relationship between surface air temperature and solar radiation was negative. Solar radiation, therefore, was not included as an explanatory variable for this research as it is expected that temperature should have a positive relationship with solar radiation where an increase in solar radiation would also increase the temperature of a site (Huang et al., 2008). The distribution of the sensors was reviewed and contrasted against the seasonal change in potential incoming solar radiation (PISR). It was determined that while sampling from north-facing aspects, regions on the landscape that experienced regular topographically driven shading were not being represented in the sampling framework. With an improved distribution of stations by sampling from areas represented by end members of the PISR range could improve the relationship between observed temperatures to be more congruent with paralleled research.

This model process assumed a linear relationship between all the explanatory variables, i.e. slope, elevation, and TPI, as well as treeline representing a significant spatial delineation. The model also assumes that processes within the watershed occur equally on a spatial basis and the relationship between surface air temperature and the explanatory variables does not change within the bounds of the basin. This represents an issue as a reality of this network of sensors is that the data is unable to model or predict the cold-air drainage influence that does not occur within the sensor array are. It does not model temporal shifts in cold air drainage before they reach the sensor network or that occur within different regions of the WCW. Further, the higher in elevation yet low slope regions up valley could have differing temperature regimes that are not being sampled from. Moreover, this work focuses on the change in temperature over the landscape with elevation in a uniform manner, there maybe locations present within the landscape the do not conform to the lapse rates that have been derived for various reasons such as the lack of influence of shortwave radiation in high-elevation north-facing valleys. Unique locations within this landscape would need to be instrumented to further understand how they differ or resemble the rest of the watershed.

7.8 Applications of this Work

This research within the WCW will assist in informing other spatially coincident research, improving snowmelt and hydrological models, and providing a baseline to assess watershed level responses to a changing climate. Current and future hydrological modelling within the region by Anderson (2014) highlights the need for improved

monitoring and station distributions within mountainous regions to improve hydrological cycle response modelling and current understanding.

As it is expected that with climate change and a shift in surface air temperatures as well as other climate variables, a shift in species ranges, both native and invasive, has been observed and is expected to continue (Hamann & Wang, 2006; Lenoir et al., 2008; Chen et al., 2011; Harsch & HilleRisLambers, 2016). With temperature changes modelled of 7.1 ˚C on average (**Table 16**) between the 1981-2010 and the 2081-2100 climate normal periods for RCP 8.5, the redistribution of species sensitive to thermal ranges would shift both with latitude and elevation. This shift in community and in environmental conditions could be a concern for the management of endangered species such as *Pinus flexilis* and *Pinus albicalus* that are present within the region. Further, as edaphic and climatic conditions are often a limiting factor in vegetative distribution, it could be expected that a relatively quick shift in climate would increase the suitable range for many species, but as soil takes many years to develop (Brady et al., 1990), only sites with suitable conditions would become inhabited. Recent soil mapping and modelling efforts (Deering, *unpublished thesis*) in association with this research could be used to assess the locales within the WCW that are potentially primed for species movement with no restrictions as a result of soil conditions at a site.

To improve upon the results of this research, continued observation in partnership with further network development. The further collection of data will allow for improved

analysis and reduce any potential error with modelling as a result of only a single year of data being examined. Improvement of spatial modelling through collection of more climatological variables, implementation of air movement models, and the direct relation between influence of flora communities in the surface energy balance and surface air temperature within the WCW should be a goal. Continued research into the distribution and spatial patterns of inversion presence and the climatological implication of regions prone to inverted SLRs. Application of this work into fields such as snowpack modelling and hydrological impacts, species range and potential future distribution including treeline shift and sensitive species extirpation.

8.0 Conclusion

8.1 Summary

In completion of this research, spatial heterogeneity and temporal patterns in surface air temperature were explored within the West Castle Watershed focusing on the time between July 1st, 2017 and June 30th, 2018. As a result of this research, a new network of sensors distributed across the landscape began collecting temperature data in August 2016 and are continuing measurements at the time of this writing with plans of supplementation and expansion. An objective of this research was to compare small-scale models interpolating surface air temperature in mountainous regions to explore the potential over or underestimation. It was found that while some regions are congruent between models, a substantial proportion are asserting annual surface air temperatures that are to extremes of 4.90 ˚C above to -3.16 ˚C below the interpolated temperature of this research. This discrepancy is most likely as a result of inability of the larger models to capture the landscape within the cells of the model.

By perturbing the models to future states, this research provides insight into the potential changes to the surface air temperature fields within the WCW, an ecologically significant, biodiverse, watershed. With annual average change as great as 7.1 ˚C possible within the next 80 years, this poses a substantial threat to water resources, ecological interactions, species distribution, and sustainability of winter sports activities within the region.

Finally, inversions, surface lapse rates, and chinook patterns observed within this region were identified and explored. Inversions invents were observed for 18.5 % of the

year, and slightly more frequent during the summer as compared to the winter. Further chinooks and surface lapse rates were observed to interact with each other, exemplified by the month of January, where the surface lapse rate of the watershed was modified by the presence of frequent chinook events. This data and understanding provides valuable information that may inform broad models.

9.0 References

Adam, Hamlet, & Lettenmaier. (2009). Implications of global climate change for snowmelt hydrology in the twenty-first century. *Hydrological Processes, 23*(7), 962-972. doi:doi:10.1002/hyp.7201

AEP. (2018). *Castle Management Plan*. Retrieved from https://www.albertaparks.ca/media/6494620/castle_management_plan.pdf.

Al-Rawas, & Valeo. (2009). Characteristics of rainstorm temporal distributions in arid mountainous and coastal regions. *Journal of hydrology, 376*(1), 318-326.

Alexander, Bhatt, Walsh, Timlin, Miller, & Scott. (2004). The atmospheric response to realistic Arctic sea ice anomalies in an AGCM during winter. *Journal of Climate, 17*(5), 890-905.

Anderson. (2014). *Hydrological impacts of climate change on the Castle River Watershed, Alberta, Canada.* University of Lethbridge (Canada).

Arrhenius. (1896). XXXI. On the influence of carbonic acid in the air upon the temperature of the ground. *The London, Edinburgh, and Dublin Philosophical Magazine and Journal of Science, 41*(251), 237-276.

Bobrowsky, & Rutter. (1992). The quaternary geologic history of the Canadian Rocky Mountains. *Géographie physique et Quaternaire, 46*(1), 5-50.

Bonnaventure, & Lamoureux. (2013). The active layer: A conceptual review of monitoring, modelling techniques and changes in a warming climate. *Progress in Physical Geography, 37*(3), 352-376.

Bonnaventure, & Lewkowicz. (2013). Impacts of mean annual air temperature change on a regional permafrost probability model for the southern Yukon and northern British Columbia, Canada. *The Cryosphere, 7*(3), 935-946.

Bradley, Keimig, & Diaz. (2004). Projected temperature changes along the American cordillera and the planned GCOS network. *Geophysical Research Letters, 31*(16). doi:doi:10.1029/2004GL020229

Brady, Weil, & Weil. (1990). The nature and properties of soils.

Brinkmann. (1970). The Chinook at Calgary (Canada). *Archiv für Meteorologie, Geophysik und Bioklimatologie, Serie B, 18*(3), 269-278. doi:10.1007/BF02242880

Charlson, Schwartz, Hales, Cess, Coakley, Hansen, & Hofmann. (1992). Climate forcing by anthropogenic aerosols. *Science, 255*(5043), 423-430.

Chen, Hill, Ohlemüller, Roy, & Thomas. (2011). Rapid Range Shifts of Species Associated with High Levels of Climate Warming. *Science, 333*(6045), 1024-1026. doi:10.1126/science.1206432

Clements, Whiteman, & Horel. (2003). Cold-Air-Pool Structure and Evolution in a Mountain Basin: Peter Sinks, Utah. *Journal of Applied Meteorology, 42*(6), 752-768. doi:10.1175/1520-0450(2003)042<0752:csaeia>2.0.co;2

Cohen, Furtado, Barlow, Alexeev, & Cherry. (2012). Asymmetric seasonal temperature trends. *Geophysical Research Letters, 39*(4). doi:doi:10.1029/2011GL050582

Cohen, Screen, Furtado, Barlow, Whittleston, Coumou, . . . Jones. (2014). Recent Arctic amplification and extreme mid-latitude weather. *Nature Geoscience, 7*, 627. doi:10.1038/ngeo2234

Cowtan, & Way. (2014). Coverage bias in the HadCRUT4 temperature series and its impact on recent temperature trends. *Quarterly Journal of the Royal Meteorological Society, 140*(683), 1935-1944.

Cullen, & Marshall. (2011). Mesoscale Temperature Patterns in the Rocky Mountains and Foothills Region of Southern Alberta. *Atmosphere-Ocean, 49*(3), 189-205. doi:10.1080/07055900.2011.592130

Daly, & Bryant. (2013). The PRISM climate and weather system—an introduction. *Corvallis, OR: PRISM climate group*.

Daly, Gibson, Taylor, Johnson, & Pasteris. (2002). A knowledge-based approach to the statistical mapping of climate. *Climate Research, 22*(2), 99-113.

Daly, Neilson, & Phillips. (1994). A statistical-topographic model for mapping climatological precipitation over mountainous terrain. *Journal of Applied Meteorology, 33*(2), 140-158.

Deser, Tomas, Alexander, & Lawrence. (2010). The Seasonal Atmospheric Response to Projected Arctic Sea Ice Loss in the Late Twenty-First Century. *Journal of Climate, 23*(2), 333-351. doi:10.1175/2009jcli3053.1

Diffenbaugh, & Giorgi. (2012). Climate change hotspots in the CMIP5 global climate model ensemble. *Climatic Change, 114*(3-4), 813-822.

Dobrowski, Abatzoglou, Greenberg, & Schladow. (2009). How much influence does landscape-scale physiography have on air temperature in a mountain environment? *Agricultural and Forest Meteorology, 149*(10), 1751-1758. doi:https://doi.org/10.1016/j.agrformet.2009.06.006

Dyke, Andrews, Clark, England, Miller, Shaw, & Veillette. (2002). The Laurentide and Innuitian ice sheets during the Last Glacial Maximum. *Quaternary Science Reviews, 21*(1–3), 9-31. doi:https://doi.org/10.1016/S0277-3791(01)00095-6

Fridley. (2009). Downscaling Climate over Complex Terrain: High Finescale (<1000 m) Spatial Variation of Near-Ground Temperatures in a Montane Forested Landscape (Great Smoky Mountains). *Journal of Applied Meteorology and Climatology, 48*(5), 1033-1049. doi:10.1175/2008jamc2084.1

Friis-Christensen, & Lassen. (1991). Length of the solar cycle: an indicator of solar activity closely associated with climate. *Science, 254*(5032), 698-700.

Fyfe, & Flato. (1999). Enhanced climate change and its detection over the Rocky Mountains. *Journal of Climate, 12*(1), 230-243.

Giorgi, Hurrell, Marinucci, & Beniston. (1997). Elevation Dependency of the Surface Climate Change Signal: A Model Study. *Journal of Climate, 10*(2), 288-296. doi:10.1175/1520-0442(1997)010<0288:edotsc>2.0.co;2

Gottfried, Pauli, Futschik, Akhalkatsi, Barančok, Alonso, . . . Kazakis. (2012). Continent-wide response of mountain vegetation to climate change. *Nature Climate Change, 2*(2), 111.

Hamann, & Wang. (2006). Potential Effects of Climate Change on Ecosystem and Tree Species Distribution in British Columbia. *Ecology, 87*(11), 2773-2786. doi:10.1890/0012-9658(2006)87[2773:peocco]2.0.co;2

Harsch, & HilleRisLambers. (2016). Climate Warming and Seasonal Precipitation Change Interact to Limit Species Distribution Shifts across Western North America. *PLoS One, 11*(7), e0159184. doi:10.1371/journal.pone.0159184

Hauer, Stanford, & Lorang. (2007). Pattern and Process in Northern Rocky Mountain Headwaters: Ecological Linkages in the Headwaters of the Crown of the Continent1. *JAWRA Journal of the American Water Resources Association, 43*(1), 104-117. doi:doi:10.1111/j.1752-1688.2007.00009.x

Hays, Imbrie, & Shackleton. (1976). Variations in the Earth's orbit: pacemaker of the ice ages. *Science, 194*(4270), 1121-1132.

Held, & Soden. (2006). Robust responses of the hydrological cycle to global warming. *Journal of Climate, 19*(21), 5686-5699.

Hernández-Henríquez, Déry, & Derksen. (2015). Polar amplification and elevation-dependence in trends of Northern Hemisphere snow cover extent, 1971–2014. *Environmental Research Letters, 10*(4), 044010.

Hijmans, Cameron, Parra, Jones, & Jarvis. (2005). Very high resolution interpolated climate surfaces for global land areas. *International journal of climatology, 25*(15), 1965-1978.

Hock. (2003). Temperature index melt modelling in mountain areas. *Journal of hydrology, 282*(1-4), 104-115.

Hopkinson, McKenney, Milewska, Hutchinson, Papadopol, & Vincent. (2011). Impact of Aligning Climatological Day on Gridding Daily Maximum–Minimum Temperature and Precipitation over Canada. *Journal of Applied Meteorology and Climatology, 50*(8), 1654-1665. doi:10.1175/2011jamc2684.1

Huang, Rich, Crabtree, Potter, & Fu. (2008). Modeling Monthly Near-Surface Air Temperature from Solar Radiation and Lapse Rate: Application over Complex Terrain in Yellowstone National Park. *Physical Geography, 29*(2), 158-178. doi:10.2747/0272-3646.29.2.158

Hutchinson, McKenney, Lawrence, Pedlar, Hopkinson, Milewska, & Papadopol. (2009). Development and Testing of Canada-Wide Interpolated Spatial Models of Daily Minimum–Maximum Temperature and Precipitation for 1961–2003. *Journal of Applied Meteorology and Climatology, 48*(4), 725-741. doi:10.1175/2008jamc1979.1

IPCC. (2014). *Climate Change 2014–Impacts, Adaptation and Vulnerability: Regional Aspects*: Cambridge University Press.

Jackson, Phillips, Shimamura, & Little. (1997). Cosmogenic 36Cl dating of the Foothills erratics train, Alberta, Canada. *Geology, 25*(3), 195-198.

Jenness. (2006). Topographic Position Index (tpi_jen. avx) extension for ArcView 3. x, v. 1.3 a. Jenness Enterprises.

Jenny. (1994). *Factors of soil formation: a system of quantitative pedology*: Courier Corporation.

Jouzel, Lorius, Petit, Genthon, Barkov, Kotlyakov, & Petrov. (1987). Vostok ice core: a continuous isotope temperature record over the last climatic cycle (160,000 years). *Nature, 329*(6138), 403-408. doi:10.1038/329403a0

Kienzle. (2017). Has it become warmer in Alberta? Mapping temperature changes for the period 1950–2010 across Alberta, Canada. *The Canadian Geographer / Le Géographe canadien*, n/a-n/a. doi:10.1111/cag.12432

Kienzle, & Mueller. (2013). Mapping Alberta's surface water resources for the period 1971–2000. *The Canadian Geographer / Le Géographe canadien, 57*(4), 506-518. doi:10.1111/j.1541-0064.2013.12050.x

Kienzle, Nemeth, Byrne, & MacDonald. (2012). Simulating the hydrological impacts of climate change in the upper North Saskatchewan River basin, Alberta, Canada. *Journal of hydrology, 412*, 76-89.

Kirchner, Faus-Kessler, Jakobi, Leuchner, Ries, Scheel, & Suppan. (2013). Altitudinal temperature lapse rates in an Alpine valley: trends and the influence of season and weather patterns. *International journal of climatology, 33*(3), 539-555. doi:10.1002/joc.3444

Lenoir, Gégout, Marquet, de Ruffray, & Brisse. (2008). A Significant Upward Shift in Plant Species Optimum Elevation During the 20th Century. *Science, 320*(5884), 1768-1771. doi:10.1126/science.1156831

Lewkowicz, & Bonnaventure. (2011). Equivalent Elevation: A New Method to Incorporate Variable Surface Lapse Rates into Mountain Permafrost Modelling. *Permafrost and Periglacial Processes, 22*(2), 153-162. doi:10.1002/ppp.720

Li, & Heap. (2014). Spatial interpolation methods applied in the environmental sciences: A review. *Environmental Modelling & Software, 53*, 173-189.

Lorenc. (1986). Analysis methods for numerical weather prediction. *Quarterly Journal of the Royal Meteorological Society, 112*(474), 1177-1194.

Lorius, Merlivat, Jouzel, & Pourchet. (1979). A 30,000-yr isotope climatic record from Antarctic ice. *Nature, 280*(5724), 644-648. doi:10.1038/280644a0

Luckman, & Wilson. (2005). Summer temperatures in the Canadian Rockies during the last millennium: a revised record. *Climate Dynamics, 24*(2-3), 131-144.

Lundquist, Pepin, & Rochford. (2008). Automated algorithm for mapping regions of cold-air pooling in complex terrain. *Journal of Geophysical Research: Atmospheres, 113*(D22). doi:10.1029/2008jd009879

Mattie. (2009). *Surface Temperature as a Function of Terrain Variables in the Rocky Mountins and Foothills Region in Southern Alberta*: University of Calgary, Department of Geography.

Minder, Mote, & Lundquist. (2010). Surface temperature lapse rates over complex terrain: Lessons from the Cascade Mountains. *Journal of Geophysical Research: Atmospheres, 115*(D14), n/a-n/a. doi:10.1029/2009JD013493

Nkemdirim. (1986). Chinooks in Southern Alberta: Some distinguishing nocturnal features. *Journal of Climatology, 6*(6), 593-603. doi:10.1002/joc.3370060603

Nkemdirim. (1996). Canada's chinook belt. *International journal of climatology, 16*(4), 441-462.

Nkemdirim. (1997). ON THE FREQUENCY AND SEQUENCING OF CHINOOK EVENTS. *Physical Geography, 18*(2), 101-113. doi:10.1080/02723646.1997.10642610

NRCAN. (2019). Retrieved from https://cfs.nrcan.gc.ca/projects/3/4.

Oke. (1987). *Boundary layer climates*: Routledge.

Painter, Barrett, Landry, Neff, Cassidy, Lawrence, . . . Farmer. (2007). Impact of disturbed desert soils on duration of mountain snow cover. *Geophysical Research Letters, 34*(12).

Palmer. (2000). Predicting uncertainty in forecasts of weather and climate. *Reports on Progress in Physics, 63*(2), 71.

Pepin, Bradley, Diaz, Baraer, Caceres, Forsythe, . . . Yang. (2015). Elevation-dependent warming in mountain regions of the world. *Nature Climate Change, 5*, 424. doi:10.1038/nclimate2563

Pepin, & Lundquist. (2008). Temperature trends at high elevations: patterns across the globe. *Geophysical Research Letters, 35*(14).

Petit, Jouzel, Raynaud, Barkov, Barnola, Basile, . . . Delaygue. (1999). Climate and atmospheric history of the past 420,000 years from the Vostok ice core, Antarctica. *Nature, 399*(6735), 429-436.

Pigeon, & Jiskoot. (2008). Meteorological controls on snowpack formation and dynamics in the southern Canadian Rocky Mountains. *Arctic, Antarctic, and Alpine Research, 40*(4), 716-730.

Praskievicz. (2018). Downscaling climate-model output in mountainous terrain using local topographic lapse rates for hydrologic modeling of climate-change impacts. *Physical Geography, 39*(2), 99-117. doi:10.1080/02723646.2017.1378555

Prömmel, Geyer, Jones, & Widmann. (2010). Evaluation of the skill and added value of a reanalysis-driven regional simulation for Alpine temperature. *International journal of climatology, 30*(5), 760-773. doi:doi:10.1002/joc.1916

Raymo, & Ruddiman. (1992). Tectonic forcing of late Cenozoic climate. *Nature, 359*(6391), 117.

Reinelt. (1970). On the role of orography in the precipitation regime of Alberta. *Albertan Geographer, 6*, 45-58.

Rolland. (2003). Spatial and seasonal variations of air temperature lapse rates in Alpine regions. *Journal of Climate, 16*(7), 1032-1046.

Ross. (2017). *Weather and climate: An introduction*: Oxford University Press.

Ruddiman. (2001). *Earth's climate: past and future*: Macmillan.

Safranyik. (1978). Effects of climate and weather on mountain pine beetle populations.

Schneider. (2013). Alberta's natural subregions under a changing climate: past, present, and future.

Serreze, & Barry. (2011). Processes and impacts of Arctic amplification: A research synthesis. *Global and Planetary Change, 77*(1), 85-96. doi:https://doi.org/10.1016/j.gloplacha.2011.03.004

Singarayer, Bamber, & Valdes. (2006). Twenty-first-century climate impacts from a declining Arctic sea ice cover. *Journal of Climate, 19*(7), 1109-1125.

Smith, & Bonnaventure. (2017). *Quantifying Surface Temperature Inversions and Their Impact on the Ground Thermal Regime at a High Arctic Site* (Vol. 49).

Stahl, Moore, Floyer, Asplin, & McKendry. (2006). Comparison of approaches for spatial interpolation of daily air temperature in a large region with complex topography and highly variable station density. *Agricultural and Forest Meteorology, 139*(3), 224-236. doi:https://doi.org/10.1016/j.agrformet.2006.07.004

Stalker. (1969). A Probable Late Pinedale Terminal Moraine in Castle River Valley, Alberta. *GSA Bulletin, 80*(10), 2115-2122. doi:10.1130/0016-7606(1969)80[2115:APLPTM]2.0.CO;2

Stalker, & Harrison. (1977). Quaternary glaciation of the Waterton-Castle River region of Alberta. *Bulletin of Canadian Petroleum Geology, 25*(4), 882-906.

SWIPA. (2017). Snow, Water, Ice and Permafrost in the Arctic (SWIPA) 2017.

Taylor, Nixon, Eley, Burgess, & Egginton. (1998). *Effect of atmospheric temperature inversions on ground surface temperatures and discontinuous permafrost, Norman Wells, Mackenzie Valley, Canada.* Paper presented at the Proceedings of the Seventh International Conference on Permafrost, Yellowknife, NWT, Université Laval, Quebec, Collection Nordicana.

Wang, Hamann, Spittlehouse, & Carroll. (2016). Locally Downscaled and Spatially Customizable Climate Data for Historical and Future Periods for North America. *PLoS One, 11*(6), e0156720. doi:10.1371/journal.pone.0156720

Wang, Hamann, Spittlehouse, & Murdock. (2012). ClimateWNA—high-resolution spatial climate data for western North America. *Journal of Applied Meteorology and Climatology, 51*(1), 16-29.

Way, & Bonnaventure. (2015). Testing a reanalysis-based infilling method for areas with sparse discontinuous air temperature data in northeastern Canada. *Atmospheric Science Letters, 16*(3), 398-407.

Wood, Marshall, & Fargey. (2019). Daily measurements of near-surface humidity from a mesonet in the foothills of the Canadian Rocky Mountains, 2005–2010. *Earth System Science Data, 11*(1), 23-34.

Xu, Cao, Hansen, Yao, Joswia, Wang, . . . Yang. (2009). Black soot and the survival of Tibetan glaciers. *Proceedings of the National Academy of Sciences, 106*(52), 22114-22118.

Young. (2003). Top-down and data-based mechanistic modelling of rainfall–flow dynamics at the catchment scale. *Hydrological Processes, 17*(11), 2195-2217.

Appendix

Table 18: The average monthly temperature in the WCW for the year of study and perturbed monthly averages along RCP 2.6, 4.5, and 8.5 to three future climate normals.

		2017-2018	2011-2040	2041-2070	2071-2100
RCP 2.6	January	-4.95	-3.58	-2.90	-2.07
	February	-11.60	-10.45	-8.56	-8.28
	March	-4.04	-1.88	-0.60	-0.47
	April	-0.37	1.63	3.21	2.43
	May	8.57	11.34	11.71	11.44
	June	9.69	13.32	13.74	13.78
	July	16.93	19.91	20.31	20.05
	August	14.90	17.98	18.60	18.38
	September	8.50	11.25	10.70	10.62
	October	1.22	4.06	3.76	3.42
	November	-4.48	-3.42	-2.87	-2.84
	December	-9.06	-7.60	-6.77	-6.45
		2017-2018	**2011-2040**	**2041-2070**	**2071-2100**
RCP 4.5	January	-4.95	-3.25	-2.33	-1.07
	February	-11.60	-9.67	-7.63	-6.45
	March	-4.04	-1.86	-0.39	0.89
	April	-0.37	1.66	2.64	4.18
	May	8.57	10.74	11.10	12.21
	June	9.69	13.64	15.12	15.03
	July	16.93	19.61	21.58	22.82
	August	14.90	17.85	19.53	20.48
	September	8.50	10.88	12.19	12.53
	October	1.22	3.74	4.51	5.08
	November	-4.48	-3.43	-2.45	-2.29
	December	-9.06	-8.11	-6.07	-5.73
		2017-2018	**2011-2040**	**2041-2070**	**2071-2100**
RCP 8.5	January	-4.95	-2.70	-1.16	1.22
	February	-11.60	-9.15	-7.60	-4.06
	March	-4.04	-1.63	0.77	3.45
	April	-0.37	1.34	3.36	5.68
	May	8.57	11.37	12.19	14.23
	June	9.69	13.35	15.25	17.93
	July	16.93	20.08	23.28	26.17
	August	14.90	18.23	20.64	24.27
	September	8.50	10.47	12.94	16.67
	October	1.22	4.10	5.35	7.92
	November	-4.48	-3.68	-1.53	0.56
	December	-9.06	-7.50	-5.11	-3.51

Table 19: The rate of change of temperature in the WCW between perturbed future climate normal scenarios for individual RCP models and months.

		2020-2050	2050-2080	Average
RCP 2.6	January	0.68	0.82	0.75
	February	1.89	0.28	1.08
	March	1.28	0.13	0.70
	April	1.58	-0.78	0.40
	May	0.37	-0.27	0.05
	June	0.41	0.04	0.23
	July	0.40	-0.27	0.07
	August	0.62	-0.22	0.20
	September	-0.55	-0.08	-0.31
	October	-0.31	-0.34	-0.32
	November	0.55	0.04	0.29
	December	0.84	0.32	0.58
		2020-2050	**2050-2080**	**Average**
RCP 4.5	January	0.92	1.26	1.09
	February	2.04	1.18	1.61
	March	1.48	1.28	1.38
	April	0.98	1.54	1.26
	May	0.36	1.11	0.73
	June	1.48	-0.09	0.69
	July	1.96	1.24	1.60
	August	1.68	0.94	1.31
	September	1.31	0.34	0.83
	October	0.77	0.57	0.67
	November	0.98	0.17	0.57
	December	2.04	0.34	1.19
		2020-2050	**2050-2080**	**Average**
RCP 8.5	January	1.54	2.38	1.96
	February	1.54	3.54	2.54
	March	2.40	2.68	2.54
	April	2.02	2.31	2.17
	May	0.82	2.04	1.43
	June	1.89	2.68	2.29
	July	3.20	2.90	3.05
	August	2.41	3.63	3.02
	September	2.47	3.72	3.10
	October	1.25	2.56	1.91
	November	2.14	2.09	2.12
	December	2.39	1.59	1.99

Table 20: The average climate normal (˚C) of all station locations within the WCW for the period of 1981-2010 as calculated by ClimateNA (Wang et al., 2012).

Month	Climate Normal (1981-2010)
January	-8.13
February	-7.32
March	-3.45
April	0.44
May	5.14
June	9.57
July	13.15
August	12.66
September	8.41
October	2.73
November	-4.67
December	-9.20